Development and characterisation of copper solution-based artificial synapses

Andreia Silva
Mestrado em Engenharia Física
Departamento de Física e Astronomia
2022

Orientador
Dra. Catarina Dias, Faculdade de Ciências

Coorientador
Prof. Dr. João Ventura, Faculdade de Ciências

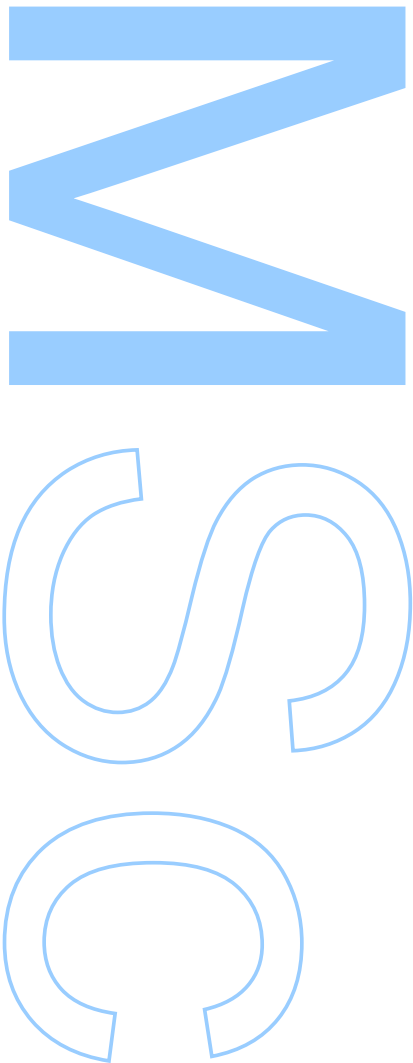

U.PORTO

FACULDADE DE CIÊNCIAS
UNIVERSIDADE DO PORTO

Todas as correções determinadas pelo júri, e só essas, foram efetuadas.

O Presidente do Júri,

Porto, _____/_____/_____

UNIVERSIDADE DO PORTO

MASTERS THESIS

Development and characterisation of copper solution-based artificial synapses

Author:
Andreia SILVA

Supervisor:
Dra. Catarina DIAS

Co-supervisor:
Prof. Dr. João VENTURA

A thesis submitted in fulfilment of the requirements
for the degree of MSc. Engineering Physics

at the

Faculdade de Ciências da Universidade do Porto
Departamento de Física e Astronomia

November 24, 2022

Sworn Statement

I, Andreia Catarina Vieira da Silva, enrolled in the Master Degree of Engineering Physics at the Faculty of Sciences of the University of Porto hereby declare, in accordance with the provisions of paragraph a) of Article 14 of the Code of Ethical Conduct of the University of Porto, that the content of this dissertation reflects perspectives, research work and my own interpretations at the time of its submission.

By submitting this dissertation, I also declare that it contains the results of my own research work and contributions that have not been previously submitted to this or any other institution.

I further declare that all references to other authors fully comply with the rules of attribution and are referenced in the text by citation and identified in the bibliographic references section. This dissertation does not include any content whose reproduction is protected by copyright laws.

I am aware that the practice of plagiarism and self-plagiarism constitute a form of academic offense.

Andreia Catarina Vieira da Silva
October 12, 2022

Acknowledgements

First and foremost, I would like to thank my supervisor, Doctor Catarina Dias, for her guidance throughout all the years we have been working together, for being patient, understanding and for doing everything in her power to help me develop and grow. I am truly thankful to her, for believing in me and in my work ethic, and for the around the clock availability to help. Without her, none of this work would have been possible.

I would also like to extend my gratitude towards my co-supervisor, Professor João Ventura, for all the help, advice and guidance provided.

A special thank you to Doctor Ana Teresa Brandão, from the Chemistry Department, who tirelessly helped me with not so comfortable subjects and provided me with all the tools I needed, and more, to be able to further my research. Your kindness and readiness to help was noted. I would also like to thank Professor Carlos Pereira for all the help provided.

To the members of IFIMUP, I would like to thank for the sympathy, the help and the great work environment.

For these five years of, in lack of better words, an eventful roller coaster, I would like to thank my friends Maria, Miguel, João Silva, João Carvalho, Trovão, Tiago and Nuno, for putting up with me in my most stressful and cranky times and for believing in me, more than I could ever believe in myself. You made hard times go by fast and good times feel like forever.

To my family and to those who, even though are not blood related, are family as well, I cannot put into words how thankful I am for you. For pulling me up every time I was feeling down, for all the sacrifices you made for me, which were many, and for never doubting, not even for a second, of my abilities. I owe everything to you.

Finally, I want to thank my other half, for putting up with a, at times, very stressed absent girlfriend, for being my safe harbor every time and for supporting and loving me all through these five years. I could not have asked for a better partner to go on this roller-coaster ride, that is life, with me. You make me happy.

Yours truly,
Andreia Silva

UNIVERSIDADE DO PORTO

Abstract

Faculdade de Ciências da Universidade do Porto
Departamento de Física e Astronomia

MSc. Engineering Physics

Development and characterisation of copper solution-based artificial synapses

by Andreia SILVA

With computer technology moving closer to its limits regarding Moore's law, a hardware solution is needed that can process large quantities of data efficiently and accompany the ever-growing computer software development. With this is mind, scientists turned to the most efficient computational entity known as inspiration, the human brain, by the means of neuromorphic computing. The brain is composed of neurons and synapses that process and transmit information, due to memory and learning abilities. A promising candidate for the mimicking of neurons and synapses in the brain is a new generation of devices that present resistive switching (RS), a process that is similar to the biological synaptic behaviour. Since many of the mechanisms of RS are dependent on the movement of ions in an active layer, the use of liquids proves to be promising for the improvement of electrical properties of such devices. Furthermore, it presents great potential for implantable and flexible devices, as the liquid nature allows them to be fabricated in many shapes. With that in mind, the present work proposes a new RS device composed of a copper(II) sulphate pentahydrate ($CuSO_4.5H_2O$) solution as its active layer, a copper active electrode and a top electrode whose material was varied. Furthermore, to characterise it, several parameters were varied such as solution concentration, applied range of potentials, distance between electrodes, temperature of the solution and material of the top electrode, and the device response was analysed. The device showed to have the best behaviour for a solution concentration of 0.5 mol/l, operation voltage $<$300 mV, distance between electrodes of 1.20 mm, room temperature operation and, finally, a Pt top electrode with a diameter of 0.1 mm. Properties like bipolar RS, endurance and data retention were achieved, all under low operation voltage. The device presented non-volatile resistive switching behaviour explained by the diffusion of copper atoms in the solution

when an electric field in being applied. Furthermore, potentiation and depression characteristics were also achieved, that are of great importance, because they are believed to be the responsible for the learning behaviour in the human brain. Such properties were attained with potential pulses of -60 and 90 mV that are similar to those of action potential of biological cells. Finally, with the increase in the use of ionic liquids as a way to improve conduction properties of several devices, a study of how its mixture with the copper sulphate would behave in the present device was of great curiosity. However, ionic liquids are hard to make, and, for the most part, pollutant, so deep eutectic solvents (DESs), solvents that present similar electrical and physical characteristics as ionic liquids, even though chemically different, proved to be the best option. So, in the last part of this thesis, a DES composed of choline chloride and glycerol was mixed with the copper sulphate and the resulting liquid was used as the active layer of the device. RS was achieved, with best results for a potential of $<$3 V, endurance over 500 cycles, and potentiation and depression observed. The RS behaviour was improved due to higher ratio between states, however, its mechanism proved to be different from the previous device, with further research needed for a better understanding of the physics behind it. Data retention was not achieved due to a change in volatility from the device, from non-volatile to volatile. An attempt to gel the solution was also made, with overall similar results as to those obtained without the gel process. The neuromorphic properties shown here, with particularly low power operation when compared to other reports, reveal the great potential of this system for energy efficient brain-like electronics. Furthermore, due to its liquid nature, it can be used in varied forms and shapes, expanding, therefore, its possible applications.

UNIVERSIDADE DO PORTO

Resumo

Faculdade de Ciências da Universidade do Porto
Departamento de Física e Astronomia

Mestrado em Engenharia Física

Desenvolvimento e caracterização de sinapses artificiais baseadas em uma solução de cobre

por Andreia SILVA

Com a tecnologia de computadores a aproximar-se do seu limite no que diz respeito à lei de Moore, é necessária uma solução física capaz de acompanhar o rápido desenvolvimento de computação, nomeadamente, que seja capaz de processar grandes quantidades de dados eficientemente. Com isto em mente, os cientistas recorreram à entidade computacional mais eficiente conhecida pelo homem como inspiração, o cérebro humano, para uso em computação neuromórfica. O cérebro é composto por neurónios e sinapses, que processam e transmitem informação, e que estão na origem da memória e aprendizagem. Um candidato promissor à tarefa de imitar os neurónios e sinapses do cérebro é uma nova geração de dispositivos que apresenta comutação resistiva, ou *resistive switching* (RS), como é conhecido, que é um processo que se assemelha ao comportamento sináptico biológico. Uma vez que muitos dos mecanismos de comutação resistiva dependem do movimento de iões numa camada ativa, o uso de líquidos revela-se promissor para a melhoria das propriedades elétricas nos dispositivos. Além disso, apresentam um grande potencial para dispositivos implantáveis e flexíveis, uma vez que a sua natureza líquida permite a sua fabricação adaptável a várias formas. Com isto em mente, o presente trabalho propõe um novo dispositivo que apresenta RS composto por uma solução de sulfato de cobre penta-hidratado ($CuSO_4.5H_2O$) como camada ativa, um elétrodo ativo de cobre e um elétrodo superior cujo material foi sendo variado. Para além disso, a sua caracterização foi feita e, para isso, vários parâmetros foram variados, tais como a concentração da solução, gama de potenciais aplicados, distância entre elétrodos, temperatura da solução e material do elétrodo superior, e a resposta do dispositivo foi analisada. O dispositivo mostrou ter o melhor comportamento para uma concentração de

solução de 0.5 mol/l, tensão de funcionamento de $<$300 mV, distância entre elétrodos de 1.2 mm, temperatura ambiente de operação e, finalmente, elétrodo superior feito de platina com diâmetro de 0.1 mm. Propriedades como comutação resistiva bipolar, tolerância, retenção de dados e comportamento não-volátil foram alcançados, tudo sob baixa tensão de operação. O dispositivo apresentou comportamento de comutação resistive não-volátil que pode ser explicado pela difusão de átomos de cobre na solução, quando um campo elétrico lhe está a ser aplicado. Além disso, foram também alcançadas características de potenciação e depressão, que são de grande importância, porque se acredita serem as responsáveis pelo comportamento de aprendizagem no cérebro humano. Tais propriedades foram atingidas com pulsos de -60 e 90 mV, que são semelhantes aos dos potenciais de ação de células biológicas. Finalmente, com o aumento do uso de líquidos iónicos como forma de melhorar as propriedades de condução de vários dispositivos, um estudo do comportamento que a sua mistura com o sulfato de cobre teria provou ser de grande interesse. No entanto, os líquidos iónicos são difíceis de fazer e, na sua maioria, poluentes, então, solventes eutécticos, também conhecidos como *deep eutectic solvents* (DESs), são solventes que apresentam características elétricas e físicas semelhantes aos líquidos iónicos, ainda que quimicamente diferentes, e que se revelaram como a melhor opção para estudo no dispositivo. Assim, na parte final desta tese, um DES composto de cloreto de colina e glicerol foi misturado com o sulfato de cobre e o líquido resultante foi usado na camada ativa do dispositivo. O fenómeno de comutação resistiva foi obtido, com melhores resultados para um potencial de $<$3 V, sendo que tolerância ao longo de 500 ciclos e potenciação e depressão também foram observados. O comportamento de comutação resistiva foi melhorado devido a um maior rácio entre estados de resistência, no entanto, o seu mecanismo de condução é diferente do dispositivo anterior, sendo que uma pesquisa mais profunda será necessária para compreensão da física por detrás do fenómeno. A retenção de dados não foi conseguida, devido a uma mudança de volatilidade do dispositivo, de não-volátil para volátil. Foi também feita uma tentativa de gelificar a solução, com resultados globais semelhantes aos obtidos sem o processo de gelificação. As propriedades neuromórficas aqui mostradas, com potência de operação particularmente baixa quando comparada com outros trabalhos, revelam o grande potencial deste sistema para dispositivos eletrónicos energeticamente eficientes. Além do mais, devido à sua natureza líquida, podem ser usados de variadas formas e feitios, expandindo, portanto, as suas possíveis aplicações.

Contents

List of Figures

List of Tables

Glossary

CPU	Central Processing Unit
RRAM	Resistive random-access memory
STDP	Spike-timing-dependent plasticity
LTP	Long-term potentiation
LTD	Long-term depression
STP	Short-term potentiation
STD	Short-term depression
LTM	Long-term memory
STM	Short-term memory
ISI	Interspike interval
LRS	Low resistive state
HRS	High resistive state
RS	Resistive switching
CMOS	Complementary metal oxide semiconductor
PCM	Phase change memory
DW	Domain wall
DES	Deep eutectic solvent
DEs	Deep eutectic solvent
IL	Ionic liquid

To my family, for their unwavering love, support and belief.

Chapter 1

Introduction

1.1 Motivation

Computation and adaptation are intrinsic virtues of which our society was built upon. Computation, however, has been evolving faster than the hardware that sustains it. This becomes obvious with the increasing use of artificial intelligence, machine learning, and algorithms, in general, that use large data and complex numerical calculations. The current hardware in which computers are based off - von Neumann architecture - separates its processing unit (CPU) and its memory, which means that, for each operation performed, information needs to travel between these two segments. Upon the processing of large data, this configuration becomes a real issue due to the traffic and traction created, known as the von Neumann bottleneck. As a consequence of this phenomenon, there is an increase in energy usage as well as decreasing of speed operation.

Simultaneously, computer technology is evolving faster than the hardware that sustains it, approaching the limit of Moore's law regarding the number of transistors and their ever decreasing size that are still capable of processing large data efficiently without reasonable high energy consumption, cost, and heat dissipation, making it imperative to find the next generation of devices that are capable of performing with better efficiency and minimal loss, to accompany the progression of technological needs and the ongoing miniaturization of electronics [1].

Keeping all these aspects in mind, scientists turned their ways into other possibilities in which to build their computers upon, such as quantum and neuromorphic computing. The latter uses the human brain as inspiration as it is the most efficient computational entity known - it has memory retention and learning capabilities, with very low power

consumption - and tries to mimic its composition - a network of neurons and synapses being that the first one processes information and the second one transmits the information. A generation of devices capable of mimicking the previously mentioned aspects, such as the processing and storing information in one place, are called memristors [2]. These memristors are two terminal devices in which current and voltage present non-linear relations and function based on a process that resembles synaptic behaviour called resistive switching, defined as the transition between two or more states of resistivity [3, 4]. Research has already shown that this process can be replicated in either solid or liquid medium [5]. The special interest in liquids and in liquid-based artificial synapses arises from the fact that liquids, such as ionic liquids, present high ion mobility, which is ideal for a device that relies on ion diffusion since smaller fields are involved in its operation. Furthermore, the device can be fabricated in many shapes due to the liquid nature and being the main transport systems in humans liquid-based, this allows for a better biocompatibility with living beings [6]. Besides, liquid-based devices are often cheaper and easier to produce than solid-state ones since they do not require access to clean rooms and their cutting-edge nanotechnology deposition methods, at least not as much as solid-state ones.

With the promising qualities that liquid-based devices have shown to have, a deep dive into a liquid system made of a copper solution will be pursued, namely its characterisation based upon properties such as presence of RS behaviour, endurance, retention, potentiation and depression, in the hopes it will be of use for new and promising high technology.

1.2 Objective

This dissertation has the main goal to create and characterise an artificial synapse-based memristor device made from a copper-based solution. For that, a device was engineered, a measuring setup was constructed, and its characterisation (electrical, in temperature, and in materials used) was performed.

1.3 Document Overview

The document is divided into 5 main chapters: introduction, literature review, experimental data, device characterisation and conclusion.

The first chapter briefly explains the motivation behind the work exposed in the dissertation as well as its main goals.

The second chapter overviews the literature related to the subject in study, mainly related to memristors, and all its key points and definitions in order to understand future references in the work, namely in the characterisation of the device phase.

The third chapter relates to the experimental part of the work, so it deals with the explaining of the different processes made, the different measurements executed, and the measuring setup used.

The device characterisation chapter portrays all the analysis performed on the created device and the main conclusions one can draw from the obtained results.

Finally, the conclusion chapter is intended to be a summary of all the main conclusion drawn from the results obtained by the device. It will also include the future work necessary to fill in the gaps in knowledge that arose from this experiment.

Chapter 2

Literature Review

2.1 Brain Architecture

The brain is an impressive organ with unique characteristics, such as learning capabilities and memory retention. It is composed of a complex network of two fundamental units: neurons and synapses (fig. 2.1). A neuron is composed of a lipid membrane that separates intra and extracellular spaces (fig. 2.1a). Along the lipidic membrane there are several ions distributed with different concentrations: Na^+ and Cl^- are more concentrated in the extracellular space and K^+ in the intracellular space. When no potential is applied through the membrane, it is at a resting state of about -60 mV derived from the distribution of ions through the membrane. However, when and external stimuli is applied, the depolarization of the resting state membrane happens, increasing the membrane potential. This depolarization is often called action potential firing and is caused by the change in the ion distribution in the membrane (fig. 2.1c). The depolarization state does not last long, due to the existence of Na^+/K^+ ion pumps that act towards re-establishing the membrane equilibrium by moving ions in order to achieve resting phase concentration distribution, again (elastic behaviour). While the phenomena described refers to a particular site in the neuron, when the external stimuli strike the cell, it propagates the action potential all the way from the dendrites to the nerve endings, moving on to the synapses and to the following neuron, if the trigger is strong enough [7].

Synapses are the junctions between neurons where signals, chemical or electrical, are transmitted, from the pre- to the post-synaptic neuron, by means of neurotransmitters (fig. 2.1b) , when an action potential (fig. 2.1c) generates a gradient of ionic concentrations in the cell. These neurotransmitters bind to the receptor sites (receptor proteins that are

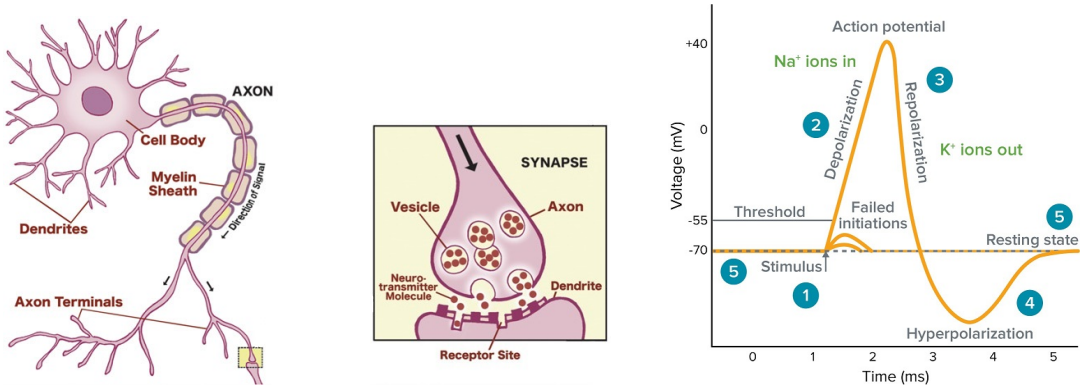

(A) (B) (C)

FIGURE 2.1: Schematic of (A) a neuron and (B) a signal being transmitted through a synapse connecting two neurons. Adapted from [9]. (C) Graphic representation of an action potential through a membrane. Adapted from [10].

activated by a neurotransmitter) leading to an excitatory or inhibitory firing on the post-synaptic neuron [8]. Therefore, synapses provide an altered or converted input signal to a neuron that is related, proportionally, to the output signal of the previous neuron.

In fig. 2.1a a nervous cell and its constituents are illustrated. Furthermore, in fig. 2.1b, a zoom of the synapse is illustrated, where one can see the signal moving from the pre-synaptic neuron to the post-synaptic neuron, where neurotransmitters, which are responsible for a change in the membrane's conductivity [11], are being released to the synapse and captured by the post-synaptic neuron.

Biologically, memory is then stored in the synapses in the form of synaptic strength, the strength that bonds two neurons together, being that learning mechanisms can alter this strength due to neural activities [12]. This process is called synaptic plasticity and it is what enables learning and memorizing in the brain.

In the latest years, models have been developed to help understand how the brain works, especially in terms of learning capabilities. Even though a lot of effort has been put in place, till this day, no model has successfully described all the possibilities of plasticity observed in nature. Some, however, have remained has the foundation from which to build upon, namely, Hebbian learning. Hebbian learning is described as, by Hebb in 1949, "when an axon of cell A is near enough to excite a cell B and repeatedly or persistently takes part in firing it, some growth process or metabolic change takes place in one or both cells such that A's efficiency, as one of the cells firing B, is increased". Essentially "units that fire together, wire together", meaning that the synaptic weight between two neurons who are connected and firing together increases due to successive stimuli and the bond

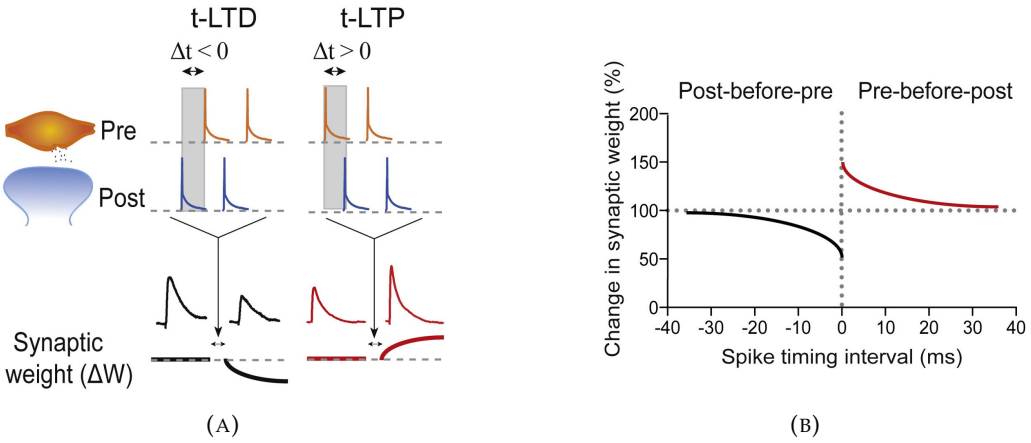

(A) (B)

FIGURE 2.2: (A) Schematics of LTD and LTP and the respective synaptic weight change. (B) Graphical representation of the change synaptic weight with dependence on the spike timing interval, for both post-synaptic spike before the pre-synaptic spike and post-synaptic spike before post-synaptic spike. The longer the time interval the least amount of change in synaptic weight is recorded. Adapted from [14].

between these strengthens [13].

Another model worth mentioning is the spike-timing-dependent plasticity (STDP) model that states that the changes verified in synaptic strength and sign are directly related to the timing of the firing of the spikes. It can be divided into two categories, timing-dependent long-term potentiation (LTP), and timing-dependent long-term depression (LTD). In the first, consecutive patterned activation of a presynaptic cell immediately before it spikes into a postsynaptic cell strengthens their relation, lasting hours or longer. As for the second, consecutive patterned activation of a presynaptic cell immediately after it spikes into a postsynaptic cell weakens their relation, lasting, again, hours or longer (fig. 2.2a). This model is "Hebbian" in the sense that there are synaptic inputs that lead to post-synaptic firing, but it adds concepts of temporal order that are relevant to determine the direction, strength and patterns of synapses and their modification [14]. The main factor that needs to be considered when referring to STPD is, therefore, the interspike interval (ISI): the time that occurs between action potentials in the pre- and post-synaptic neurons. The shorter the time between two consecutive spikes, the more change is induced in both LTP and LTD. However, for an ISI bigger than 80 ms, changes are no longer observed, as it is possible to see in fig. 2.2b, where the variation of synaptic change, according to the spike time interval, is represented for both LTP and LTD [15].

As far as memory goes, as previously mentioned, it is believed to occur due to plasticity, in particular two kinds of plasticity: short-term potentiation (STP) and long-term potentiation (LTP). STP relates to the strengthening of a particular connection, which quickly

returns to its initial state. LTP relates to the strengthening of a particular connection with repeated stimuli, that can possibly cause a permanent change in connection, taking much longer to return to its initial state (years even) [16].

2.2 Artificial Neural Networks

Artificial neural networks (ANNs) are an attempt of mimicking the biological, structural, and functional properties of the human nervous system [17]. They are expected to be able to learn and maintain that knowledge and "can be defined as a set of processing units, represented by artificial neurons, interlinked by a lot of interconnections (artificial synapses), implemented by vectors and matrices of synaptic weights" [18]. This means that the weight between two interconnected neurons is what determines the network's behaviour [19]. Over the past decades, leading research in computational models for this exact same objective have been carried out, with already great advances and results. However, most of these simulations and models are carried out in regular computers, with the von Neumann architecture, that are not able to fully scale the human brain without massive energy consumption and massive data consumption. Thus, the development of hardware capable of mimicking the relations of neurons and synapses of the brain is essential for the growth of ANNs [17].

This kind of technology can be significant in solving fundamental day-to-day issues in diverse areas such as science, engineering, economics, and medicine that cannot be solved with standard computers and be decisive in achieving ground-breaking developments in those areas. Some notorious applications of ANNs are in medical diagnosis [20], with cancer diagnosis being an important one, speech [21] and pattern [22] recognition, market segmentation [23], and so on.

2.3 Memristors

The concept of memristor, memory-resistor, was introduced in 1971 by Chua. It was introduced as the fourth basic circuit element, alongside the already known resistor, capacitor, and inductor. There are four fundamental variables in which the previous circuit elements are based upon: current i, voltage v, charge q, and magnetic flux ϕ. These fundamental variables can be arranged, two at time, in six different ways, being that each relates either a known law or the known relationship between variables in the three basic circuit

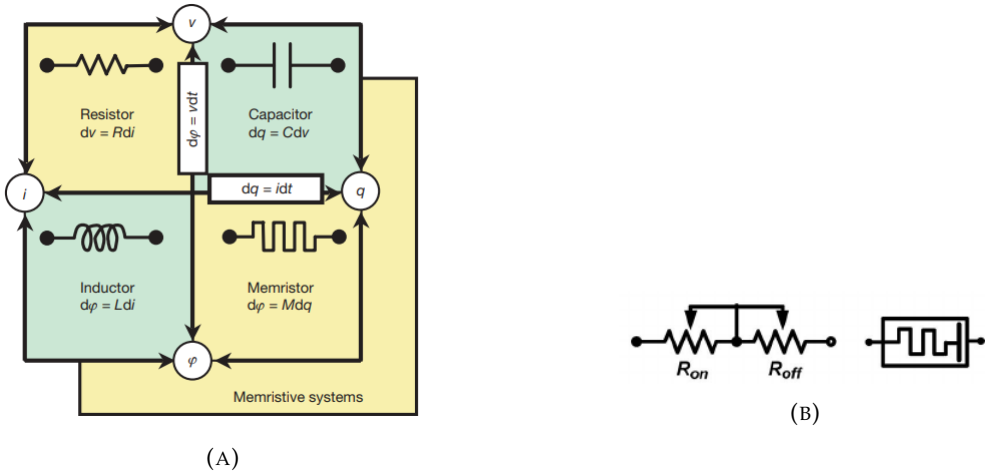

(A) (B)

FIGURE 2.3: (A) Scheme representing the four fundamental variables (q, ϕ, i, v) and their possible six combinations. Adapted from [25]. (B) Electrical memristor circuit (on the left, where R_{On} represents the minimum memristance and R_{Off} the maximum memristance) and electrical symbol (on the right, where the black bar represents the polarity: when current flows from the left to the right, memristance is decreased and vice-versa). Adapted from [26].

elements resistor, capacitor and inductor (eqs. 2.1-2.5). One combination is left missing, given rise to the memristor, that states a relation between flux and charge (eq. 2.6), where R, C, L, M, and t are, respectively, resistance, capacitance, inductance, memristance and time [24]. Memristance can be defined, then, as the variation of resistance according to the history of charge that has moved through the memristor. It is the non-linear relation of resistance with current and potential (see fig. 2.3).

$$Current : dq = I\,dt, \tag{2.1}$$

$$Faraday's\ law : d\phi = V\,dt, \tag{2.2}$$

$$Resistor : dV = R\,dI, \tag{2.3}$$

$$Capacitor : dq = C\,dV, \tag{2.4}$$

$$Inductor : d\phi = L\,dI, \tag{2.5}$$

$$Memristor : d\phi = M(q)\,dq. \tag{2.6}$$

After the memristor was theorized, it took several years to prove its existence (2008). This was achieved by the work of Strukov et al. [25]. A nano-device was built, with composition $Pt/TiO_2/Pt$, that showed, after a sinusoidal voltage was applied, a pinched-hysteretic I(V) loop, related to the movement of charged dopants, that came in accordance with the theory postulated before, proving its physical existence.

Following this breakthrough, memristors have become one of the most sought after topics of research, especially in regards to the post-complementary metal oxide semiconductor (CMOS) industry [27, 28].

2.3.1 Formal theory

The memristor can be defined in terms of the relation between current, charge, voltage, and flux. A current-controlled memristor has the form presented in eqs. 2.7 and 2.8, being that $M(q(t))$ has resistance dimensions, with $q(t)$ representing the flow of charge in the device. A voltage-controlled memristor is repesented by eqs. 2.9 and 2.10, being that $W(\phi(t))$ has units of conductance and $\phi(t)$ represents the magnetic flux in the system [29]. If there is no dependence with time, eq. 2.7 turns into Ohm's equation.

$$v(t) = M(q(t))i(t), \tag{2.7}$$

$$M(q) = d\phi(q)/dq, \tag{2.8}$$

$$i(t) = W(\phi(t))v(t), \tag{2.9}$$

$$W(\phi) = dq(\phi)/d\phi. \tag{2.10}$$

Expanding eqs. 2.7 and 2.9, one is left with eqs. 2.11 and 2.12.

$$v(t) = M\left(\int_{-\infty}^{t} i(t)dt\right) i(t), \tag{2.11}$$

$$i(t) = W\left(\int_{-\infty}^{t} v(t)dt\right) v(t). \tag{2.12}$$

These equations show that the value of memristance has a dependence with the history of current that moves through the device. This means that, when current moving through the device is stopped, it retains the last value of memristance until a new change, in the form of current again, is applied to it [29].

A few years after Chua proposed the concept of memristor, he proposed a new definition for memristors that included a larger spectrum of nonlinear dynamical systems called memristive systems [30], that were described by eqs. 2.13 and 2.14 (in regards to current-controlled memristive systems), where w can refer to a set of state variables [25].

$$v(t) = R(w, i, t)i(t) \tag{2.13}$$

$$\frac{dw}{dt} = f(w, i, t) \tag{2.14}$$

When a memristor is fed with a periodic signal, it presents a distinct pinched hysteresis loop in an I(V) characteristic curve, passing through the origin point, and limited to the first and third quadrants of the graph. Due to this behaviour, the memristor has the ability to memorize and remember its state. With high enough frequencies of the input signal, memristive systems tend to operate as a linear resistor and with low enough frequencies they tend to operate as a non-linear resistor (see fig. 2.4). This is due to the fact that for higher frequencies the state variable is not able to adjust in the amount of time it

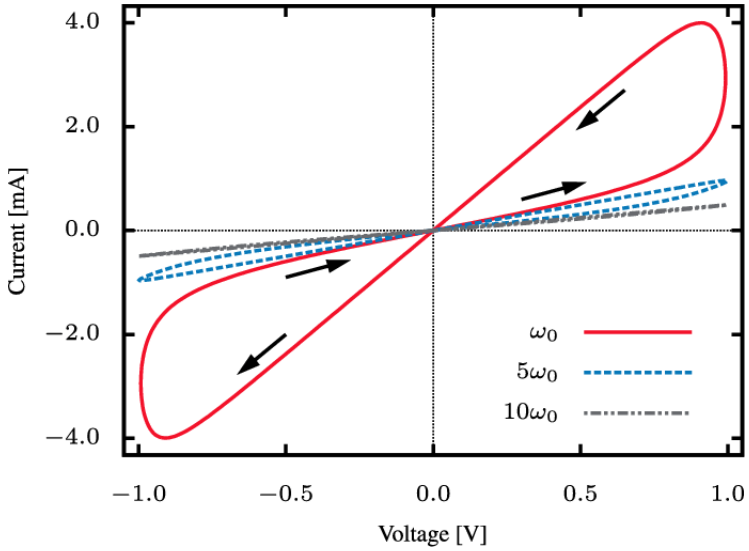

FIGURE 2.4: I(V) curves for different frequencies of input signal. It is possible to notice a collapse of the hysteresis as frequency increases up to ten times. Adapted from [32].

has, when compared to lower frequencies. Arising from all these characteristics, memristive systems have found several applications in which to be merged into such as resistive memories, soft computing, neurocomputing and more [29, 31].

2.3.2 Overview of existing devices

After decades since the theoretical memristor was proposed and not much more than 10 years from the first proof of its existence, memristors have suffered a boom in research. Because of that, nowadays there are already several types of memristors that can be differentiated by several parameters such as source of stimulation, mechanism of conduction, and materials used.

2.3.2.1 Resistive switching

These devices display resistive switching (RS), which is, by the name indication, a transition between different resistive states, a low resistive state (LRS) and a high resistive state (HRS), when an external bias applied [33]. When the device is switched from the HRS to the LRS, the set process (or write process), as it is called, occurs, and when the device is switched from the LRS to the HRS, the reset process (or erase process) occurs (see fig. 2.5a and 2.5b). Initially, some devices with filamentary switching may require an electroforming step as a first measure into having a work ready device. The RS phenomenon can be

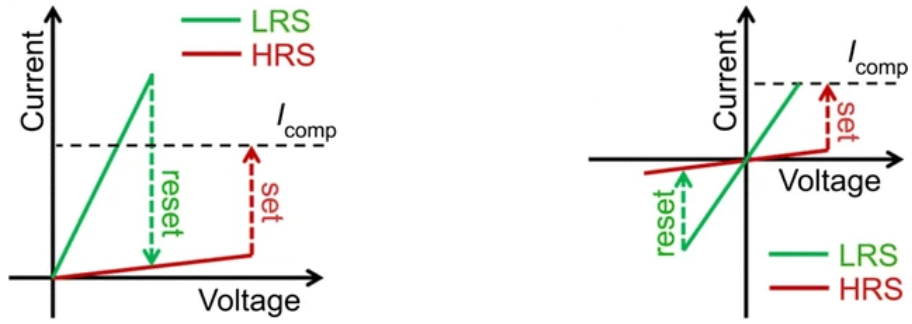

(A) (B)

FIGURE 2.5: I(V) curves for (A) unipolar RS and (B) bipolar RS. Adapted from [35]

classified as unipolar or bipolar. In unipolar RS, switching does not depend on the polarity of the applied signal but on its amplitude (see fig. 2.5a). In bipolar RS, the polarity of the input signal dictates the switching process (see fig. 2.5b) [34].

2.3.2.2 Source of stimulation

According to source of stimulation, memristors can be separated into five different groups: electrical stimulus, optical stimulus, magnetic stimulus, pressure stimulus and thermal stimulus. Electrical stimulus is the most common one, with an already considerable amount of literature on it. Besides electrical stimulus, optical stimulus is the second most developed one, especially due to its desirable characteristics such as a higher transmission speed and less likelihood of crosstalk and noise problems, with the downside of an issue in optoelectrical conversion [36]. A diagram that summarizes the different sources of stimulation is present in fig. 2.6.

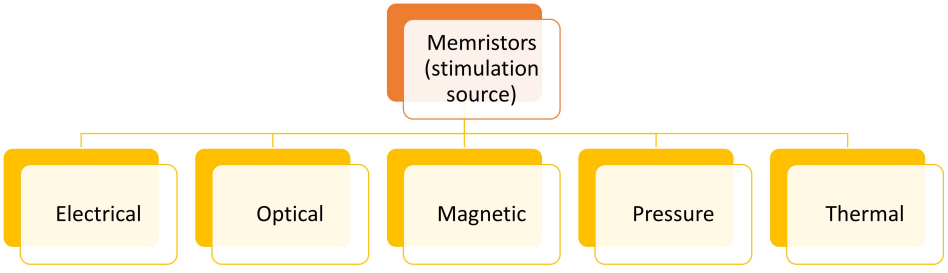

FIGURE 2.6: Diagram of the main types of memristors according to their stimulation source.

2.3.2.3 Switching mechanism

According to switching mechanism, memristors can be divided into four main categories: filament-based devices, charge trapping devices, phase change memory (PCM) based devices, and interfacial-based based devices.

Filament-based devices can be further divided into two categories: electrochemical metallization memory (ECM) and valence change memory (VCM). The first is related to the creation and destruction of a metal conductive element inside the active layer. When a bias is applied to the ECM device, the active electrode is partially ionized, providing cations to the switching layer. When in the active layer, those same cations can capture electrons to then be reduced to atoms, that combine and form the conductive filament, that will send the device into the low resistive state (LRS) (see fig. 2.7a, 2.7b, 2.7c and 2.7d). To put the device back into the high resistive state (HRS), the bias applied must be reversed, in order to rupture the formed filament (see fig. 2.7e). As for the second, VCM, its conductive mechanism relies on the transfer of vacancies in the active layer. This rearrangement of vacancies promotes the migration of electrons that rearrange in the form of conductive filament changing the state of the device in a similar manner as the ECM (see fig. 2.7f) [36].

Phase change memory-based devices rely on the change of the phase of the material in the switching layer, to change its resistance state. These kinds of devices use strong electrical pulses in order to heat and melt an insulator material, that is in contact with the switching layer, that is then rapidly quenched. This allows for the switching layer to change from a crystalline to an amorphous state, that leads to resistance change in the device. To reverse the state, an electrical adjusted pulse is applied in order to anneal and crystallize the layer (see fig. 2.7g) [36].

Interfacial-based devices have a switching mechanism that is rooted on the interfacial processes between electrodes and insulator material. It can happen for materials such as oxygen, where its distribution alongside the interface of the electrode can cause conductivity changes in the device. It can also happen in materials such as ferroelectrics (FE), ferromagnetics (FM) (see fig. 2.7h) and semiconductors [36, 37].

Finally, for charge trapping devices the switching mechanism takes place due to the charge transition between a charge trapping layer and a channel or switching layer. What happens is that when charge is passed on from the charge trapping layer of the device to its channel, the structure of the switching layer changes and becomes conductive. This

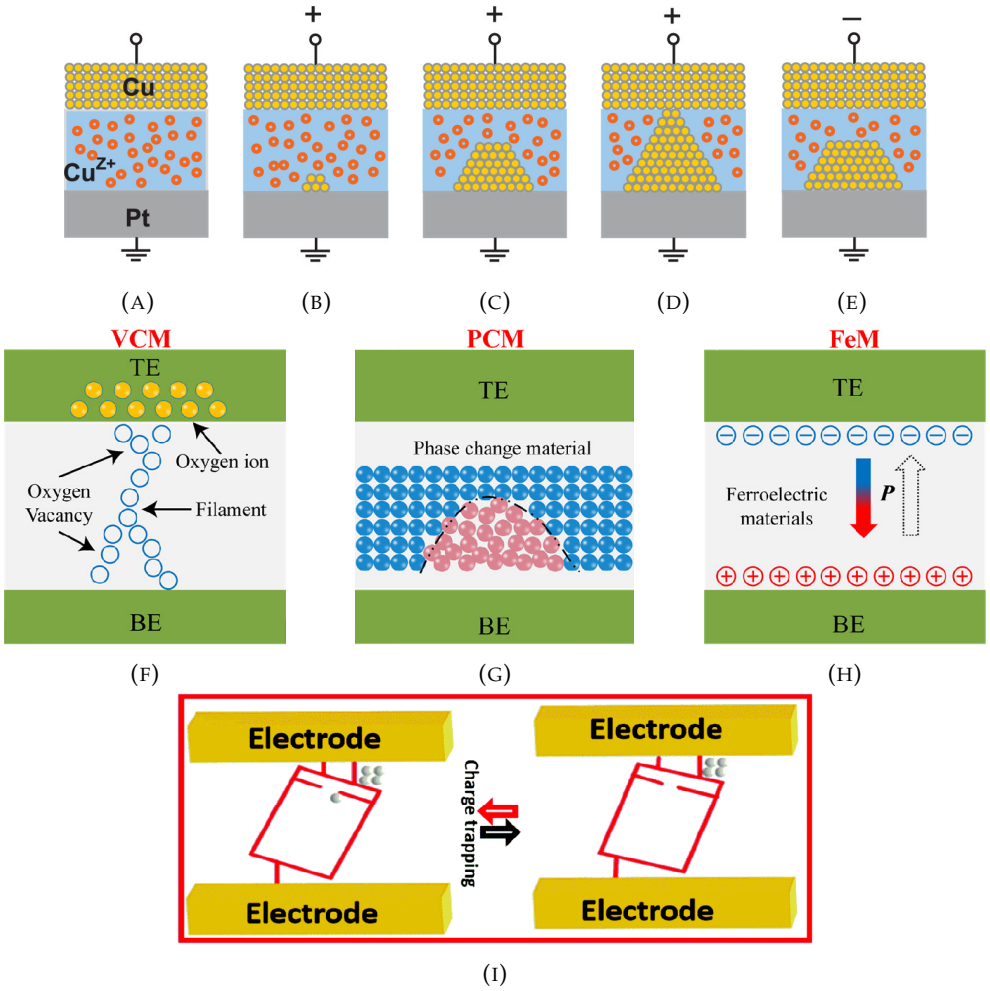

FIGURE 2.7: (A) - (E) Process of filament formation and destruction in electrochemical metallization memory-based devices. The example depicted has a stack configuration of Cu/chalcogenide/Pt. Adapted from [38]. Scheme of the switch mechanism for (F) valence change memory-based devices, (G) phase change memory-based devices and (H) interfacial-based devices composed of ferromagnetic (and ferroelectric) materials. Adapted from [39]. (I) Switching mechanism for charge trapping-based devices. Adapted from [40].

kind of devices can be further divided into two categories: interference-based and floating gate (FG) systems . What differentiates them both is the fact that in the interference-based one, the charge trapping layer and the channel are in direct contact with each other, while for the floating gate one, there is a floating gate separating the charge trapping layer and the channel. In the first, the electrons and holes will move directly through the interface between layers while in the second, quantum tunnelling and thermal emission are the cause for the movement of electrons and holes from the charge trapping layer towards the floating gate, that can trap them or not, manipulating the channel conductance in that manner (see fig. 2.7i) [36].

A diagram that summarises the information above is present in fig. 2.8.

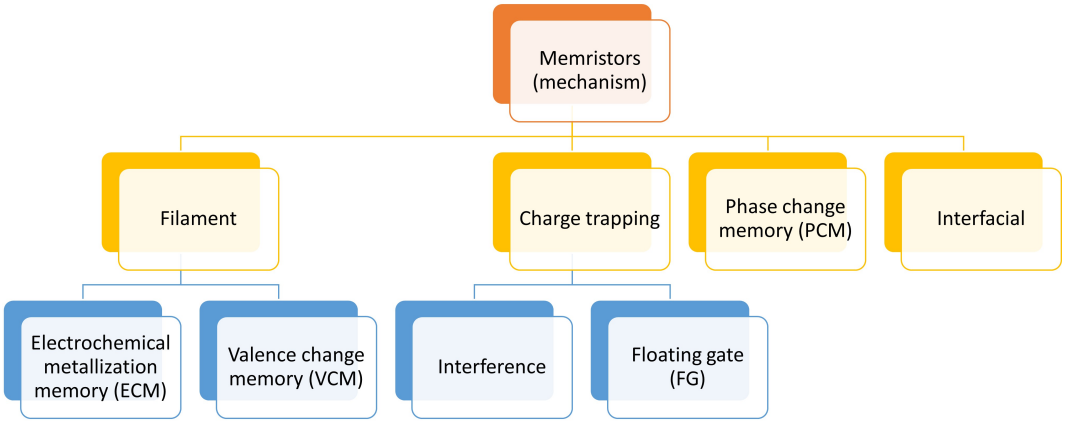

FIGURE 2.8: Diagram of the main types of memristors according to their switching mechanism.

2.3.2.4 Volatility

Memristors can be separated into two different groups when it comes to their volatility properties: volatile or non-volatile. The difference between these two is that the volatile device presents spontaneous decay of its conductance in the LRS, while the non-volatile one can hold its conductance, no matter the state, for longer periods of time [41]. Both kinds of devices present different yet useful characteristics for the mimicking of synaptic and neuromorphic characteristics in hardware, namely, short-term adaptation for volatile devices and long-term adaptation for non-volatile devices [42]. Volatile memristors can be used for access devices, neuromorphic computers, hardware security applications and others.

2.3.2.5 Short-term memory and long-term memory

As the name indicates, memristor, memory resistor, presents memory properties. It is believed that memory, in the human brain, is a result of two kinds of plasticities: short-term plasticity and long-term plasticity. Plasticity is known to be the ability to alter neural circuit functions and ramifications due to the experience of an activity. In order words, it is the altering of strength or efficacy of synaptic transmission in synapses, due to a stimulation [43]. Short-term memory (the circuit equivalent of short-term plasticity) is attained with stimulation that presents low repetition rates, which leads to the improvement in synaptic connection that rapidly decays to its initial state. Long-term plasticity (the circuit equivalent of long-term plasticity), however, is attained by stimulation with high repetition rates that cause permanent change in connections between neurons, that

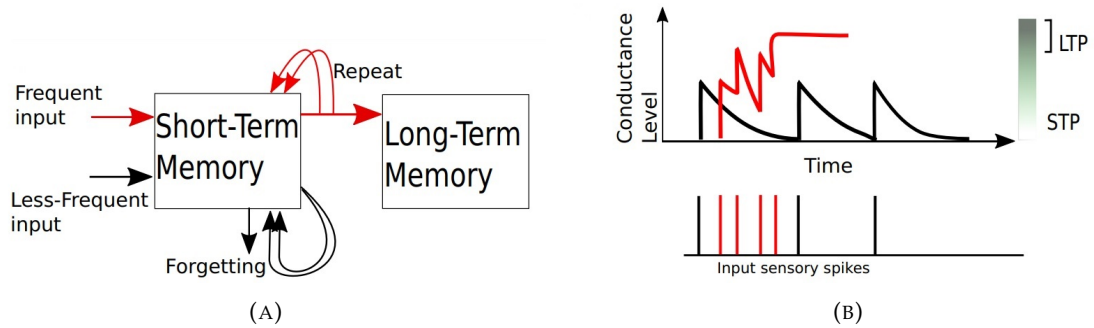

FIGURE 2.9: (A) Diagram of the rehearsal process that leads to the transition from STM to LTM. (B) Representation of the conductance level of STM and LTM, as a function of time between the input spikes. Adapted from [46].

enable the memristor to hold its state for long period of times, besides natural forgetting, without the need of additional stimuli [44]. The transition between short-term memory (STM) and long-term memory (LTM) is possible, and can be achieved through repeated stimulation, as Chang *et al.* proved in their work [45]. They created a device based on the movement of oxygen vacancies inside a WO_x film that presented the transition between STM and LTM through what is called rehearsal (repetitions; see fig. 2.9a and 2.9b) and very complex molecular mechanisms and structural changes at various levels. They saw significant improvement in retention times from STM to LTM and a high dependence on the time interval of the stimuli.

2.3.2.6 Class of materials

The main materials used for the construction of **solid-state** memristor devices can be divided into seven main groups, namely metal-oxide, chalcogenide, carbon-based, natural biomaterials, synthetic polymer, halide perovskites and nanoparticles (see fig. 2.10).

Metal oxides are extremely important materials when it comes to technology because they present very desirable optical and electrical properties, stability, and adaptability. They can be divided in two main groups, binary oxides, and oxide junctions. Binary oxides, such as HfO_x, TaO_x, WO_x and ZnO_x, are widely used due to their properties such as low power consumption, high data transfer speed and scalability. In recent years, oxide heterojunctions in memristors have been getting more predominance, with the use of two different dielectric materials in order to control parameters like tunnelling and ion diffusion rate, that relate directly to the resistance of the device. Some examples of materials used for this purpose are GaO_x, SiO_x, $PbZr_{0.2}Ti_{0.8}O_3$ and $SrRuO_3$. However, this kind of memristors has several disadvantages as well, such as very likely uncontrollable

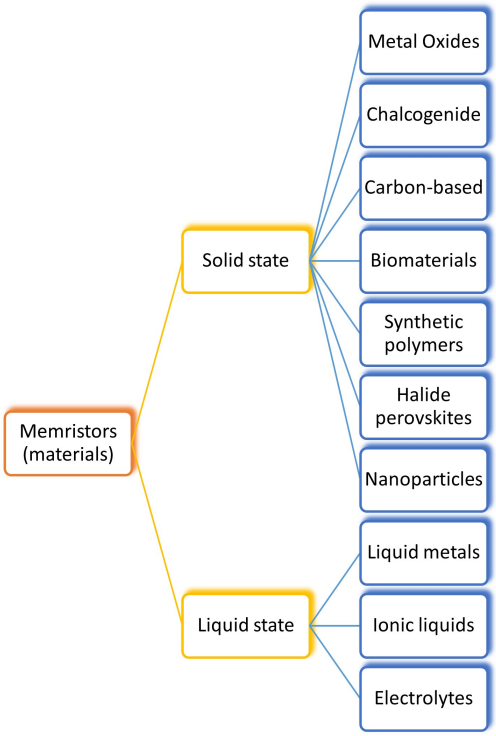

FIGURE 2.10: Diagram of the main types of memristors according to the materials they are composed of.

filament formation and ion migration, unreliability, some degree of toxicity and high cost, which means they cannot emulate every property and function of the brain and are not very environmentally friendly [47–50].

Chalcogenides are materials that present one or more chalcogen anions (e.g., S, Se, Te) and one or more electropositive element (e.g., Ag, Cu). This class of materials presents high ion mobility, which promotes very good filament formation and conduction for electrochemical metallization-like devices and high R_{Off}/R_{On} ratios and it also presents structural characteristics that promote phase-change-like devices (e.g., Ag_2Se, Cu_2Se, Ag_2S) when temperature variation is applied to them. However, disadvantages like high variability in RS for filament-based devices is present, as well as high cost of fabrication due to the use of lithography processes [48].

As far as carbon-based materials go, they can have several forms, such as amorphous carbon, graphene, reduced graphene oxide [51], carbon nanotubes, fullerene, carbon-based allotropes, and carbon-based derivatives. They present very good thermal, electrical, chemical, and physical properties, provide, overall, very good RS behaviour and are usually low cost, nontoxic, biocompatible, tuneable, and flexible. However, they lack in endurance and retention properties when compared to metal-oxides [47, 48].

Biopolymers are a class of materials that can be divided in proteins, DNA/RNA, and carbohydrates. They are eco-friendly, flexible, biocompatible, and easily degradable materials (biodegradable), which makes them extremely desirable for the development of green electronics. They present complex structures, which makes them the hosts of several different switching mechanisms. Some materials such as silk, keratin, egg albumen (proteins), DNA, chitosan, dead leaves, and glucose (carbohydrates) were tested with RS mechanism proven to be present. However, these materials' sensitivity towards the environment, such as humidity or temperature, can affect their stability. Furthermore, they lack on large-scale reliability and repeatability [48].

Synthetic polymer materials can take several shapes, forms and consistencies. Their microstructure can be divided into linear macromolecules, branched macromolecules, semicrystalline structures, slightly cross-linked, and highly cross-linked polymers. They present promising qualities such as their structure flexibility, solution processability, cheap cost, versatility, and, overall, great RS behaviour. However, the complexity of molecule structure these materials present leads to an unclear understanding of switching mechanisms, and also, due to the great size of molecule chains, scalability of the device is an issue [48, 52].

Finally, the latest emerging materials to be used and researched for the purpose of artificial synapses are halide perovskites and nanoparticles. Halide perovskites have desirable properties such as rapid ion migration, tuneable bandgap, solution process availability and long charge-carrier diffusion length. They can also be fabricated in both 3D and 2D. However, they have lead in their composition, that is highly toxic and bad for the environment. As far as nanoparticles, they present, especially silver nanoparticles, qualities that are able to enhance properties of the material in which they are inserted. They can lower power consumption and switching voltages, can better the formation of silver filaments and make it more orderly [47].

2.4 Liquid-based memristor devices

When it comes to **liquid-based** memristor devices, they have taken a more predominant position in research in the last few years [53]. Solid-state devices, even though they present many good qualities, ultimately, have limited ion diffusion when compared to the real ionic movement in the synapses [54]. So, with that in mind, liquids have been pointed as one of the materials that can fill that role. Liquids and solutions present qualities such

as high ion mobility, easy production, low cost, flexibility, adaptability and possible biocompatibility, that make them truly promising for memristor applications [6, 54–57]. The main types of liquids present in literature, at the moment, for memristor applications are liquid metals, ionic liquids (ILs) and electrolytes (see fig. 2.10) [56].

Liquid metals, as the name indicates, are metals (or metal alloys) that are in liquid form in room or near room temperature. Some examples of liquid metals and alloys are mercury, gallium, caesium and eutectic gallium-indium [58]. The literature on the application of liquid metals in memristor devices is very short and composed, mainly, of their use for liquid electrodes. M. Zaheer *et al.* [59] built a device with a EGaIn (eutectic gallium-indium) liquid metal alloy top electrode, a polymer insulator layer and a ITO thin film (indium tin oxide) bottom electrode (see fig. 2.11a). This liquid metal top electrode enabled the use of several different polymer insulator layers such as PDMS, PVDF and PMMA, because it induced RS behaviour that otherwise would be difficult to obtain with solid metal electrodes and these same polymer layers. Liquid metals have the ability to form conductive filaments in organic materials in an easier way than most solid metals (fig. 2.11b). Furthermore, besides RS, the built device showed low switching voltage, high resistance ratio, good endurance and data retention characteristics, being a promising candidate for the use in wearable and soft electronics. Another example of a device that used liquid metals as their electrodes is the one by H. Koo *et al.* [55]. They used the same liquid metal as the previous example, EGaIn, to build a device composed of two liquid metal electrodes separated by two thin layers of hydrogel doped with polyelectrolytes (see fig. 2.11c). The respective liquid alloy is quite popular due to its low viscosity, high surface tension, and high thermal and electrical conductivity (being the latter its most important property) [58]. The device also showed RS with reliable long-term behaviour (see fig. 2.11e). After a single device was produced, a crossbar array of devices was created (see fig. 2.11d), that was tested and showed that each node was able be operated independently without crosstalk phenomena. Since the hydrogels were biocompatible and the conduction mechanism was ionic, this device has great capabilities to be used in bioelectronic systems and brain-like structures.

Ionic liquids (ILs) can be defined as salts in the liquid state that are solely made of ions [62], such as compounds based on the 1-ethyl-3-methylimidazolium (EMIM) cation. They are known for enhancing electrical and ionic properties of several devices. As far as their application on memristors go, ILs have already been widely studied in literature.

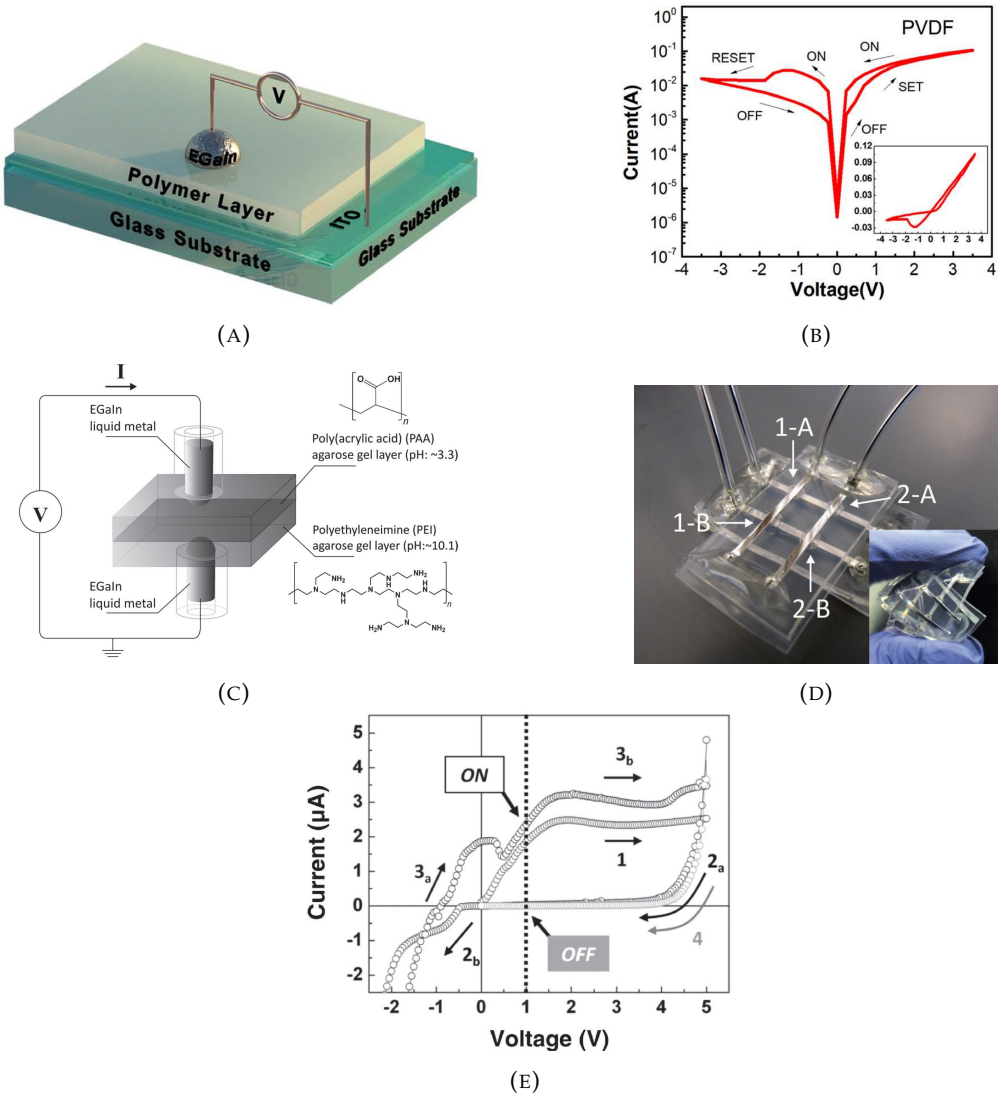

FIGURE 2.11: (A) Memristor device composed of a EGaIn liquid metal electrode, polymer layer and ITO bottom electrode, and its respective (B) RS cycle, for a polymer layer composed of PVDF. Adapted from [59]. (C) Memristor device composed of two EGaIn liquid metal encapsulated electrodes and two polymer active layers in between and (D) crossbar array of the same single devices. (E) I(V) curves retrieved from the device, at a sweep rate of 0.04 V/s. The dotted line represents the reading bias. Adapted from [55].

ILs have been used, generally, in mixture with other solutions or materials (e.g., polymers and gels), in order to enhance the ionic properties of the devices. An example of the use of ILs in mixture with other solvents or solutions is the one by M. Chougale *et al.* [60]. They built a two-terminal ionic liquid-based device composed of two copper electrodes and aqueous ionic liquids 1-butyl3-methylimidazolium bromide [Bmin][Br] and 1-ethyl3-methylimidazolium bromide [Emin][Br], encapsulated in a sample tube (see fig. 2.12a). This device presented bipolar RS, frequency-dependent-limiting linear characteristics and analogue memory characteristics (see fig. 2.12b). All of this was achieved with

very low switching voltage (1 V; solid state memristors usually work under higher voltages), stable RS and desirable memory window. In addition, a work by K. Rajan *et al.* [61] utilized BMIM-TFSI IL to test its effect on a device. This device was composed of two gold electrodes with a spin coated polymer nanocomposite matrix separating them both. The matrix was made of the polymer Poly(vinylidene fluoride-hexafluoropropylene) (PVDF-HFP) (used because it presents high dielectric constant, good mechanical strength and chemical stability), silver nitrate ($AgNO_3$; electrolyte) and the said IL (to improve the ionic transport in the polymer matrix; see fig. 2.12c). To clearly tell apart what role the ionic liquid had in the device's properties, the researchers tested the exact same device with and without the IL in the polymer matrix. For the device without the IL, high voltage operation was necessary, and volatile behaviour was present. Once the room-temperature ionic liquid was added into the mix, there was a switch in the memory volatility of the device, from volatile to non-volatile, and a decrease in the set voltage for the RS, that was attributed to the changes the IL caused in the device such as better ionic mobility, reduced viscosity and reduced crystallinity of the polymer matrix (see fig. 2.12d). The mechanism of conduction can be attributed to the formation and dissolution of a silver

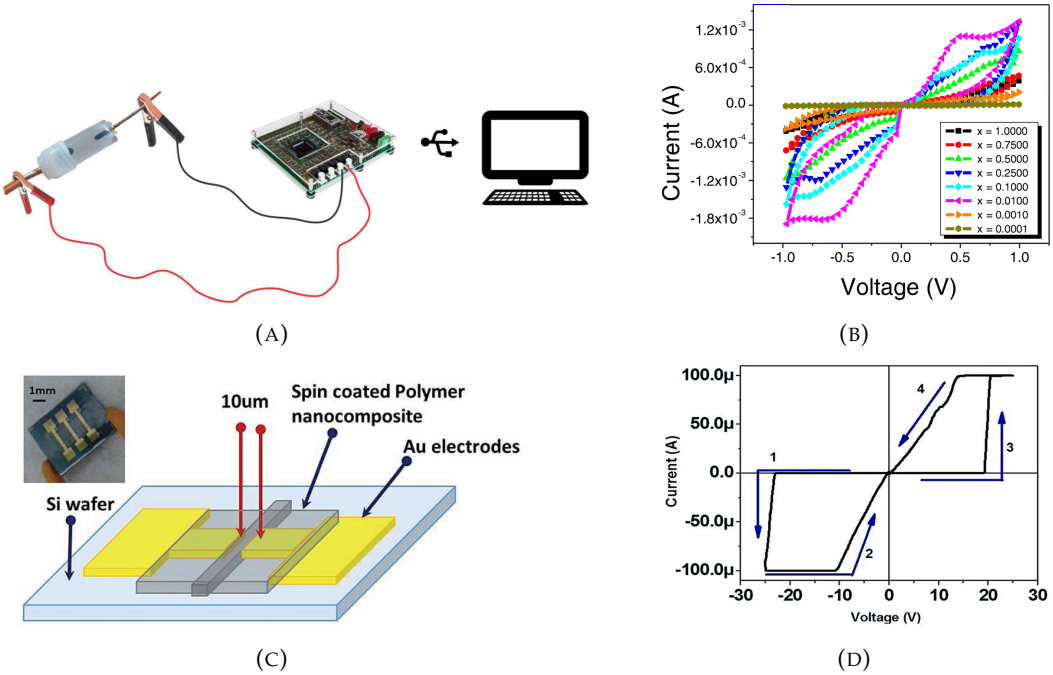

FIGURE 2.12: (A) Memristor device composed of two copper electrodes and a encapsulated ionic liquid by the name of [Bmin][Br] or [Emin][Br]. (B) RS obtained from the device, for several IL molar fractions and an input signal frequency of 0.80 Hz. Adapted from [60]. (C) Memristor device composed of two gold electrodes with a spin coated polymer nanocomposite on top of it made out of PVDF-HFP, $AgNO_3$ and ionic liquid BMIM TFSI, and its (D) attained RS curve. Adapted from [61].

filament between electrodes. Good retention, endurance and high resistance ratio were also observed.

Finally, electrolytes are defined as compounds that, upon dissolution in a solvent, such as water, produce ions that can conduct electric current through their movement in a medium [63], being sodium chloride, NaCl, the most known. Some other examples include silver nitrate, copper sulphate and others. In the literature, they have been used either in their sole aqueous form in the active layer, or mixed with other materials, usually polymers, gels or hydrogels. An example of the use of successful liquid electrolyte solutions is the work of D. Kim *et al.* [54], that built a two-terminal device composed of electrodes, Na_2TP, Nafion, and a NaCl solution (see fig. 2.13a) capable of emulating biological synapses, in which the conductance of the device is dictated by the concentration of sodium atoms in the solution and the concentration of sodium atoms trapped in the Na_2TP layer. This device showed synaptic characteristics such as potentiation, depression, short-term potentiation, long-term potentiation and spike time-depending plasticity (see fig. 2.13b). Another example of the same authors [6] is of a silver-based device (see fig. 2.13c), similar to the one present in this dissertation, composed of a silver bottom electrode, a silver nitrate solution and a gold inert top electrode, that presented a filamentary conduction mechanism and synaptic properties such as RS behaviour, endurance, data retention, potentiation, depression, paired-pulse facilitation and excitatory post-synaptic current, all with very low power consumption (< 0.1 V; see fig. 2.13d). As far as the use of electrolytes in mixtures with other materials, one can recall the work by K. Rajan *et al.* [61], already previously mentioned, where a polymer matrix active layer composed of PVDF-HFP, an ionic liquid and an electrolyte, $AgNO_3$ was built and spin coated onto the two gold electrodes, presenting RS properties that were explained by the diffusion of silver atoms in the polymer matrix when an electric field was being applied.

Nevertheless, fully solution-based devices present some disadvantages, one of the main ones being the fact that they are not reliable for long periods of time, when operated in a non-controlled environment, present difficulty in reproducibility, sustaining its shape or not leaking. Because of that, and as the examples previously mentioned prove, the scientific community has turned their ways into another category of materials, soft materials, materials that are easily deformed, such as polymers, biopolymers, gels and hydrogels, where solutions and liquids can be incorporated and that usually rely on simple and less cost worthy fabrication techniques than for solid materials. They have been

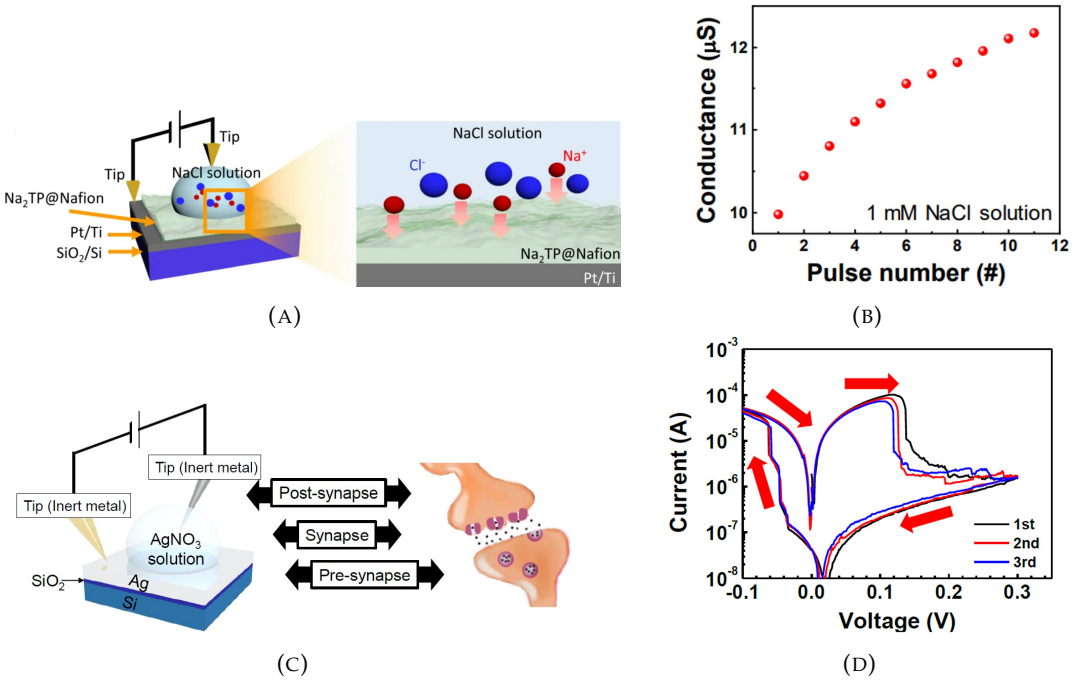

FIGURE 2.13: (A) Memristor device composed of a NaCl solution, Na_2TP@Nafion reservoir layer and electrodes, in which the conduction mechanism is determined by the movement of Na^+ ions in the solution and through the reservoir layer. (B) Potentiation behaviour acquired from the device, for a NaCl solution concentration of 1 mM. Adapted from [54]. (C) Memristor device composed of a silver nitrate solution, silver bottom electrode and gold tip top electrode, in which the conduction mechanism is determined by the creation and dissolution of a silver filament in the solution when an electric field is being applied. (D) RS cycle obtained for the solution concentration of 0.1 mol/l. Adapted from [6].

rising in popularity for the use in soft electronics for the most diverse applications, one being, for example, for healthcare purposes such as skin implantations [57, 64].

2.4.1 Copper(II) sulphate pentahydrate

Copper(II) sulphate pentahydrate, also described as copper(II) sulphate pentahydrate or cupric sulphate, is an inorganic salt that presents high solubility in water. Its crystalline granules or powder present a bright blue colour (see fig. 2.14), containing, as the name indicates, 5 molecules of water for each molecule of copper sulphate. The molecular formula is $CuSO_4.5H_2O$, the molecular weight is 249.68 g/mol, the melting point is 110°C and it turns white when dehydrated. It is considered an electrolyte because, when dissolved in water, its molecules split up into positive and negative ions, that move freely in the solution. Copper sulphate is mainly used in agriculture, as an algaecide, pesticide, bactericide, herbicide and fertilizer. However, it has also been used as a reagent in analytic chemistry, electrolyte for batteries, electroplating baths, and in the medical field, with

several veterinary uses. Since copper is present in this salt, one must know, as well, that since it is a noble metal, its properties include high thermal and electrical conductivity, low corrosion, alloying ability, and malleability [65].

2.4.2 Deep eutectic solvent (DES)

Deep eutectic solvents (DESs) are a class of solvents that presents similar characteristics as those of ILs even though their chemistry is different. DESs are composed of a eutectic mixture of Lewis or Brønsted acids and bases that contain plenty of cationic and/or anionic species (ILs are composed of one type of discrete anion or cation). Their formation is attributed, for the most part, to the complexation of quaternary ammonium salt (for example, choline chloride) with either a metal salt or a hydrogen bond donor. The name arises from the fact the liquids are close to the eutectic composition of the mixtures, as in the lowest melting point achieved for the molar ratio of the components present. DESs composed of choline chloride and hydrogen bonds have been particularly studied, due to their ability to solvate most of transition metal species. Usually, DESs present high viscosity and high ionic conductivity, comparable to those of ionic liquids. Their electrical conductivity properties are shown to be tuneable and dependent on factors such as temperature and molar ratio of species. DESs have advantages such as simplicity of preparation, low cost, passiveness in water and biodegradability. Since many hydrogen bond donors can be used, namely amides, carboxylic acids, and alcohols, they are also very adaptable, with each one having different physical properties that can be used for distinct purposes. It has also been shown that some transition metals can be integrated in ambient temperature eutectics and that they are able to ionize.

FIGURE 2.14: $CuSO_4.5H_2O$ powder.

Some of the applications known to use these solvents are the processing of metal oxides, the removal of glycerol from biodiesel, and the synthesis of derivatives of cellulose [62, 66–68]. More specifically, DESs have recently been studied for the use, as electrolytes, in green energy storage applications [69]. Up until now, no known research dedicated to the use of DESs in memristors has been performed, being the present work a first contact.

Chapter 3

Experimental Details

3.1 Copper(II) sulphate pentahydrate preparation

In order to study the effect of different solution concentrations on the devices' working parameters, three solutions of copper sulphate were produced: 0.1, 0.5 and 1 mol/l. In order to do that, pre-calculated amounts of copper(II) sulphate pentahydrate powder were mixed with deionized water and later stored in 2 mL eppendorfs. The copper(II) sulphate pentahydrate is a blue powder by Fluka with a purity percentage of $\geq$99.0%. The quantities of powder and water were weighted in the Kern ABT100-5M high precision scale.

3.2 Choline Chloride + glycerol (DES) preparation

The choline chloride + glycerol preparation was performed as mentioned by A. Brandão *et al.* [70]. The choline chloride was dried overnight, in an oven, at 60°C, prior to use. The mixture of the two components was performed by stirring them at 60°C, in the molar ratio of 1 ChCl: 2 G, until a homogeneous, transparent liquid was formed. The choline chloride used was by Sigma Aldrich at 99% purity and the glycerol used (it was used as received) was also by Sigma Aldrich at >99%.

3.3 Mixture of copper(II) sulphate pentahydrate with the deep eutectic solvent

Eutectic liquids (or DES) are known to enhance conductivity of electrolytes. Therefore, a mixture of the electrolyte copper sulphate with the eutectic liquid was fabricated and later

studied and characterised. To achieve a homogenous mixture of these two compounds, initially, the eutectic liquid was placed in a beaker on top of a hotplate, at 60°C, for 30 min in order to evaporate any possible water absorbed and to lower its viscosity. While this process was taking place, a pre-calculated amount of powder of the copper(II) sulphate pentahydrate was weighted, in order to achieve a desired concentration of 0.5 mol/l of the same reagent for a volume of the eutectic liquid of 20 mL, and was grinded in order to minimize the size of the crystals for better and faster dissolution when mixed with the eutectic liquid. After the 30 min of sole heating of the DES, a magnet was placed in the solution and the magnetic stirrer function was activated at 900 rpm. The powder of copper sulphate was added to the solution and after about 30 min, with the heating always working at the mentioned temperature, it was fully dissolved. It was then stored in a plastic container.

The quantity of powder needed was weighted in the Kern ABT100-5M high precision scale and the volume of choline chloride + glycerol needed was measured in a graduated flask. The copper(II) sulphate pentahydrate powder used was the same as mentioned in the previous section.

3.4 Gelling of the copper(II) sulphate pentahydrate mixture with a deep eutectic solvent

For the gelling of the copper(II) sulphate pentahydrate mixture with a choline chloride based deep eutectic solvent (DES), the method produced by S. Hong *et al.* [66] was mostly used. The materials needed for this step were the copper(II) sulphate, DES (choline chloride and glycerol mixed with the $CuSO_4.5H_2O$), ammonium peroxy-disulphate (APS), acrylamide (AM), methylene-bisacrylamide (MBA), and cellulose. Initially, the APS was dissolved in the DES with a 3:100 mass ratio, in order to facilitate its dissolution and set off polymerization in the next steps. Next, cellulose, with a 4 wt.% in regard to the weight of the AM, was mixed with the DES (20 g) for 2 hours at 100°C, after which it was left to cool at room temperature. Following that, AM and MBA were added to the DES, with a mass of 3 g and 0.03 g, respectively, and were stirred for 30 min at 40°C. The resulting mixture was then cooled till 25°C and 1.2 g of APS-DES were added to it, remaining in a stirrer, for 5 min. Finally, the final mixture was added into a mould and was dried for 24 hours at 60°C to complete the polymerization process.

3.5 Measuring setup

Firstly, to study the dependence of the height of the top electrode immersed in the liquid, a micrometre screw was attached to a metal base, that enabled the control of the electrode position.

Secondly, to study the implication of temperature in the device, a Peltier module TEC1-12715 was attached to the base of the setup, in order to heat or cool the bottom electrode layed on top of it.

The top electrode was varied between two platinum wires of diameter 0.1 and 1.0 mm, a copper and a silver wire of diameter 1.0 mm, and a probe gold tip with diameter 2.4 μm. The bottom electrode was a copper sheet with 0.4 mm thickness that was connected to the setup via a gold POGO tip, and that was sanded before any measurement in order to clean any possible impurities.

To measure properties such as RS, endurance, and data retention, an existing LabView routine was used, initially. For that, the top electrode and bottom electrode were connected to a Keithley 2400-C SourceMeter, which both applied the potential to the device and read the current response. Later, a device called ArC ONE, which allowed for a better control of pulse width, achieving lower times than the SourceMeter, was also used. A UniVolt DC power supply, model DT305DS, was used to control the Peltier cell and a thermocouple was used to record its temperature. This thermocouple was in contact with the Peltier by a silver paste, for better conduction, and connected to a PicoLog, model Pico TC-08 USB Thermocouple Data Logger, that was able to show the temperature, in real time, in a computer.

A representation of the experimental setup is shown in fig. 3.1, and the real setup used is shown in fig. 3.2.

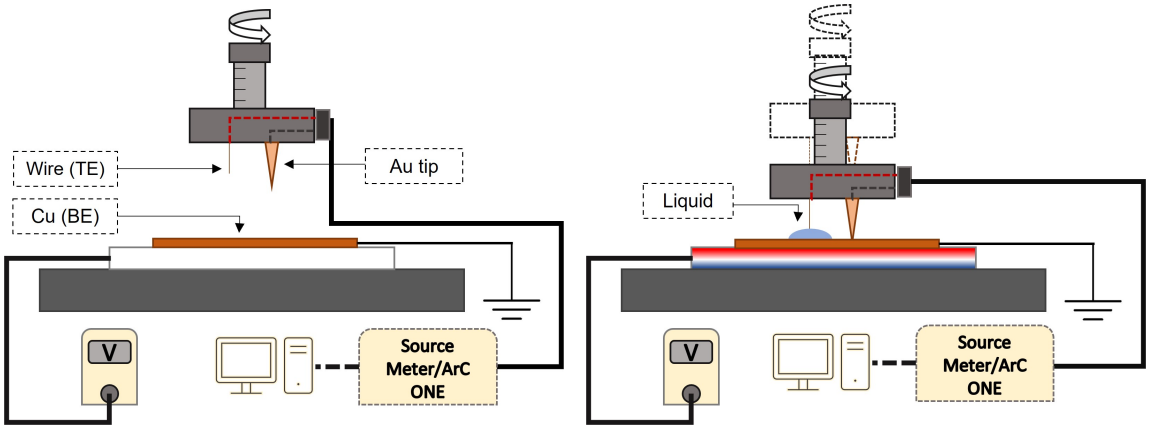

(A) (B)

FIGURE 3.1: Scheme of the experimental setup used to characterise the devices, (A) before and (B) during measuring operation. The setup is composed of a micrometre screw that moves a platform in which an electrode wire and a gold POGO retractable tip are attached, a copper sheet (bottom electrode), the liquid that acts as the active layer in the memristor, a Peltier module connected to a power source (to heat or cool the system), a SourceMeter or ArC ONE device (to apply signals defined by the user in the computer, and read the system's response) and a computer. In order to perform measurements, the top electrode must be in contact with the liquid, the liquid must be on top of the bottom electrode, and the gold POGO tip must be in contact with the bottom electrode, also. The POGO tip shall be connected to the SourceMeter or ArC ONE has the ground terminal, and the top electrode has the positive terminal.

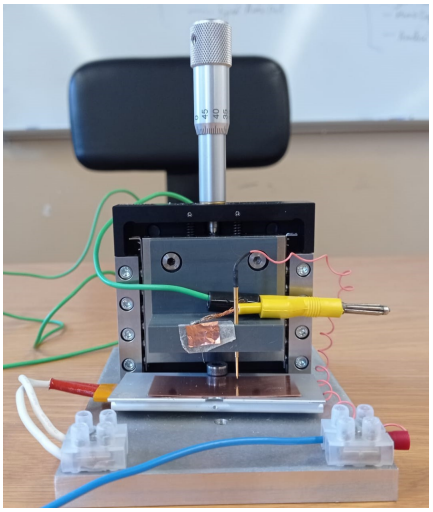

FIGURE 3.2: Experimental setup developed.

3.6 Description of the types of measurements performed

3.6.1 Resistive switching

For the RS measurements, ramps of potential were applied to the device, in order to set it and reset it. The set process of the device corresponded to the negative values of potential and the reset to the positive values of potential, with the bottom electrode grounded. The ramps start at zero value, move towards the negative potential, return to zero, move towards the positive potential and return, again, to the zero potential (0 V $\rightarrow$ -V $\rightarrow$ 0 V $\rightarrow$ +V $\rightarrow$ 0 V).

The default conditions were a solution concentration of 0.5 M, a distance between electrodes of 1 mm, platinum with 0.1 mm in diameter as top electrode and room temperature. The exceptions are for the sections in which a given parameter is being studied, keeping all other at default values.

For the copper(II) sulphate pentahydrate solution, a Keithley 2400 SourceMeter connected to a Labview routine was used. The pulse parameters have a width of about 200 ms, the lowest achieved by the device, and a step voltage of 0.01 V. The range of applied voltage used was [-300, 300] mV (the exception being for when this parameter was studied), and a current compliance of 2 mA was defined.

As for the copper(II) sulphate pentahydrate mix with the DES, the platform ArC ONE from ArC Instruments was used at a step voltage of 0.01 V, being that the width and amplitude parameters were object to study. When the gelling took place, pulse parameters remained the same, except for the applied potential, that was, once again, object to a study. Current compliance was not adopted in this case.

3.6.2 Retention and endurance

As for the endurance measurements, two types of methods were used: individually retrieving the On and Off resistances of several consecutive applied voltage sweep cycles and the pulsed method. The first one was used solely in the study of endurance for the three concentrations of the copper(II) sulphate pentahydrate solution, and the last one was used for the verification of endurance in the copper(II) sulphate pentahydrate solution, for the concentration of 0.5 M, the copper(II) sulphate pentahydrate mix with the DES and the study of endurance of the gel. The first method used a developed Python

routine, where, for each cycle , the On and Off current states were registered, at a reading voltage of either 50 or 20 mV, and plotted in order to assess the behaviour of current with each new cycle. The second method relied on the application of a negative pulse that could transit the device to the low resistive state and on the application of a positive pulse that could transit the device to the high resistive state, consecutively, for as long as possible. For that, a pulse study was performed and for the copper(II) sulphate solution, the pulses were of -100 and 100 mV with pulse width of 100 ms and interpulse width of 1 ms, for the copper(II) sulphate mix with the DES, the pulses were of -200 mV and 90 mV with pulse width of 10 ms and interpulse of 1 ms and, for the gel, the pulses were of -1 V and 90 mV, with pulse width of 10 ms and interpulse of 1 ms.

For the data retention measurements, similar methods were used, where the device was placed in either the On or Off state by a half or a full RS cycle using the SourceMeter or ArC ONE instruments, and the evolution of current over time was registered by the same equipment, with a small reading pulse of 20 mV.

3.6.3 Neuromorphic properties

To achieve potentiation or depression, the device was put under a series of consecutive positive and negative pulses, and its conductance was then retrieved and plotted in function of the number of applied pulses or cycles. The default number of consecutive pulses was 10, except for a few cases where 30 was tested. For each type of solution, a pulse study was performed, and the higher performing parameters used were: for the copper(II) sulphate solution - pulses of -60 and 90 mV with 100 ms pulse width and 1 ms interpulse width; for the copper(II) sulphate mix with the DES – -200 and 90 mV, 10 ms pulse width and 1 ms interpulse; and, finally, for the gel – -1 V and 90 mV, with 10 ms pulse width and 1 ms interpulse. Since the ArC ONE returns the values as resistance, these were inverted to give conductance.

Chapter 4

Device Characterisation

4.1 Copper(II) sulphate pentahydrate solution

One of the key properties of synapse-like devices such as memristors is the existence of dynamic RS, as previously mentioned. Thus, a first step in the device characterisation was the verification of the existence of this property, its type and mechanism, and how it varies when parameters like applied potential, solution concentration, temperature, type of inert electrode and height of top electrode are changed.

4.1.1 Determination of the type and mechanism of switching

A voltage sweep was performed, with negative and positive potentials for a grounded bottom electrode, with results seen in fig. 4.1a. The type of switching that the devices present is bipolar switching. This means that the polarity of the input voltage is what determines the switching of the device, from HRS to LRS or vice-versa. The set process of the device, or write, occurred for negative potentials (black arrows in fig. 4.1a) and the reset process, or erase, occurred for positive potentials (red arrows in fig. 4.1a). The high-resistive state and low-resistive state (HRS and LRS, respectively) of the device are also represented in the same figure by HRS and LRS, respectively.

One of the important aspects one needs to determine when it comes to memristors is which mechanism is responsible for the RS behaviour, to understand the underlying phenomena. A method often used for this determination is the log vs log analysis, where both the applied voltage and the current response of the device are set to a logarithm scale, and the behaviours of the LRS and HRS are studied. According to literature written on this subject [71, 72], if the slope equals 1, then ohmic conduction is present in the device

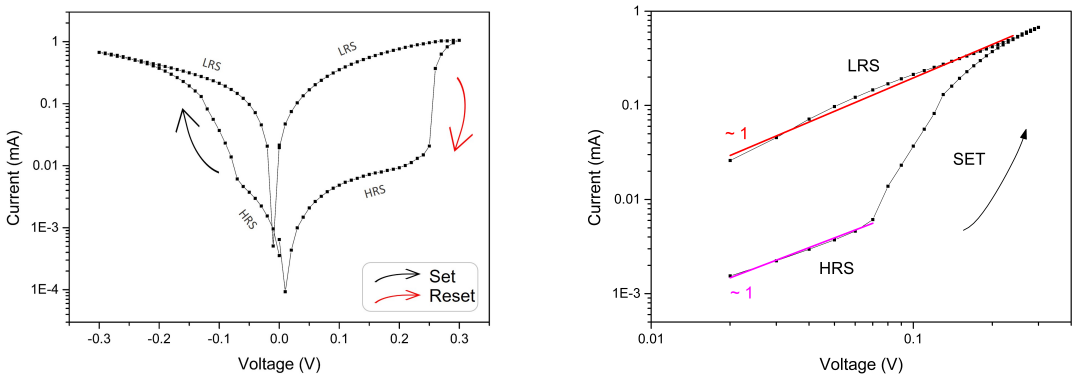

(A) (B)

FIGURE 4.1: (A) RS cycle obtained from a voltage sweep ranging from -300 to 300 mV, electrode distance of 1.3 mm at solution concentration of 0.5 M, at room temperature. The set process, that occurs for negative potentials, and reset process, that occurs for positive potentials, are represented with black and red arrows, respectively. Furthermore, the high-resistive state (HRS) of the device and the low-resistive state of the device (LRS) are also portrayed. (B) Log(I) vs log(V) of the negative portion of the voltage of (A) and the respective fit of the HRS and LRS.

and if the slope equals 2, then space charge limited conduction is present. However, more than one conduction mechanism can be present simultaneously. Thus, in order to determine the predominant mechanism during set, a voltage sweep (fig. 4.1a) was analysed on the negative potential application (fig. 4.1b). As one can see, for both LRS and HRS, the slope is approximately 1 (the rest of the curve is not considered due to it being a transition phase), which means ohmic conduction is the main mechanism of conduction for the device (the relation between current and potential in these states is linear: follows Ohm's law). One important advantage of this device, in the liquid-state, is that is does not need an electroforming step, as often happens with solid-state materials, because, since the structure is more fluid, there is no need for a high initial electrical field to be able to cut through that same structure. Initially, the liquid is composed of disperse ions of copper and sulphate (see fig. 4.2a). When a negative bias is applied, the copper bottom electrode is oxidised, releasing copper ions to the solution that migrate towards the top inert electrode, where their reduction takes place, leading to the creating of copper atoms (fig. 4.2b) . This is called the set process. These formed atoms begin to agglomerate, from the top to the bottom electrode, in a filamentary way. When the filament connects both top and bottom electrode, the device arrives to its On State (LRS; 1.09×10^4 Ω), the state of low resistivity (see fig. 4.2c). When the polarity of the applied bias is switched, the filament ruptures (reset process), leading the device to the state of high resistivity (HRS;

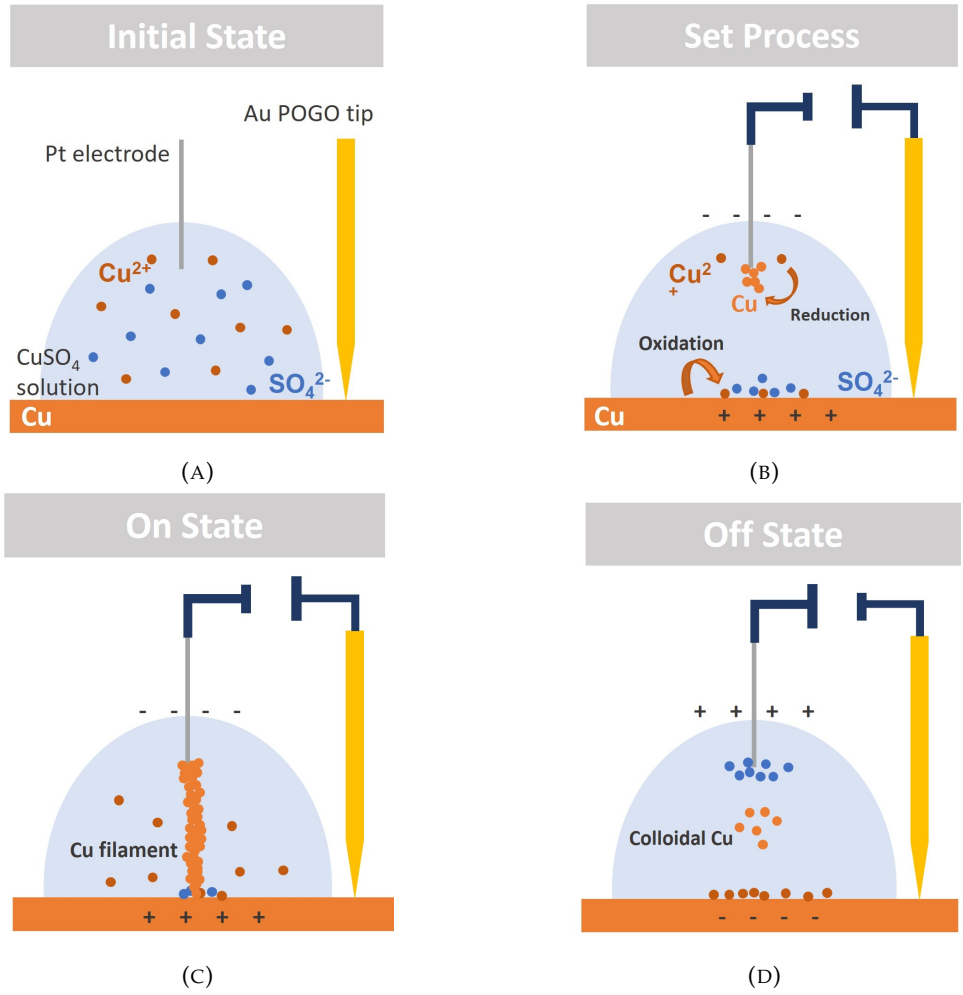

FIGURE 4.2: Visual representation of the switching mechanism of the device. (A) Initial state with disperse ions in the solution. (B) Set process: with an applied bias, reduction of Cu^{2+} to Cu atoms take place at the top electrode while oxidation of the copper bottom electrode occurs, releasing Cu^{2+} ions into the solution, that are a source for filament formation. (C) On state: the Cu atoms form a filament connecting both electrodes and conduction takes place. (D) Off state: with an applied bias with reverse polarity (reset process), the Cu filament is ruptured, leaving some of its atoms disperse in the solution.

$1.98 \times 10^5\ \Omega$; fig. 4.2d). Even though most of the copper atoms are oxidised in this stage, some remain in the solution in colloidal form. This is further proven by the fact that the solution is light clear blue at the beginning of measurements (see fig. 4.3a) and turns to a nebulous light blue with orange surroundings at the end of measurements (see fig. 4.3b). The R_{Off}/R_{On} ratio for this curve was of 18.

The chemical equations that define the reduction and oxidation of copper, during the set process, on both the top and bottom electrode, respectively, are

$$Cu^{2+}(aq) + 2e^- \rightarrow Cu(s), \tag{4.1}$$

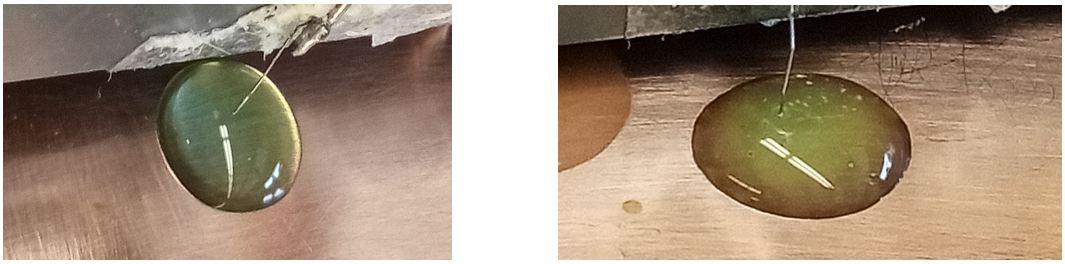

(A) (B)

FIGURE 4.3: Drop of the copper sulphate solution (A) before any electrical stimuli, and (B) after several electrical stimuli.

and

$$Cu(s) \rightarrow Cu^{2+}(aq) + 2e^{-}. \tag{4.2}$$

4.1.2 Applied potentials

In order to achieve optimal operation, there must be an equilibrium between two main aspects: lowest potential possible applied to the device, with the highest R_{Off}/R_{On} ratio possible as response. Thus, measurements of different RS cycles were applied for various voltage ranges and the results are present in fig. 4.4.

As shown, the On current reaches approximately the same value for the different voltage ranges applied to the device, which means that the LRS state of the device is similar for all. Furthermore, it is possible to see that the device has an abrupt set and reset processes, no matter the applied potential, which means that the change in state is fast ($< 10^2$ ms). It is also clear that, in the negative part of the voltage sweep, there is a crossing of the RS curve (at about -200 mV). This phenomenon may be explained by the occurrence

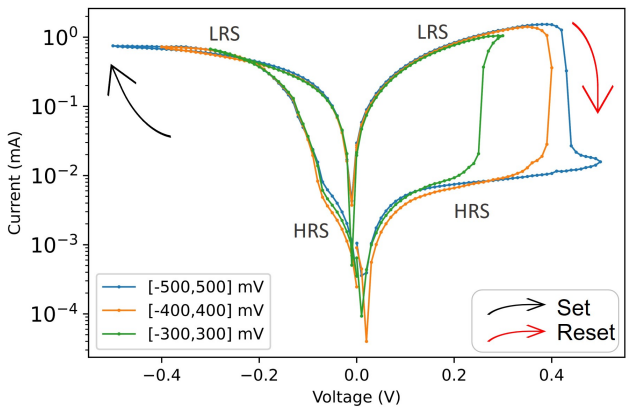

FIGURE 4.4: RS cycle for three different ranges of applied potential: [-300, 300], [-400, 400], and [-500, 500] mV.

of nucleation of copper atoms in the top electrode for some measurements, but a more in-depth analysis will be presented in section 4.1.8.2. Additionally, the minimum of current for each curve suffers from a potential shift about the 0 V. This shift can be explained by the nano-battery effect, that is thoroughly explained in section 4.1.8.1. The set process takes place at the same potential value for each potential range, and the reset process takes place at slightly different potential values, that increase with increasing potential range, as one can tell by fig. 4.5a. For the potential range of [-300, 300] mV, the reset process is forced by the limits of the voltage sweep (V_{reset} is 300 mV). As far as the other potential ranges go, the minimal difference they present in V_{reset} is most likely due to some undissolved copper from the nucleation process that, even though is not enough to significantly improve the device's current response, can make for the reset process to start at slightly higher voltages. The ratio of the Off and On resistances was calculated for each range of applied potentials, with the On and Off resistances of each range represented in fig. 4.5b. They all show very close values, within the same order of magnitude: 54 for [-300, 300] mV, 68 for [-400, 400] mV and 53 for [-500, 500] mV. The medium range obtained slightly higher ratio, which is probably due to measure-to-measure variability since it is not significantly higher. As previously mentioned, a higher R_{Off}/R_{On} ratio is desired because it translates into a better separation between the two operation states and overall low current is also desired, since it implies lower power consumption [73]. Furthermore, as previously mentioned, since the filament formation occurs in a liquid, the lower the current involved, the lower the chance of heating due to Joule effect and to, consequently, evaporate. This is highly desirable to achieve better reliability and stability for the device.

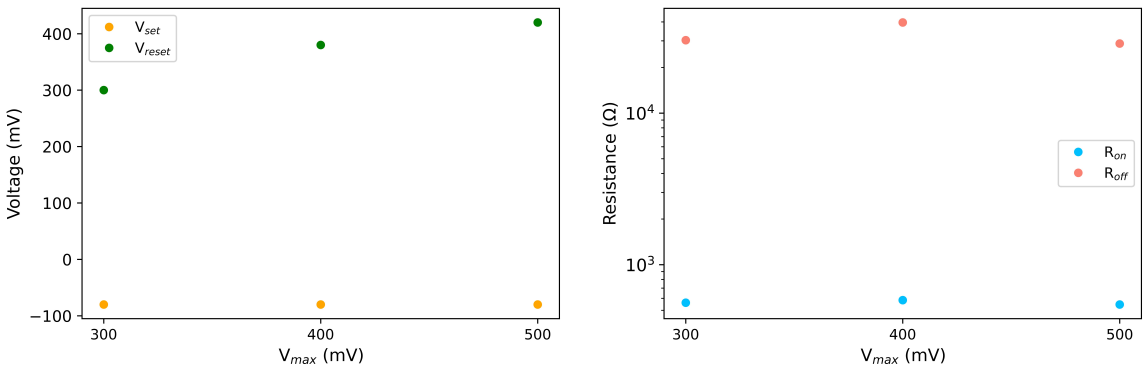

(A) (B)

FIGURE 4.5: (A) V_{set} and V_{reset} and (B) R_{On} and R_{Off} of each voltage sweep range, at a reading voltage of 50 mV.

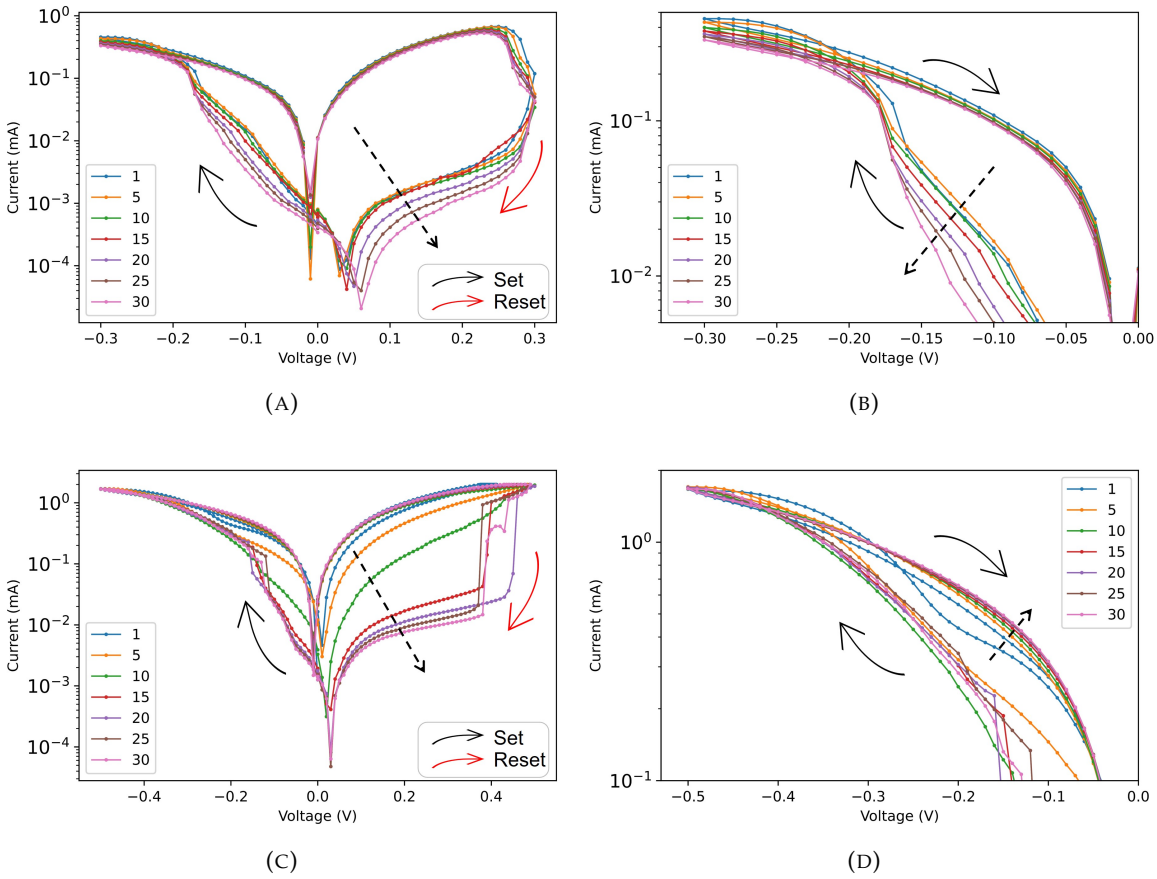

FIGURE 4.6: (A) RS curves of cycles 1, 5, 10, 15, 20, 25 and 30 of voltage sweeps with range [-300, 300] mV and a (B) zoom of their negative potential portion in linear scale. (C) RS curves of cycles 1, 5, 10, 15, 20, 25 and 30 of voltage sweeps with range [-500, 500] mV and a (D) zoom of their negative potential portion in linear scale. The dashed arrow represents the tendency of the curves.

Finally, it is also desirable that the device operates with as little input voltage as necessary. With all these aspects in mind, and given the previous mentioned analysis, the [-300, 300] mV potential range (<1.5 mA) is the most appropriate for further measurements.

To further experiment with the applied potentials, 30 consecutive cycles of RS for the voltage ranges of [-300, 300] and [-500, 500] mV were applied, with results for the cycles 1, 5, 10, 15, 20, 25 and 30 shown in figs. 4.6a and 4.6c, respectively. Figs. 4.6b and 4.6d show the portion of the negative potential applied in detail. It is possible to notice that, with cycling, the current of both On and Off states tends to diminish (resistance tends to increase), with this being more evident for the smaller range of applied voltage and the On state. This is due to the fact that the filament formed is not as thick as the filament formed for higher potentials, so it does not hold the state as well for a large number of consecutive applied voltage cycles. As for the Off state, the increase in resistance is more evident in

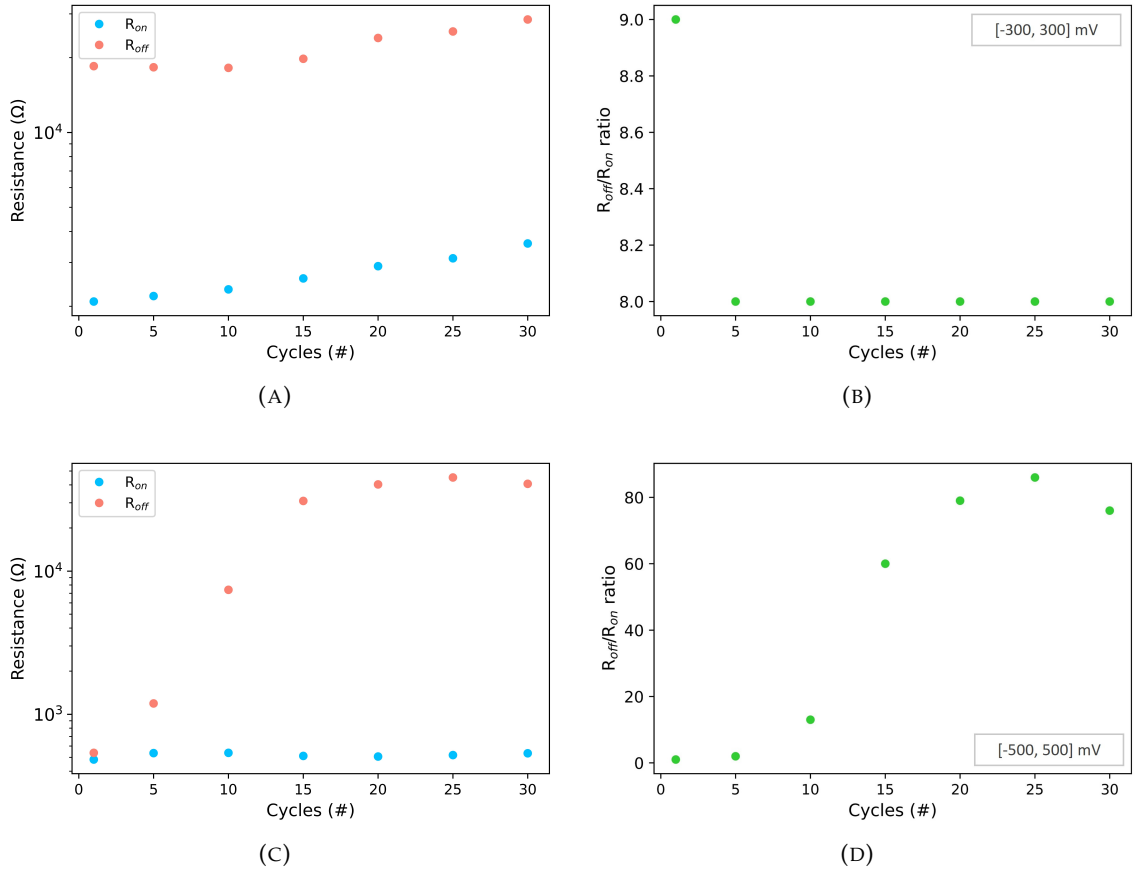

FIGURE 4.7: (A) R_{On} and R_{Off} and (B) R_{Off}/R_{On} ratio obtained for each represented cycle of voltage sweeping from -300 up to 300 mV. (C) R_{On} and R_{Off} and (D) R_{Off}/R_{On} ratio obtained for each represented cycle of voltage sweeping from -500 up to 500 mV, at a reading voltage of 50 mV.

the larger applied voltage range (see figs. 4.7a and 4.7c). Both voltage ranges show good reproducibility in the device, except for the first few cycles of the larger voltage range, due to it taking time to adapt to the voltage sweeps, since other kinds of measurements were being performed before. When it comes to the resistance state ratios obtained for each of the voltage sweep ranges, it was noted that, for the smaller range, the ratio stayed practically the same as cycles went on, always with the same order of magnitude (see fig. 4.7b) and, for the larger range, there was an initial increase (due to what was previously mentioned about adaptation in the first few cycles) and then a convergence to similar values, as more cycles went on (see fig. 4.7d). The larger range of potential led to larger ratios of Off and On resistances as cycles of potential sweeps were applied to the device, which is desired. However, it also reached higher currents, which leads to more power consumption from the device.

4.1.3 Solution concentration

In order to achieve the device with the best performance possible, the concentration of the solution is an important parameter to consider. As part of the study of the device's behaviour, three different concentrations of aqueous copper(II) sulphate pentahydrate were fabricated, namely 0.1, 0.5 and 1 mol/l. Maintaining the distance between electrodes, room temperature and same range of voltage of operation, a voltage sweeping cycle was performed for each one of the different solutions, with the result being shown in fig. 4.8.

In the three curves it is possible to observe similar hysteretic shapes, characteristic of the RS phenomenon. It is observed that, with increasing concentration, there is an increase in current response by the device. This is due to the fact that, for higher solution concentrations, more copper ions are disperse in the solution, making for a quicker formation of the filament that connects both electrodes but also a thicker one, therefore providing higher On currents (the On current is believed to be proportional to the filament size) [6]. Furthermore, calculations of the Off and On resistances were performed, as shown in fig. 4.9a, with a clear decrease in the Off resistance and a less pronounced decrease in the On resistance as the concentration of the solution increased. The determination of the ratio between Off and On resistances, for each concentration, was also performed, as shown in fig. 4.9b, revealing that its lowest value was achieved for the 1.0 M concentration, with a ratio of approximately 16, when compared with the 54 achieved by 0.5 M concentration and 116 achieved by the 0.1 M concentration. A high ratio is desired, because it means lower leakage probability, so better overall performance. However, another point that needs to be considered is the reliability of the device.

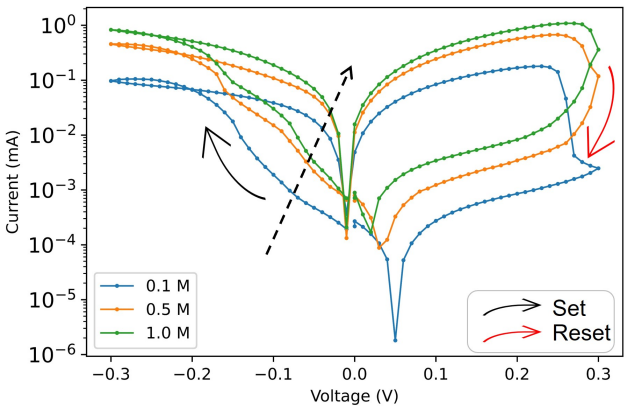

FIGURE 4.8: RS behaviour in a solution of copper(II) sulphate at three different concentrations: 0.1, 0.5, and 1.0 M. The dashed arrow represents the tendency of the curves.

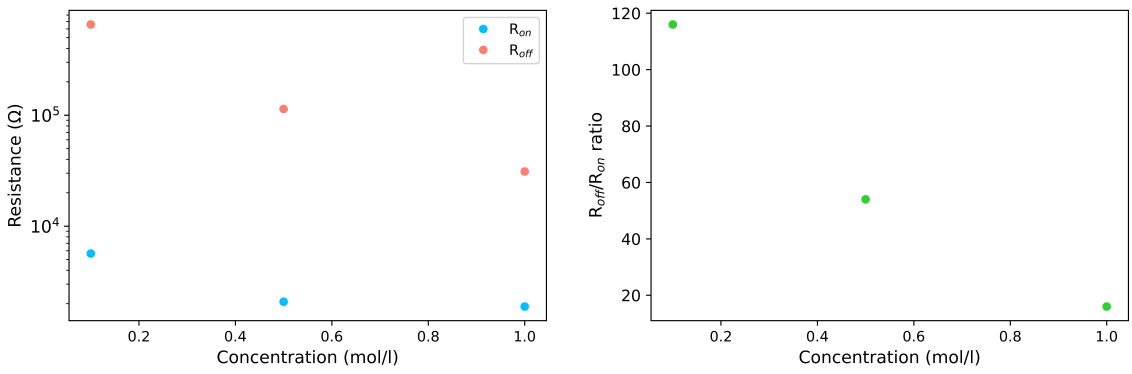

(A) (B)

FIGURE 4.9: (A) R_{On} and R_{Off}, and (B) R_{Off}/R_{On} ratio obtained for each solution concentration, at a reading voltage of 20 mV.

To further test how the device behaves for each concentration, an endurance test was performed where several cycles of voltage sweeping were carried out. The results can be seen in fig. 4.10a, 4.10b and 4.10c. For the higher concentration, switching becomes more unstable as cycles go on, most likely due to overheating issues that evaporate the water out of the solution and saturate it faster. As far as the lower concentration goes, it was unable to sustain the states for more than about 60 cycles, a poor number, especially considering its main purpose. Therefore, an intermediate concentration, such as 0.5 M, seems to be the best option for endurance purposes.

Nevertheless, we still observe a decrease in the current with cycling for all concentrations (about 68% in the On state and 94% in the Off state for 0.1 M; about 71% in the On state and about 96% in the Off state for 0.5 M, and about 78% in the On state and 81 % in the Off state for 1.0 M, comparing the first and the last read currents, before the collapsing of the state), due to degradation in the device. There are a multitude of factors than can play into why this is happening, although, the most obvious one seems to be temperature. With the continuous application of voltage bias, the temperature in the solution starts to increase. This has a known impact on the endurance of the device because it incites the growth of activation processes of diffusion and ion migration [74]. At the nanoscale, it also provokes the vibration of atoms, which can lead to a more difficult movement of electrons that transport current, leading to an overall decrease of current in the LRS. Another theory that can justify this decrease, as reported by Kim *et al.* [6] is the fact that, for each cycle, copper ions are oxidised from the bottom electrode and reduced into copper atoms to form a filament, to then return to the copper electrode later, when

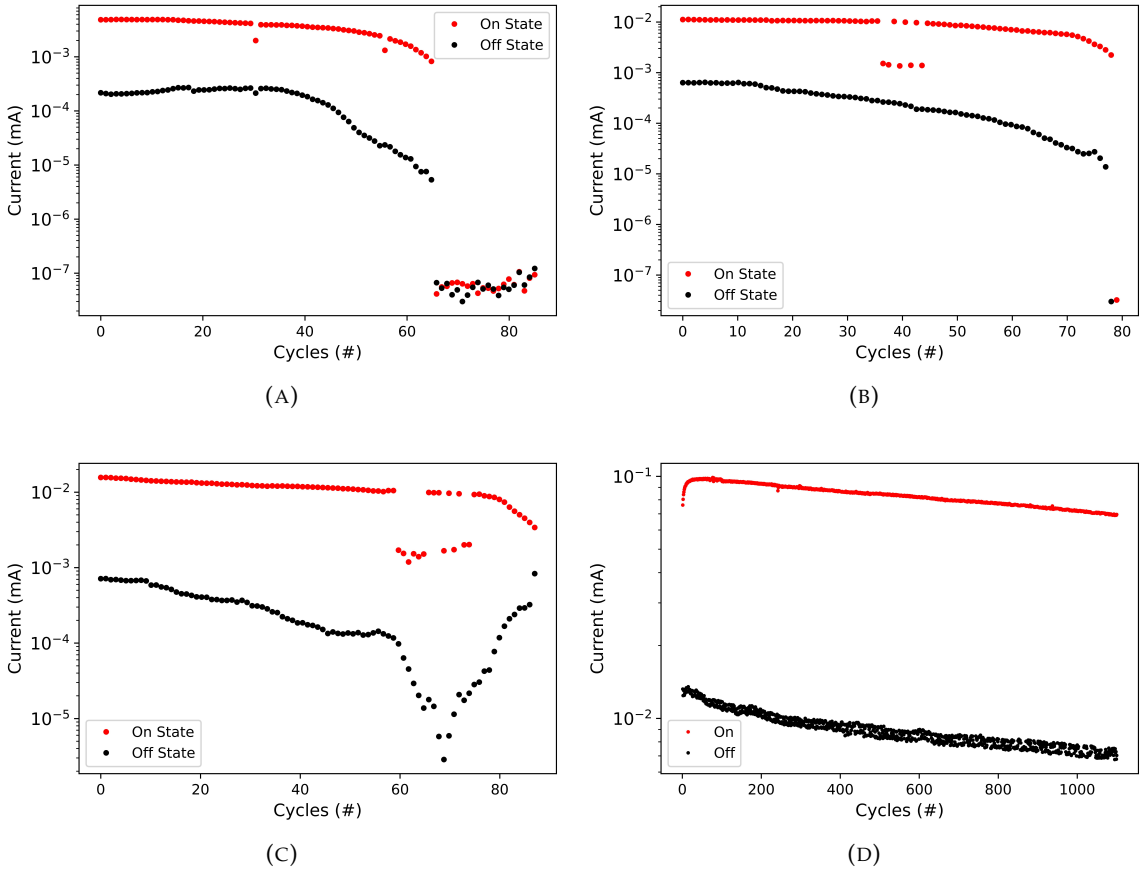

FIGURE 4.10: Endurance behaviour in the On and Off states for the solution concentrations of (A) 0.1 M, (B) 0.5 M and (C) 1.0 M, by the application of several voltage sweeps. (D) Endurance achieved by a pulsed method, for the solution concentration of 0.5 M. Reading voltage of 50 mV.

the reset process occurs. However, not all copper atoms are able to return to the copper electrode, accumulating in the solution as colloidal copper where it remains disperse [75]. These colloidal particles, when immersed in electrolytes, are usually charged due to the adsorption of ions which, therefore, attracts ions of the opposite charge to accumulate around its surface, in a bid to establish a net equilibrium [76]. These systems that are present in the solution and that increase as cycling moves on, remain disperse and can become a physical barrier in the formation of filaments, generating the said decrease in current. However, this is a theory hard to verify, even though copper colloids do seem to be created in the solution, as previously mentioned and justified. For the concentration of 0.5 M, further endurance measurements were performed, with a pulsed approach (pulses of 100 and -100 mV with width of 100 ms and interpulse width of 1 ms). The results are shown in fig. 4.10d. As one can tell, a large number of cycles were achieved without the

collapse of the state (>1000). This is largely due to less heat being generated for each measurement, since each set/reset transition is achieved by a single pulse and not a voltage sweep that takes longer and goes to higher potentials. The states also remained constant, specially when compared with the first method used, in particular the On state, with little voltage decrease detected (8% for the On state and 47% for the Off state).

Finally, a data retention test was made over 10^3 s for all three concentrations to assess the better concentration for a maintenance of a state for long periods of time. The results are shown in fig. 4.11. As it is possible to see, all three concentrations have a current decrease as time went on, justified by the same arguments as the ones used for the decrease in endurance, with the least decrease being seen in the smaller concentration and the largest decrease in the higher concentration, especially in the On state, where a filament is connecting both electrodes. So, one can say that the more stable device in terms of sustaining its state is the 0.1 M one and the least stable device is the 1.0 M one.

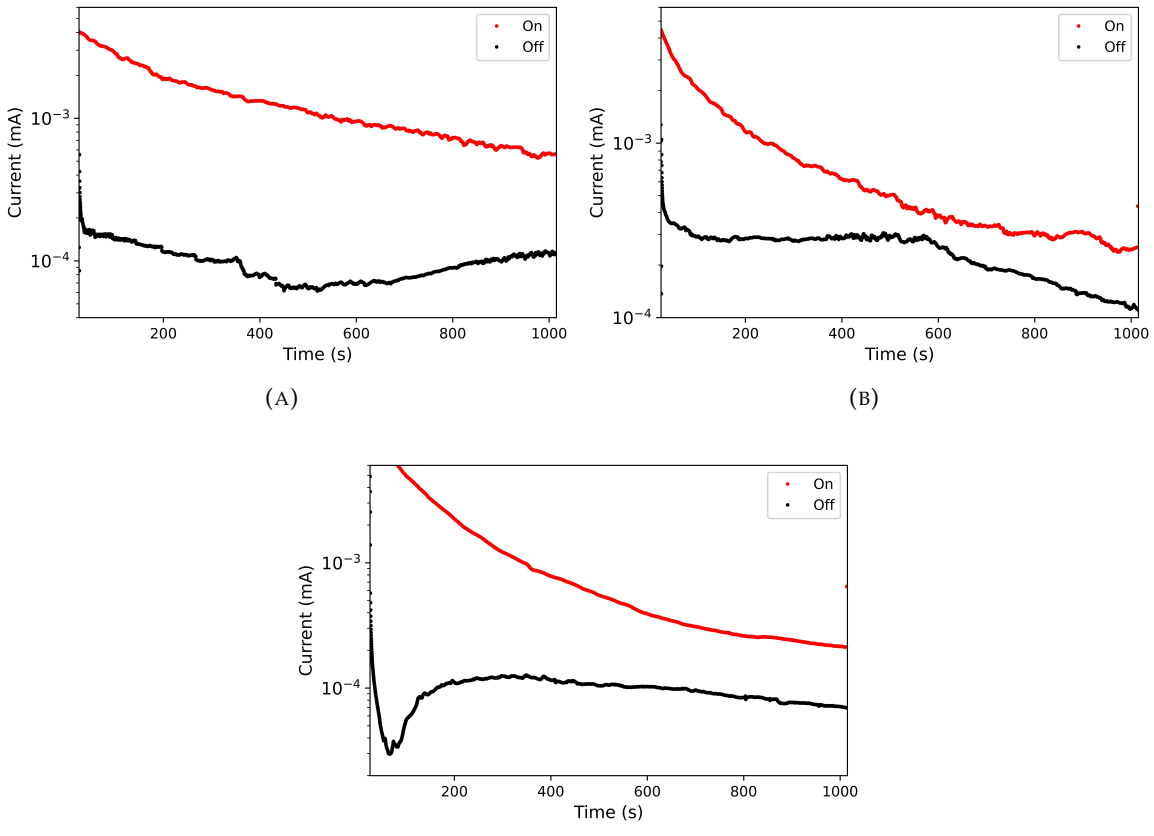

(A) (B)

(C)

FIGURE 4.11: Data retention behaviour in the On and Off states for the concentrations of (A) 0.1, (B) 0.5 and (C) 1.0 M, at a reading voltage of 50 mV.

With every property mentioned previously in mind, the best balance between reliability, stability and high R_{Off}/R_{On} ratio lies in the middle concentration, 0.5 M.

4.1.4 Solution temperature

The influence of the temperature on the RS behaviour was also studied. For that, a Peltier cell was placed on the bottom of the copper bottom electrode either to warm up or cool down (between 11 and 72 °C) the solution on top. Initially a calibration was done to understand if the temperature of the Peltier cell was the same as the one of the copper electrode and, therefore, the liquid. The calibration led to the conclusion that the temperature was very similar between Peltier and bottom electrode, being that, the relation was either 1 or approximately one for cooling (fig. 4.12a) and heating (fig. 4.12b). The results obtained for each voltage sweep from the cooling process are represented in fig. 4.13a and the ones from the warming are represented in fig. 4.13b.

From this study, there seems to be an overall decrease in current with decreasing temperature, or in other words, R_{On} and R_{Off} increases with decreasing temperature (see fig. 4.14a). However, as we inferred before that the conduction mechanism should be ohmic, the opposite behaviour would be expected. One factor that can contribute to this behaviour is the degradation of the device with cycling, which naturally leads to a decrease in current, but also the lack of certainty about the real temperature in the device, since the rate of decrease of temperature was rather high to oppose the increase of temperature caused by other side of the Peltier cell. Note, however, that the disparity between current

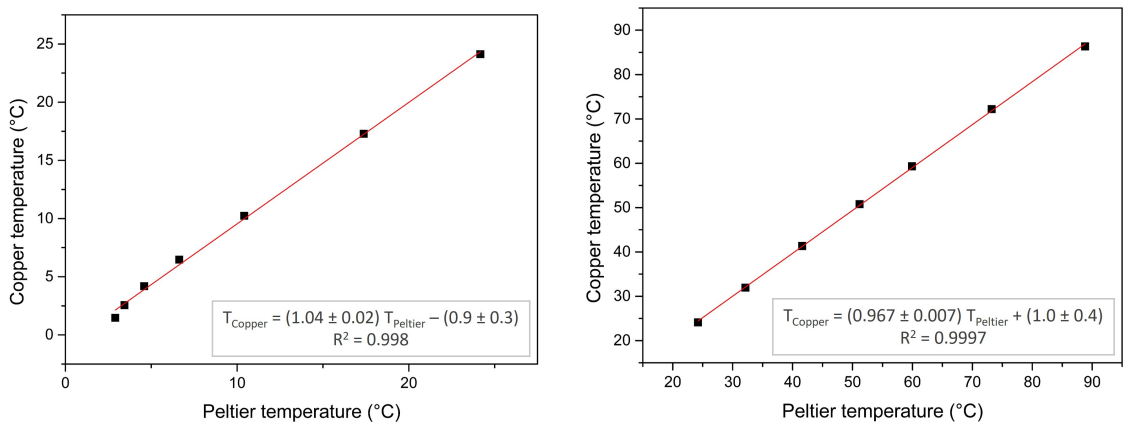

(A) (B)

FIGURE 4.12: Temperature measured in the copper as a function of the read temperature in the peltier cell for both (A) cooling and (B) heating.

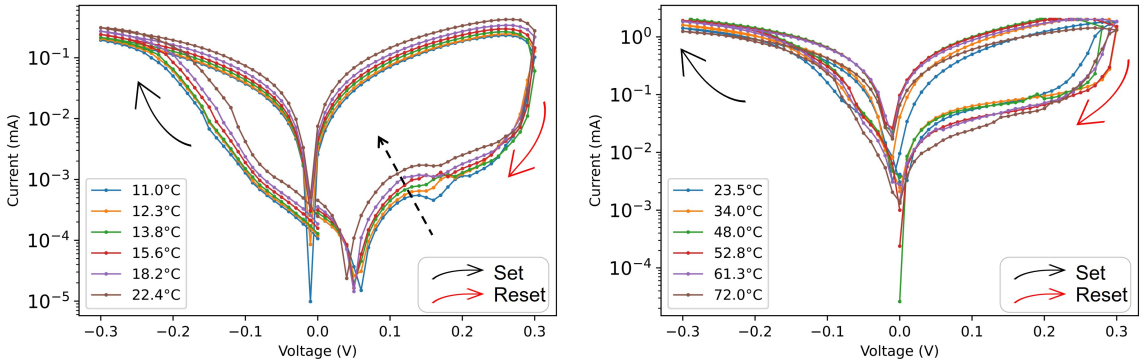

(A) (B)

FIGURE 4.13: RS cycles for different solution temperatures ranging from (A) 11.0 to 22.4°C and (B) 23.5 to 72.0°C.

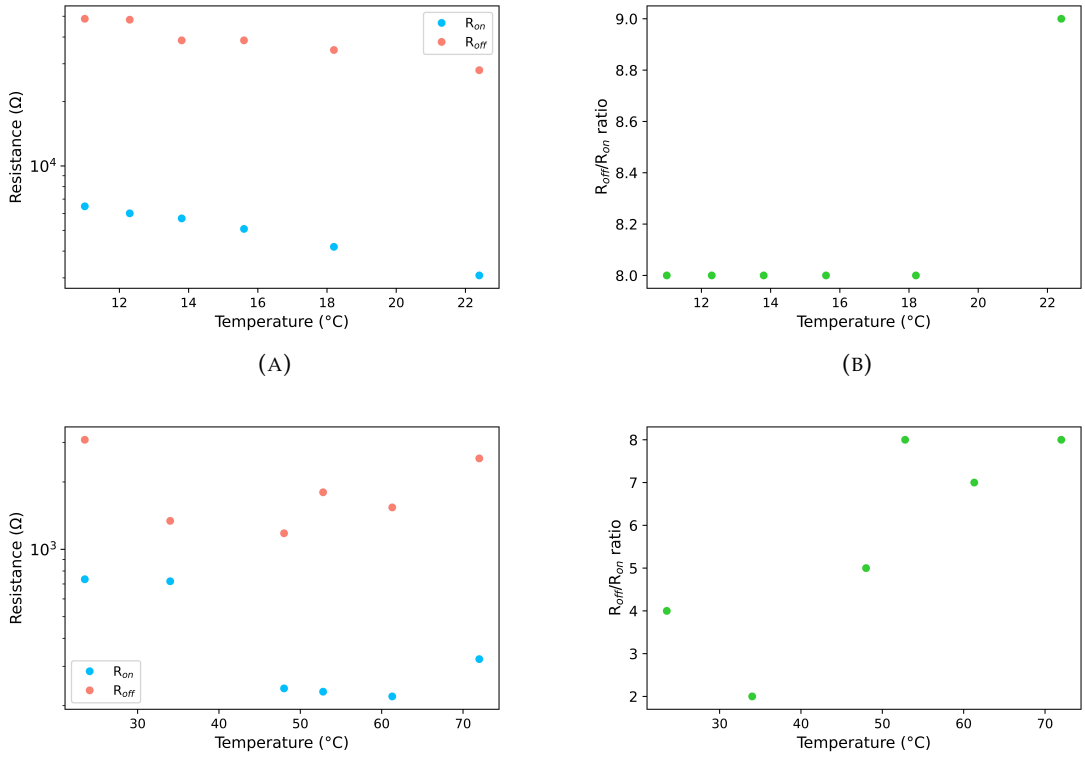

(A) (B)

(C) (D)

FIGURE 4.14: (A) R_{On} and R_{Off}, and (B) R_{Off}/R_{On} ratio obtained for each temperature in the cooling phase. (C) R_{On} and R_{Off}, and (D) R_{Off}/R_{On} ratio obtained for each temperature in the heating phase. Reading voltage of 20 mV.

responses was not significant. The ratios R_{Off}/R_{On} for the cooling phase proved to be very constant, all within the same order of magnitude, between 8 and 9 (see fig. 4.14b).

As the temperature increases past room temperature, it presents very unstable values of On and Off resistance that prevent the determination of a clear tendency (see fig.

4.14c). The first two recorded temperatures presented a rather high On resistance when compared with the rest. Past the point of about 70°C, current starts decreasing, resulting in an increase in resistance. This is probably due to the fact that vibration of the metal copper atoms increases to a point where an increase in resistance, due to the harder path of electrons through the moving atoms, happens [77]. At the same time, as temperature rises, the water content in the solution begins to evaporate quicker and quicker, creating instability and unreliability in the results, since, for each new temperature, a different volume and a different water content in the solution are present. Furthermore, the solution had to be replaced two times during these measurements, which contributed further to the inconsistent results obtained. As far as the ratio of resistances goes, it presents higher values for higher temperatures (see fig. 4.14d). Comparing the ratios of both cooling and heating, the highest achieved value was for room temperature, with a value of 9.

4.1.5 Electrode distance

Another parameter that can influence the behaviour of the device is the distance between electrodes. Since the bottom electrode is in a fixed position, the height of the top electrode, which is movable, will determine the distance between the two. The same top electrode was used for all measurements: a platinum wire with a diameter of 0.1 mm. Parameters such as potential range, temperature, and concentration remained the same for all three distances between electrodes measured, which were (1.26 ± 0.05), (0.95 ± 0.05) and (0.34 ± 0.05) mm.

A voltage sweep was performed for each distance, leading to the RS curves observed in fig. 4.15. As it is clear, the closer the two electrodes are, the higher the current response from the device, as expected. Simultaneously, as the distance between electrodes decreases, an increase in temperature in the liquid solution is verified due to Joule heating, which leads to its faster evaporation. Now, looking at fig. 4.16a and 4.16b, one can tell that, the higher the separation between electrodes, the higher the ratio between resistive states, which is highly required. Therefore, the best distance can be attributed to 1.26 mm. However, for a question of simplicity in measurement taking and in the use of the micrometre screw, 1.0 mm was used for most of the measurements.

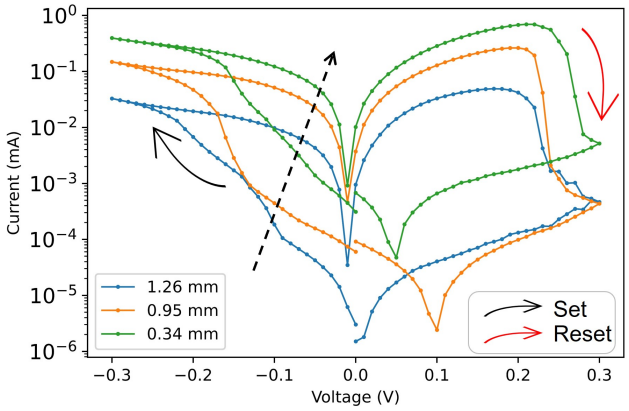

FIGURE 4.15: RS cycles for three different distances between top and bottom electrode: 1.26, 0.95, and 0.34 mm. The dashed arrow represents the tendency of the curves.

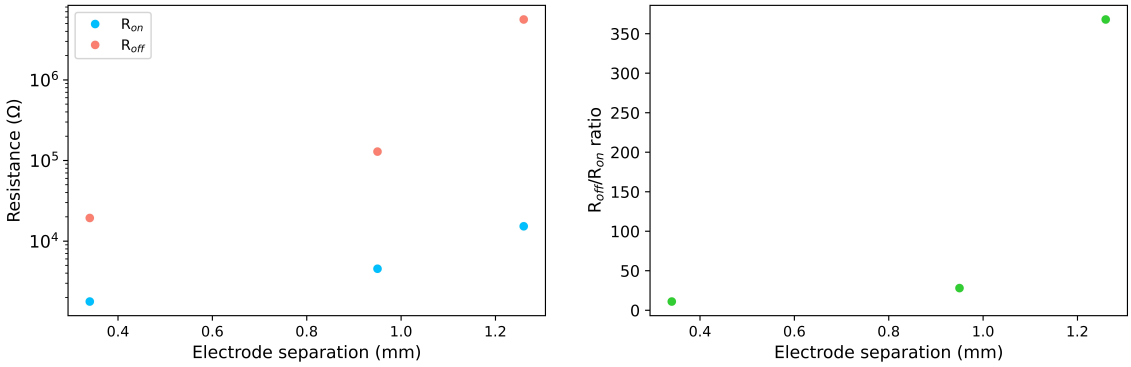

(A) (B)

FIGURE 4.16: (A) R_{On} and R_{Off} and (B) R_{Off}/R_{On} ratio obtained for each electrode distance measured, at a reading voltage of 20 mV.

4.1.6 Types of electrodes

To study the influence of the top electrode used, four different materials (platinum, silver, copper, gold) were tested with results shown in fig. 4.17. Platinum was tested with two different wire diameters, 0.1 mm (Pt 0.1), and 1.0 mm (Pt 1.0), while silver (Ag) and copper (Cu), both, had a wire diameter of 1 mm. Finally, the gold (Au) material was a probe tip with coating, being that the diameter of the probe was of 2.4 μm. To study their different behaviour, the temperature, distance between electrodes, concentration and voltage range remained the same while applying the voltage sweep.

Firstly, looking at fig. 4.17a, the higher current response of the device, reaching even the current compliance limit (2 mA), occurred for the silver electrode, followed by the platinum with larger diameter and copper electrodes. The gold and platinum (with smaller

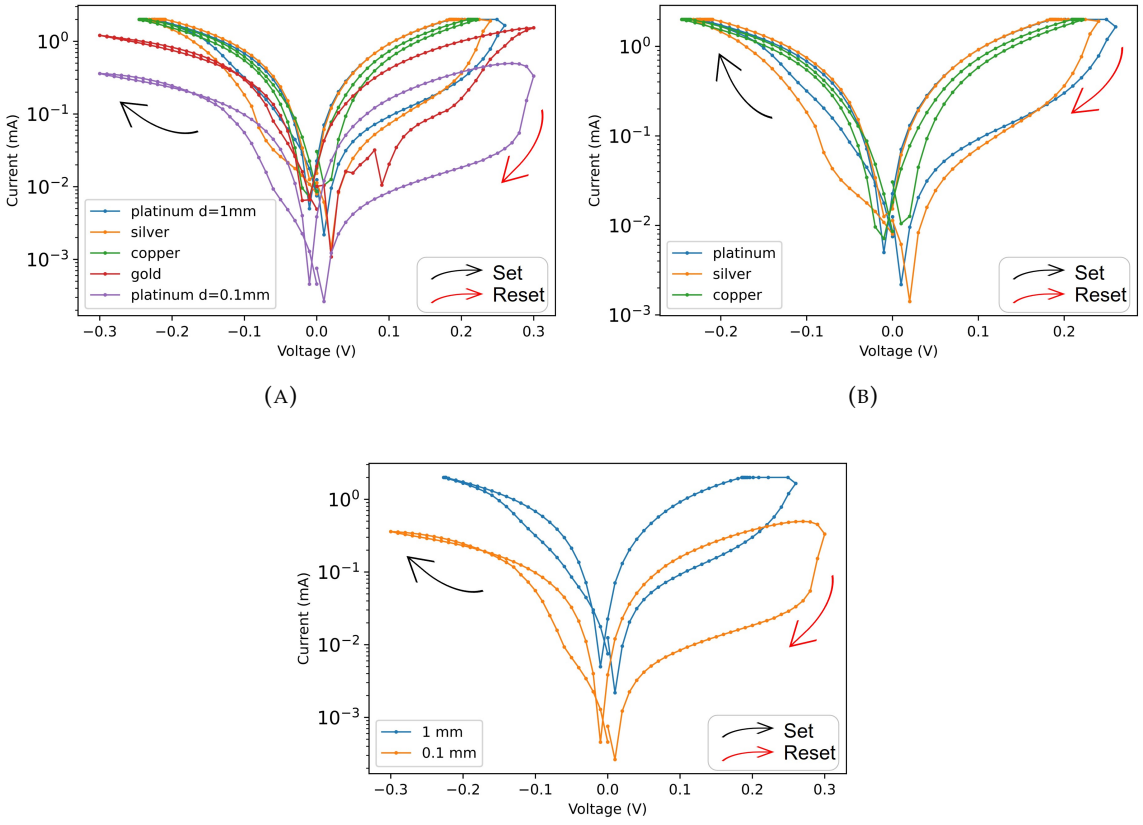

FIGURE 4.17: (A) RS cycles for every material and size electrode available: platinum wire with 1.0 and 0.1 mm diameter, silver wire with 1.0 mm diameter, copper wire with 1.0 mm diameter and probe gold tip with 2.4 μm diameter. (B) RS cycles for three different material electrodes with the same 1.0 mm diameter: platinum, silver and copper. (C) RS cycles for the same platinum material with two different diameters: 0.1 and 1.0 mm.

diameter) electrodes achieved the lowest current, higher resistance, responses by the device (see fig. 4.18a). As previously mentioned, overall low current response from the device is wanted, because it is an indication of lower power consumption by the device. To further study the different behaviours of the different electrodes, the R_{Off}/R_{On} ratios were calculated for each. The highest ratio was attributed to Pt 0.1, with a value of 14, followed by the Pt 1.0, with value of 11. Silver and copper electrodes were the ones who followed, with values of 4 and 1, respectively. Finally, the gold electrode presented a ratio of 1, however, its behaviour near 0 V showed large variability, which means the calculated ratio is not the most reliable (see fig. 4.18b). With these two characteristics in mind, Pt 0.1 proved to be the electrode with the best results.

Now comparing solely the electrodes with the same diameter, in order to study the effect of the cross-sectional area in the device's performance, it is possible to see that the

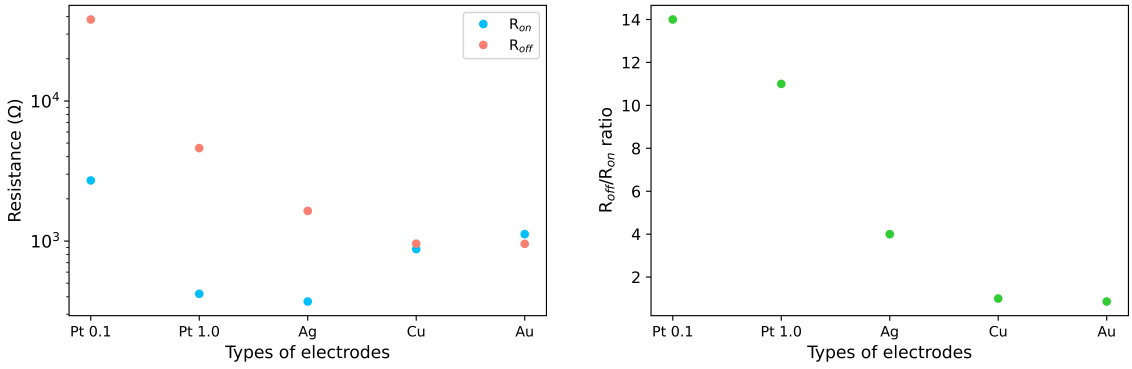

(A) (B)

FIGURE 4.18: (A) R_{On} and R_{Off}, and (B) R_{Off}/R_{On} ratio obtained for each type of top electrode used. Reading voltage of 50 mV.

silver diameter presents higher current response, followed by platinum and then copper. The values of the electrical conductivity for these metals are 6.30×10^7, 9.44×10^6, and 5.98×10^7 S/m for silver, platinum, and copper, respectively [78]. This information corroborates the fact that silver is the highest electrical conductor (lowest R_{On} of the three, as it is depicted in fig. 4.18a). However, it does not explain the relative order of copper and platinum (in the conducting state, copper should have lower R_{On} than platinum, and this is not what is occurring). A factor that can contribute to the seen difference may be that the used copper had been previously used for other types of measurements and was exposed to the environment, leading to its oxidization and some degradation. Some problems with the welding and, therefore, electrical contact of this electrode might also be a cause for this behaviour.

To understand the dependence of the data with the electrode's diameter, Pt wires were used with different diameters: 1.0 and 0.1 mm. The results can be seen in fig. 4.17c. As expected, the larger the diameter, the larger the current response (lowest R_{On}), because a larger wire diameter means more area for electrons to move through. When it comes to resistance ratios, both electrodes presented values within the same order of magnitude, with the smaller diameter electrode presenting a slightly higher value.

Platinum was the overall better performing electrode, especially with smaller diameter, because it allowed for a slight larger R_{Off}/R_{On} ratio with smaller power consumption for the device. Platinum is a commonly used electrode due to the fact that it is not needed to consider extrinsic effects of interfacial oxidization, which is critical when dealing with liquids [79].

Another aspect directly related to the electrodes used is the symmetry of the RS cycle. The closer the work functions of the two metals that compose the electrodes, the more symmetric (with respect to 0 V) the RS curves should be [80]. The work functions of the materials used as electrodes are present in Table 4.1. Since the active bottom electrode is made of copper, it is expected that the copper-copper electrodes generate the most symmetric RS curve, which is, in fact, the case. On the other hand, the gold curve is the least symmetric, followed by the platinum ones. According to the work functions, the reverse should happen. However, the gold curve displays quite an irregular behaviour, which leads us to believe that it is not performing as it should. This may be due to inconsistencies in the gold coating of the tungsten POGO tip (the tip presented a slight greyish tone instead of the expected yellow, which may symbolize that, upon deposition, some contamination occurred), due to degradation over intense use, or some connection issue between wires since the reading setup was slightly altered to accommodate this electrode. Aside from that, the symmetry of the curves behaved according to what was expected.

It is also possible to notice that, while the platinum and silver curves have a clear hysteresis pinched loop both in the set and reset portions of the device, the copper one has very little hysteresis, which is indicative of a more abrupt set and reset behaviours. More abrupt sets and resets are a product of Joule heating effect. In fact, the current increases, so do local temperatures, which leads to an acceleration in the redox processes and increase in the copper concentration in the solution. This, in turn, leads to an even larger increase in the current, that causes the abrupt set [82]. The rupture of the filament is also more abrupt because the process is more dominated by the Joule effect than the diffusion of ions controlled by the applied potential. Since this only happens with copper, one can speculate that it is because of its high conductivity and mobility but also because of the equal work functions between electrodes. Although, as previously mentioned, copper did not have the expected conductivity, which indicated some unknown issue with the

TABLE 4.1: Work functions for electrodes made of four different materials: gold, copper, platinum and silver. Collected from [81].

Material	Work function (eV)
Silver	4.26 - 4.73
Copper	4.7
Gold	5.1
Platinum	6.35

electrode, from the start.

Finally, a study of the diameter of the filament created for each one of the top electrodes was performed. From the equation of resistance in a cylindrical conductor,

$$R_{on} = \frac{\rho\, l}{A}, \tag{4.3}$$

where R_{On} is the resistance of the filament in the On state, ρ is the resistivity of copper, $\rho = 1.68 \times 10^{-8}$ Ωm [83], l is the height of the filament, which translates to the distance between electrodes, so l = 1.0 mm and A is the cross-sectional area of the filament, the diameter can be estimated.

Considering that the cross-sectional area of the filament can be approximated to that of a circle, the diameter was calculated and is represented in table 4.2.

As expected, the smaller diameter electrodes (Pt 0.1 and Au) also present the lowest diameters of the formed filament, with gold having a higher diameter since its On resistance was smaller. As for the electrodes with the same diameter, silver presented the largest diameter, followed by platinum and then copper. The filaments have diameters in the order of 10^2 nm (nano filaments), as it was expected, since the RS phenomena is mostly present at the nano scale [25].

4.1.7 Neuromorphic properties

One of the most important sought-after results for memristor devices are the presence of potentiation and depression, so the gradual increase or decrease, respectively, of the device's conductance upon stimuli repetition. Potentiation and depression are fundamental characteristics of the human synapses and are believed to be the main responsible for learning abilities. With that in mind, a pulse study was performed in the device and potentiation and depression were, indeed, proved to be present.

TABLE 4.2: Calculated filament diameter for 5 different top electrodes: platinum (Pt 0.1 and Pt 1.0), silver (Ag), copper (Cu), and gold (Au).

Top electrode	Filament diameter (nm)	Electrode diameter (mm)
Au	138	2.4×10^{-3}
Pt 0.1	89	0.1
Pt 1.0	226	1.0
Ag	240	1.0
Cu	156	1.0

The pulse study was performed by varying three different parameters, pulse amplitude, pulse width and interpulse width, and seeing the device's response to them when 10 consecutive pulses of potentiation and 10 consecutive pulses of depression were applied.

For amplitude study, several cycles of 10 pulses each, for potentiation and depression, were performed, with amplitudes ranging from 5 to 500 mV and their symmetrical, and pulse width and interpulse width fixed at 100 ms and 1 ms, respectively. The results are shown in fig. 4.19. It is evident that the larger the amplitude, the less variable the results are, and the larger the conductance achieved by the device. However, large amplitudes also present issues such as the almost constant conductance, which is not a sign of potentiation but of a current saturated device, and a slow decrease in depression after potentiation, which is not the expected behaviour. A more intermediate amplitude should present the better balance between all points considered.

For pulse width study, the same routine as for the amplitude study was implemented, except that the potentiation potential was fixed at -60 mV, the depression potential was

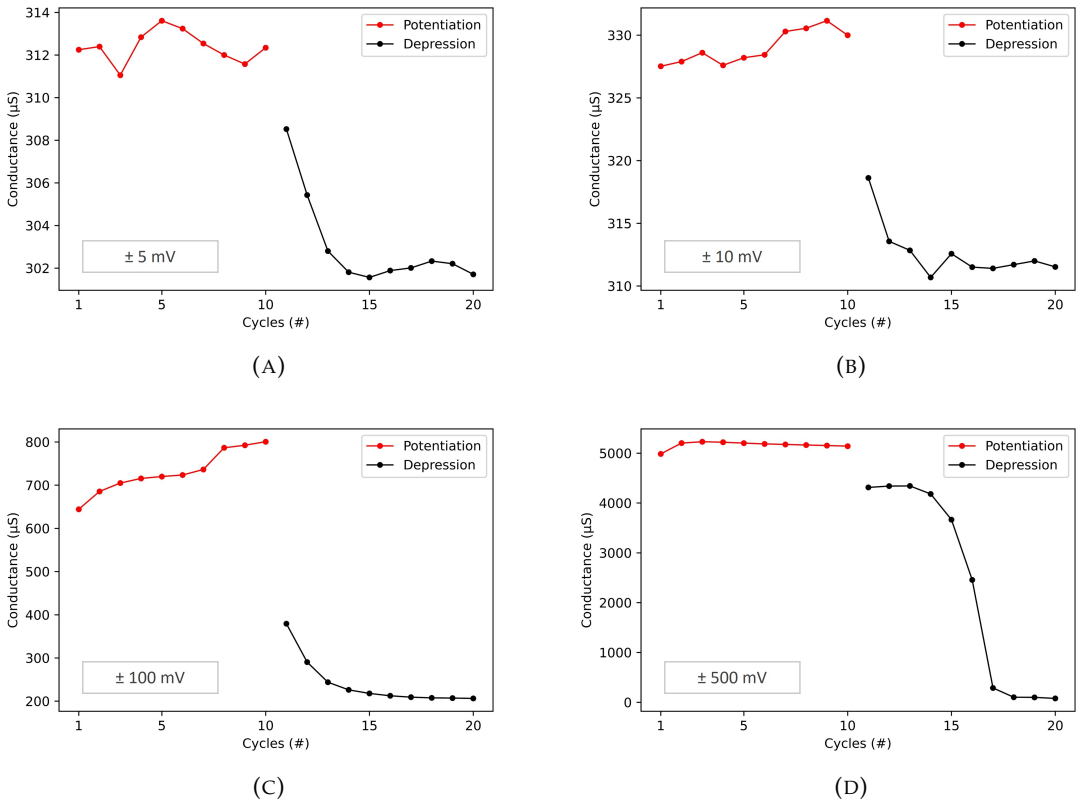

FIGURE 4.19: Behaviour displayed by the device resulting from consecutive applied pulses with pulse width of 100 ms, interpulse width of 1 ms and voltages of (A) -5 mV (for potentiation) and 5 mV (for depression), (B) -10 mV and 10 mV, (C) -100 mV and 100 mV, and (D) -500 mV and 500 mV.

fixed at 90 mV, and the dynamical variable was the pulse width, that ranged from 1 ms to 1 s. The results are shown in fig. 4.20. As one can see, pulses with very short pulse widths do not lead to potentiation (fig. 4.20a and 4.20b), leading instead to a decrease of the conductance, because their effect, in such a short period of time, is almost negligible and not felt by the device (the device is not able to reach the LRS). With increasing pulse width, the overall conductance of the device increases, and a more appropriate potentiation and depression behaviour is observed. However, with too long pulses (fig. 4.20d), such as the case for a 1 s pulse width, there is a decrease in the conductance, very low depression and no potentiation. This is probably because the device is being overloaded with the potential for such a long period of time, that it cannot adapt and respond, and also that filament rupture may occur due to Joule heating.

Lastly, a study of the interpulse width effect on the device's response was performed. For that, the pulse width was fixed at 100 ms, the potentiation amplitude was fixed at -60 mV and the depression amplitude was fixed at 90 mV. The interpulse width was varied

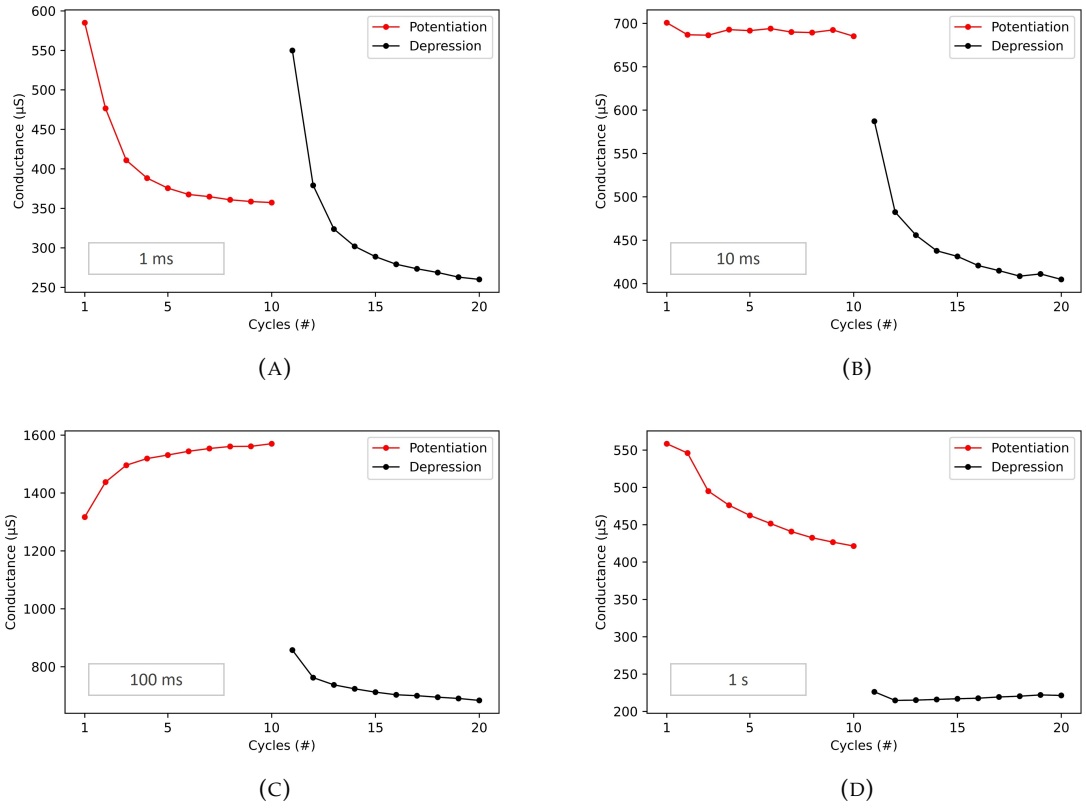

FIGURE 4.20: Behaviour displayed by the device resulting from consecutive applied pulses with voltages of -60 mV for potentiation and 90 mV for depression, interpulse width of 1 ms and pulse width of (A) 1 ms, (B) 10 ms, (C) 100 ms and (D) 1 s.

between 1 ms to 1 s. Results are shown in fig. 4.21. From the results, it is possible to conclude that a smaller interpulse time favours the device's behaviour when it comes to potentiation and depression. With less time between two pulses there is an increase in the overall conductance by the device, but also, the potentiation and depression behaviour become clearer. This happens because the shorter the time between two consecutive spikes, the more change is induced in both potentiation and depression.

Overall, the best results were obtained when the potentiation amplitude was of -60 mV, the depression amplitude was of 90 mV, the pulse width was of 100 ms and the interpulse width was of 1 ms, as one can see in fig. 4.21a. As observed, with each pulse there is an increase in conductance, for potentiation, and a decrease in conductance, for depression. These results prove to be very satisfying, especially considering the amplitudes in which they were obtained, because they are similar to the range seen in the action potential of nerve cells, therefore moving closer to their mimicking. They also prove that the device is capable of learning capabilities, demonstrated by the strengthening of

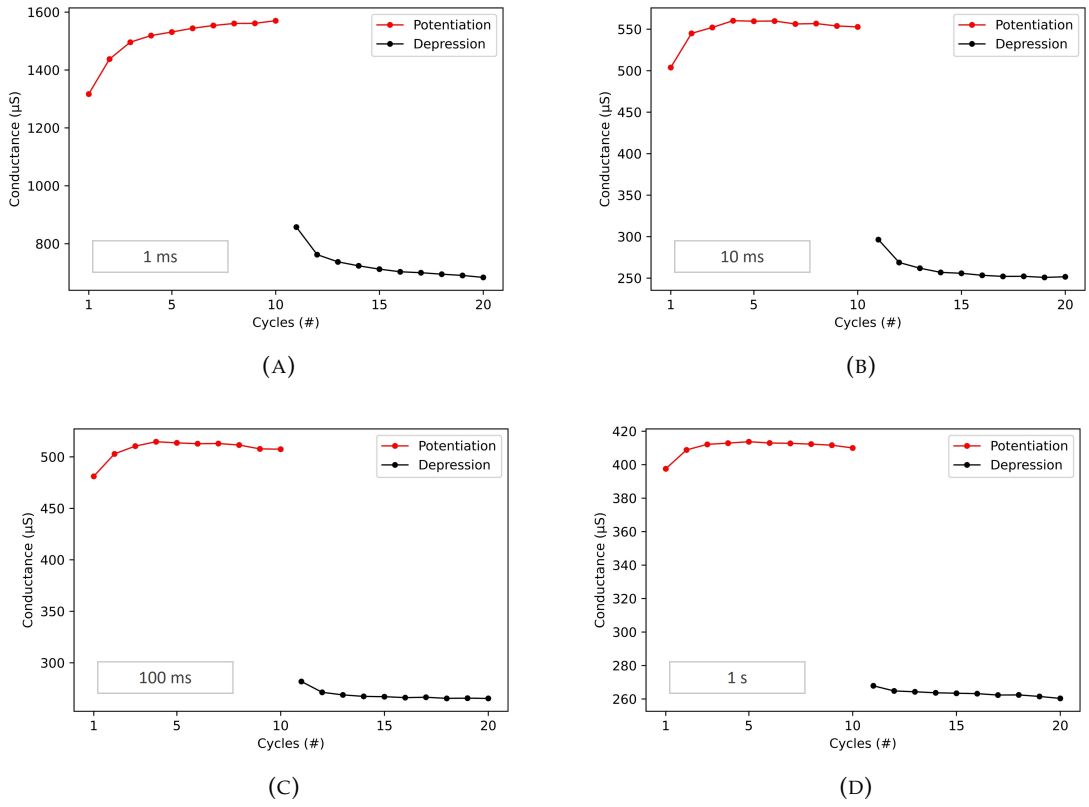

FIGURE 4.21: Behaviour displayed by the device resulting from consecutive applied pulses with voltages of -60 mV for potentiation and 90 mV for depression, pulse width of 100 ms and interpulse width of (A) 1 ms, (B) 10 ms, (C) 100 ms and (D) 1 s.

the connections between pre- and post-synaptic neuron electrodes when in potentiation mode (increase in conductance) and the weakening of connections between pre- and post-synaptic neuron electrodes when in depression mode (decrease in conductance).

4.1.8 Other phenomena

4.1.8.1 Nano-battery effect

During the study of the different RS curves obtained, it was noted that, as the curve made its ascend path from negative potentials, it did not cross the point of 0 A when the applied potential was 0 V, as it would be expected (fig. 4.22).

Such non-zero crossing of the curve at around -0.01 V can be explained by what is called the nanobattery effect [84], that it is heavily influenced by electromotive forces. From the theory presented in section 2.3.1, memristors are described by two equations, a state-dependent Ohm's law, and the state equation. This allows for a pinched I-V characteristic curve, with zero-crossing properties and is regarded as the model of such elements. However, when non-equilibrium On and Off states are present, an electromotive force (up to few hundred millivolts), derived from chemical potential gradients, transgresses the zero-crossing property.

Electromotive forces may arise from several phenomena, such as the classical Nernst potential, the diffusion potential, and the Gibbs-Thomson potential. For the case where a nanofilament is formed which results in short circuit, the Gibbs-Thomson potential is negligible. Since it is already known that the filament does, indeed, short circuit, one of

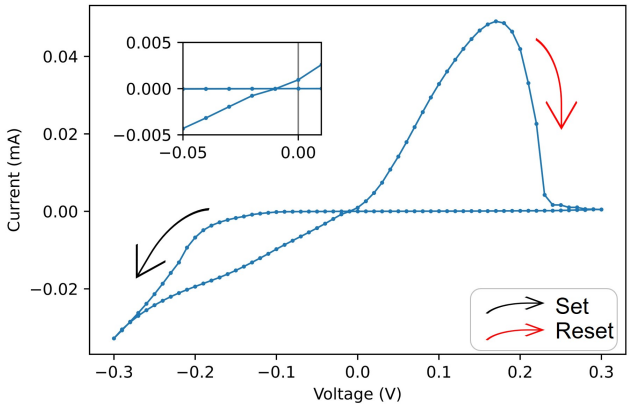

FIGURE 4.22: RS cycles where the non-zero crossing is visible (0.5 mol/l and platinum top electrode at a 1.26 mm spacing).

the conclusions to draw is that this type of potential is not responsible for the nanobattery effect observed in the device [84].

The Nernst potential relates the reduction potential of an electrochemical reaction to several factors of the chemical species involved in the processes of reduction and oxidization, such as standard electrode potential, temperature, and concentration [85]. So, it is originated, in the device, due to the difference of reactions that take place in each (active or inert) electrode/electrolyte interface.

The diffusion potential emerges when there is an excess of charged species, in concentration terms, within the electrolyte (in this case, $Cu(II)^{2+}$). This excess is usually more pronounced in the area surrounding the electrodes and promotes, therefore, the formation of an electromotive force that arises from a non-equilibrium charge distribution in the electrolyte. The potential difference found in neuron cells and responsible for the transport of electric signals arises from the diffusion potential, also [84].

This effect is also responsible for a shift in potential of the current minimum, more or less pronounced, that otherwise would happen at 0 V. The larger current seen at 0 V, compared to its minimum, suggests that an internal electric field, most likely caused by the electromotive forces, is present [86].

4.1.8.2 Crossing of the RS curve for negative potentials

During some cycles, a crossing of the curve in the negative potential region was observed, as one can see in fig. 4.23, in this particular case between -250 and -200 mV, but more generally, in the interval of -250 to -150 mV. According to the literature [88–90], this crossover

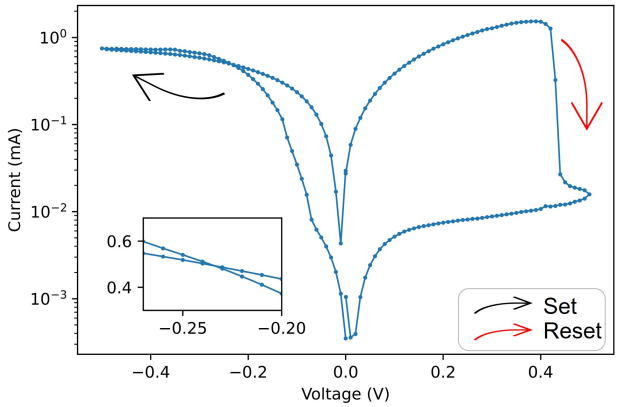

FIGURE 4.23: RS cycle with a crossing of the curve for potentials between -250 to -200 mV (0.5 mol/l and platinum top electrode at a 0.40 mm spacing).

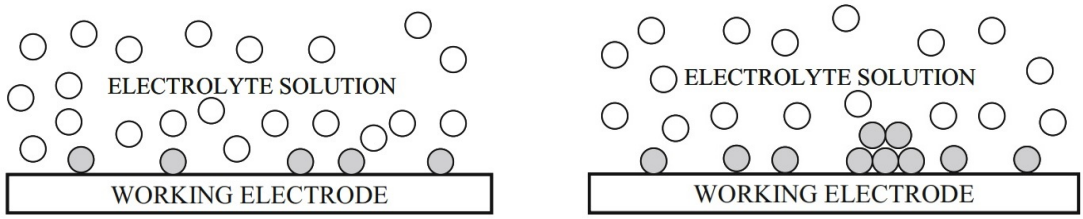

FIGURE 4.24: Electrode surface (A) before nucleation and (B) after nucleation. The white circles represent the metal ions present in the solution and the dark circles represent the metal atoms adsorbed onto the electrode surface. Retrieved from [87].

of the curve is due to the nucleation of copper atoms in the top electrode, apart from the main filament present in it. For high enough potentials, that surpass the equilibrium potential of the bulk metal crystal dipped in a solution of metal ions that create an overpotential, small clusters of atoms of the metal present in the electrolyte, copper in this case, start forming in the working electrode, which is the nucleation process previously mentioned (this process begins in the ascending phase of the curve for V $\sim$ -230 mV; fig. 4.24). However, with the decrease of voltage, when it reaches the minimum applied value, dissolution of those same clusters begins to take place, until they are mostly gone (this process begins in the descending part of the curve and ends when the potential reaches V $\sim$ -230 mV) [87]. So, the nucleation of copper atoms in the working electrode past a certain potential (that makes for a small current increase) and their dissolution (that makes for a small current decrease) are the reason for the crossing observed in some of the I-V curves. There are many reasons that can explain why, however, it does not always happen. The literature on this topic refers that several parameters can affect nucleation growth: pH of the solution, temperature, content of water in air, pressure, and others [91]. One of the main disadvantages of the measuring method is its variability: for each measurement a new drop of solution is deposited in the setup, that has a different temperature than the previous, each day the water content in the air might be different and room temperature might be different as well. Furthermore, there might be impurities in the bottom electrode, that, if not properly cleaned, can interfere with the solution. Since the nucleation process is so sensitive, and usually performed in a glove box, all these factors combined explain why nucleation takes place ever so often.

4.2 Copper(II) sulphate pentahydrate mixed with the deep eutectic solvent (choline chloride + glycerol)

With the rise of DESs and their desirable properties, a device was built where the solution was a mix between the DES and the previous used copper sulphate solution. The following sections will serve as its characterisation in terms of RS cycles, endurance, data retention and potentiation and depression. An attempt to gel this mix was also made, with results and characterisation also shown in the following sections. For all the measurements made, the copper sulphate concentration was of 0.5 M.

4.2.1 Resistive switching behaviour

Initially, in order to determine if the device presented the RS behaviour, a small study for the different applied potentials was made regarding pulse width, interpulse width, and voltage range, with results showing in fig. 4.25a, 4.26a and 4.27a, respectively. One important disclaimer is that, for all these measurements, the device ArC One was used, which presented some limitations, namely, for too high resistances near the 0 V, the data was returned as "inf" instead of a value. This leads to the implication that R_{Off} is undetermined, with the only knowledge being that it is a very high value ($>10^5$ Ω). To give some clarity on the order of magnitude of what the value might be, for each measurement, the highest reported resistance was used to substitute every single "inf" value, so that one knows, that the R_{Off} is at least higher than that. To differentiate these points from the actual resistances read by the device, in every single graph and for each curve there are two types of symbols, a circle and an asterisk, being that the first one represents real values returned by the device and the second one represents the "inf" values substituted by the highest reported resistance.

Firstly, taking a closer look at figs. 4.25a and 4.26a, for the pulse and interpulse width study, it is possible to see that a very similar LRS value was obtained in all, this being further proven by the calculated R_{On} presented in figs. 4.25b and 4.26b, roughly in the order of magnitude of 10^4 Ω. When it comes to HRS, it presented a larger variability, as one can see by the R_{Off} in figs. 4.25b and 4.26b, ranging anywhere from 10^5 to 10^9 Ω (however, as previously stated, these may not be the real values of resistance, just the smallest possible). Since higher R_{Off}/R_{On} ratios are desired, and looking at figs. 4.25c and 4.26c, where they are portrayed, the higher ratios (10^5) were obtained for pulse widths

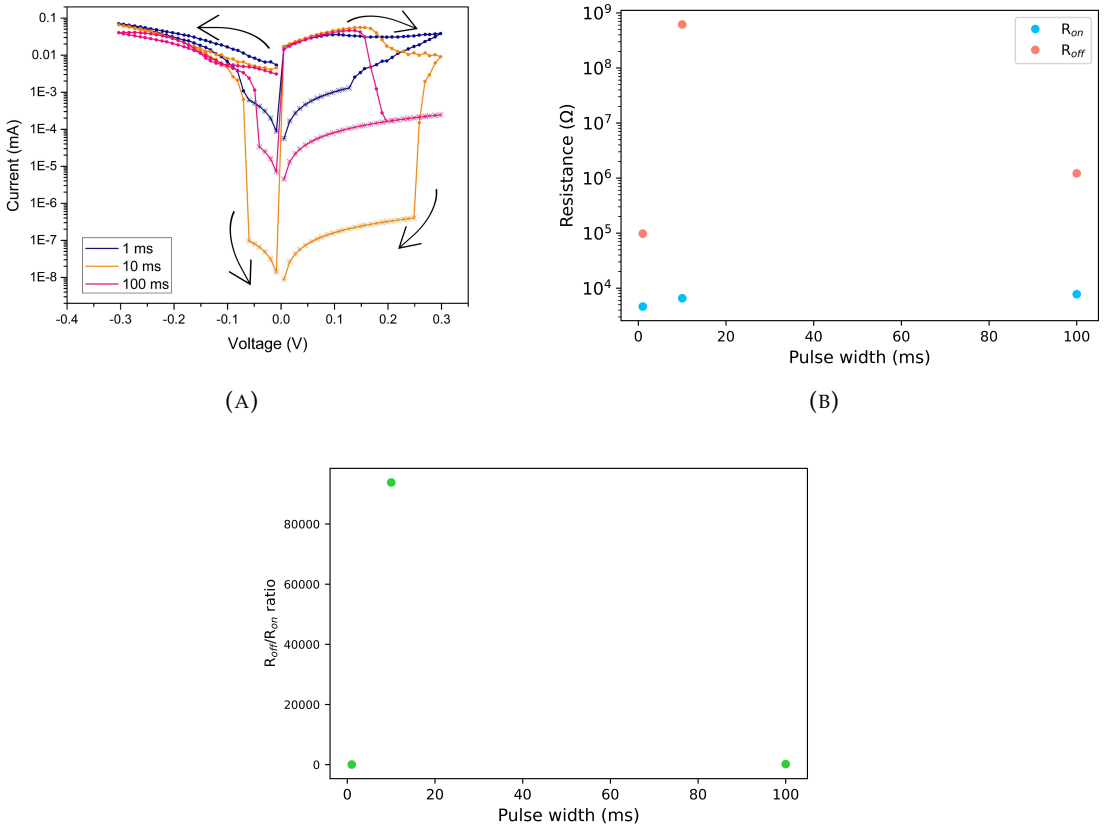

FIGURE 4.25: (A) RS cycles obtained from voltage sweeps ranging from -300 to 300 mV, with interpulse width of 100 ms and pulse width of 1, 10 and 100 ms. (B) R_{On} and R_{Off}, and (C) R_{Off}/R_{On} ratio obtained for each pulse width. Reading voltage of 50 mV.

of 10 and 100 ms. These values are already impressive because they are much higher than the reported by the previous device. Thus, these pulse parameters were used for the study of potential range. Now looking at fig. 4.27a, for that same potential range study, it is observed that the LRS remains closely the same throughout all ranges which is then verified by the R_{On} values present in fig. 4.27b, that are within the 10^4 Ω order of magnitude. As for HRS, there is not a clear tendency followed, as one can see by R_{Off} in fig. 4.27b, which may indicate that the values used do not correspond to the real ones. Now taking a look at fig. 4.27c, one can verify that the highest resistance ratio was obtained by the range of applied potential of [-3, 3] V, with a ratio of about 10^5, an extremely good value for the states' separation.

One interesting phenomenon that happened with this device has to do with its current path. As opposed to the previous device, this one started from LRS, from 0 → -300 mV, changed to HRS from -300 mV → 0 mV, went back to the initial LRS state from 0

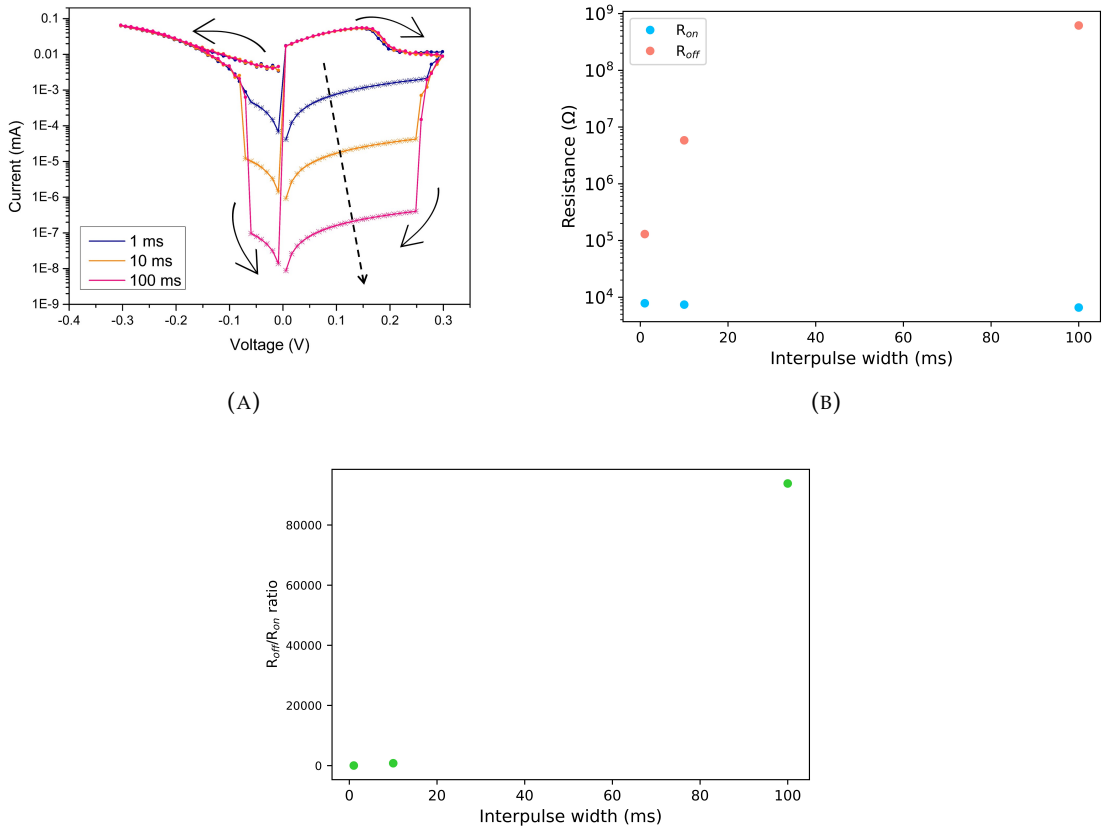

(A) (B)

(C)

FIGURE 4.26: (A) RS cycles obtained from voltage sweeps ranging from -300 to 300 mV, with pulse width of 10 ms and interpulse width of 1, 10 and 100 ms. The dashed arrow represents the tendency of the curves. (B) R_{On} and R_{Off}, and (C) R_{Off}/R_{On} ratio obtained for each interpulse width. Reading voltage of 50 mV.

$\rightarrow$ 300 mV and, finally, returned to HRS from 300 $\rightarrow$ 0 mV. So, it is naturally in the conducting state, and applied bias is responsible to the transition to HRS. This implies that a new mechanism of conduction is present; however, further study with the assistance of the Chemistry Department is needed to determine what it might be. Besides the different mechanism, the device transited from non-volatile to volatile as it moved from being composed of copper sulphate diluted in water to copper sulphate diluted in the DES. What this means is that the previous device presents a long lifetime, so the device remains stable after the set process, if no other bias is applied, however the present device presents a short lifetime, which means that it returns to its initial state when no bias is applied [92, 93]. This is more noticeable when one looks at the arrows in figs. 4.25a, 4.26a and 4.27a and sees that, after the device was set to the HRS, it did not sustain its state when the applied potential reached 0 V, switching back to its initial LRS state. One can hypothesise that when no potential is applied, the charge carriers are configured in such a way

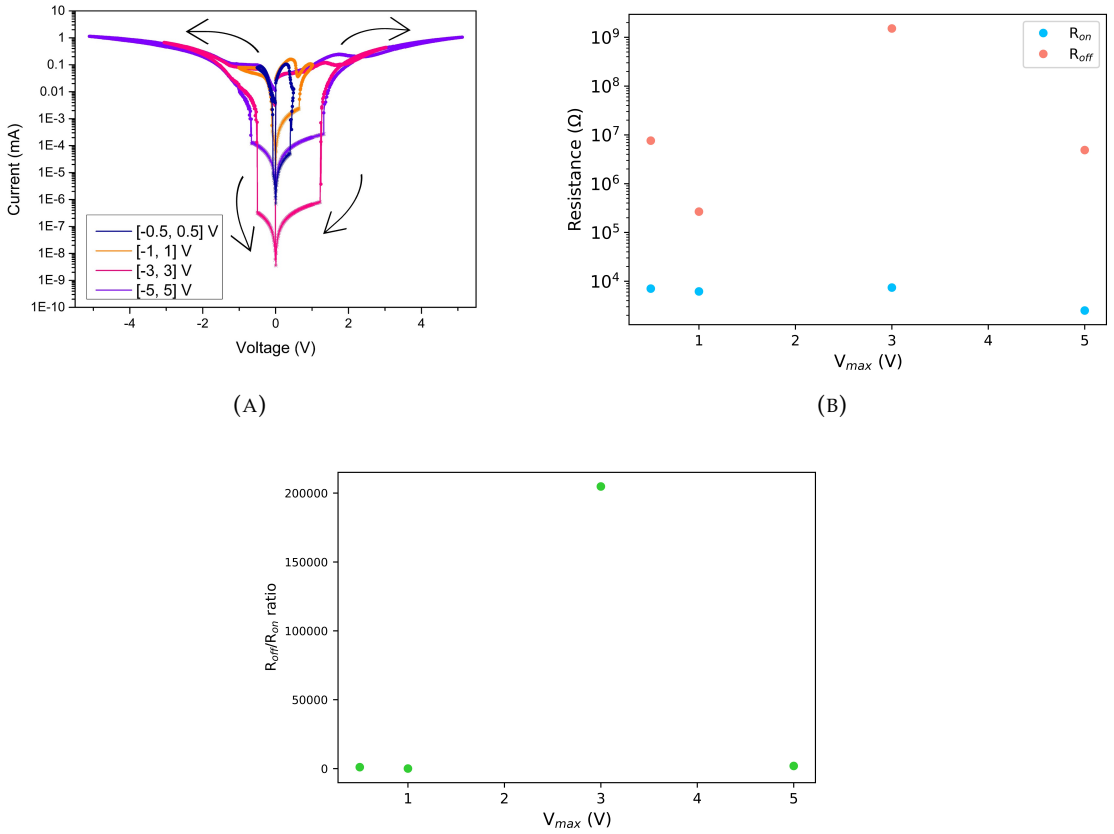

(A) (B)

(C)

FIGURE 4.27: (A) RS cycles obtained from voltage sweeps with pulse width of 10 ms, interpulse width of 100 ms and potential ranges of [-0.5, 0.5], [-1, 1], [-3, 3] and [-5, 5] V. (B) R_{On} and R_{Off}, and (C) R_{Off}/R_{On} ratio obtained for each potential range. Reading voltage of 50 mV.

that facilitates electrical conduction and, when a bias (positive or negative) is applied, a reconfiguration occurs that increases resistance. When the bias is removed, the charge carriers relax into their initial configuration, originating the volatile behaviour. Furthermore, the nucleation phenomenon also took place here, although in symmetric potentials. Since the sole difference between this device and the previous made ones is the solvent, one can assume that the solvent is the cause for this change in behaviour.

4.2.2 Endurance and data retention

To further assess the dynamic properties of the device, endurance and data retention tests were made, with results showing in fig. 4.28a and 4.28b.

As for endurance, the device presented high and stable endurance throughout the application of pulses, with a clear separation of states and with a ratio of Off and On

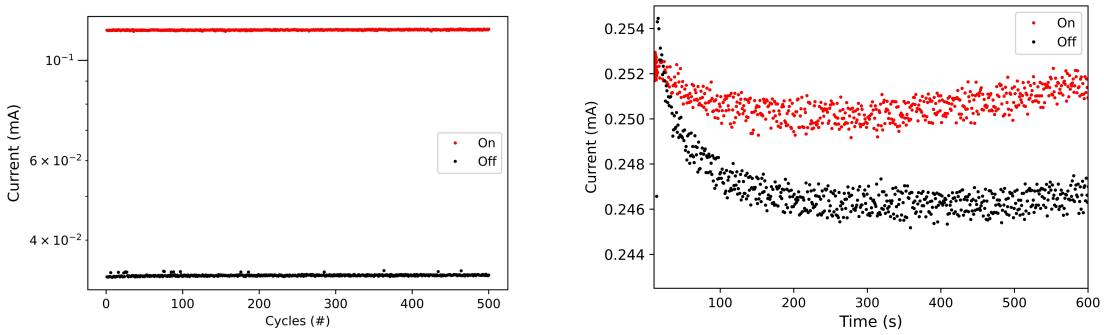

(A) (B)

FIGURE 4.28: (A) Endurance behaviour displayed by the device over 500 cycles. (B) Data retention of the device over 600 s, at a reading voltage of 50 mV.

resistances of roughly 2, all through the 500 cycles (R_{On} of about 1715 Ω and R_{Off} of about 2713 Ω). Even though stability is ensured, R_{Off}/R_{On} is still low as far as separation of states go. As for data retention, the device shows again volatility behaviour, not being able to hold the state as soon as the bias is removed, decaying rapidly and presenting a rather disperse behaviour. Despite two states being differentiated at close scale, their currents are so close that they cannot be considered distinct (the ratio of resistances is $\sim$ 1).

4.2.3 Neuromorphic properties

For a final assessment of the new device, a study of potentiation and depression was made, in order to test the device's learning abilities, in the form of a conductance increase or decrease upon repeatedly stimuli application. For that, the pulse width, interpulse width and amplitude were again varied, in order to find the best possible response from the device. The results are shown in fig. 4.29, 4.30 and 4.31.

As far as the pulse width goes, one can conclude that the best time is of 10 ms. For 1 ms of pulse width, a very short pulse, the device cannot be excited enough to move to a LRS and maintain itself there, presenting, therefore, a decaying potentiation in terms of conductance, which is not what is preferred. For 100 ms of pulse width, the pulse becomes too long, saturating the device with current, which leads to, for the potential used in the pulses, its maximum and minimum possible conductance almost right way, leaving no room for the potentiation or depression of the device to occur. For the 10 ms pulse width, even though potentiation is not expressive, probably due to a too low applied potential, the pulse is still enough to transport the device to a LRS and maintain it there and it also

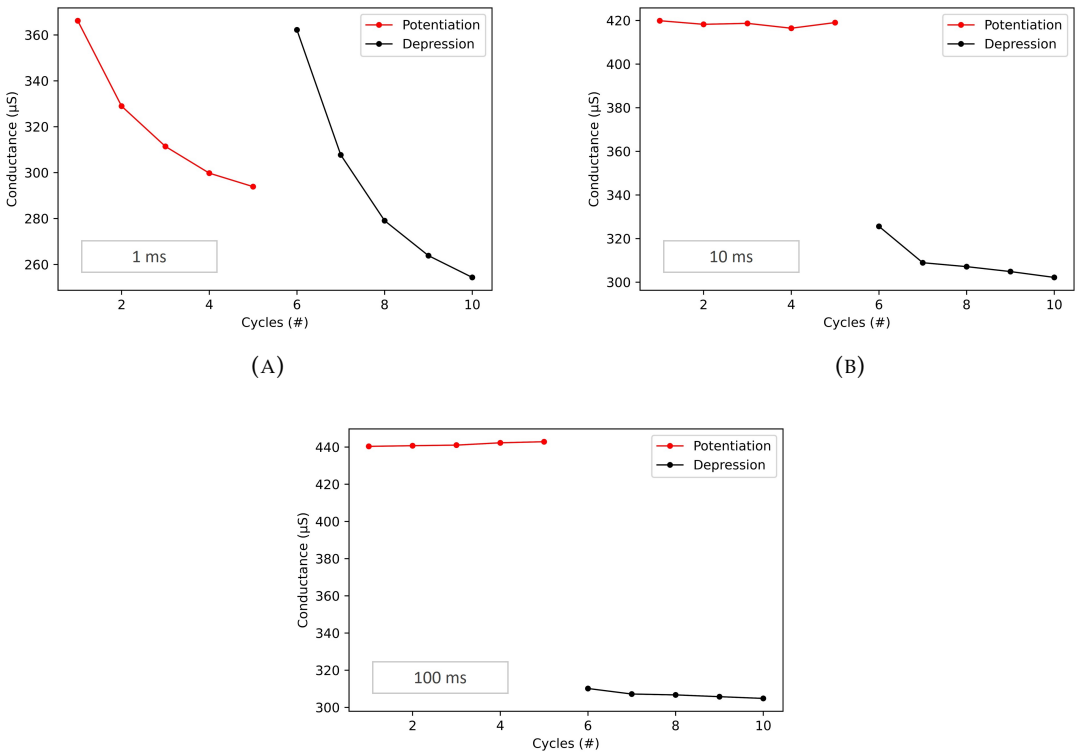

(A) (B)

(C)

FIGURE 4.29: Behaviour displayed by the device resulting from consecutive applied pulses with voltages of -60 mV for potentiation and 90 mV for depression, interpulse width of 1 ms and pulse width of (A) 1, (B) 10 and (C) 100 ms.

leads the device to a depression behaviour. It also presented similar conductance values than the ones obtained for 100 ms. With all these aspects in mind, 10 ms was the pulse width used in further measurements.

When it comes to the interpulse width, the best results occurred for the 1 ms interpulse width. As for the highest value of interpulse width, it did not show any potentiation or depression, with the conductance being stagnant as cycles went on. For the 10 ms interpulse width, depression was a little clearer, but potentiation did not happen, with the conductance being also constant as cycles went on. Both interpulse widths reached the same values of conductance for potentiation and depression, 420 and 320 μS, respectively. Finally, the 1 ms interpulse width presented the highest separation between states of potentiation and depression (with values of about 420 and 300 μS, respectively) and it also presented clearer and more pronounced depression than the rest. Potentiation was still not observed, but this is due to the low potential pulse magnitude that was used for the test, as it will be clear later. Still, the interpulse time of 1 ms presented the better properties out of all the interpulse times, being the one chosen for further measurements.

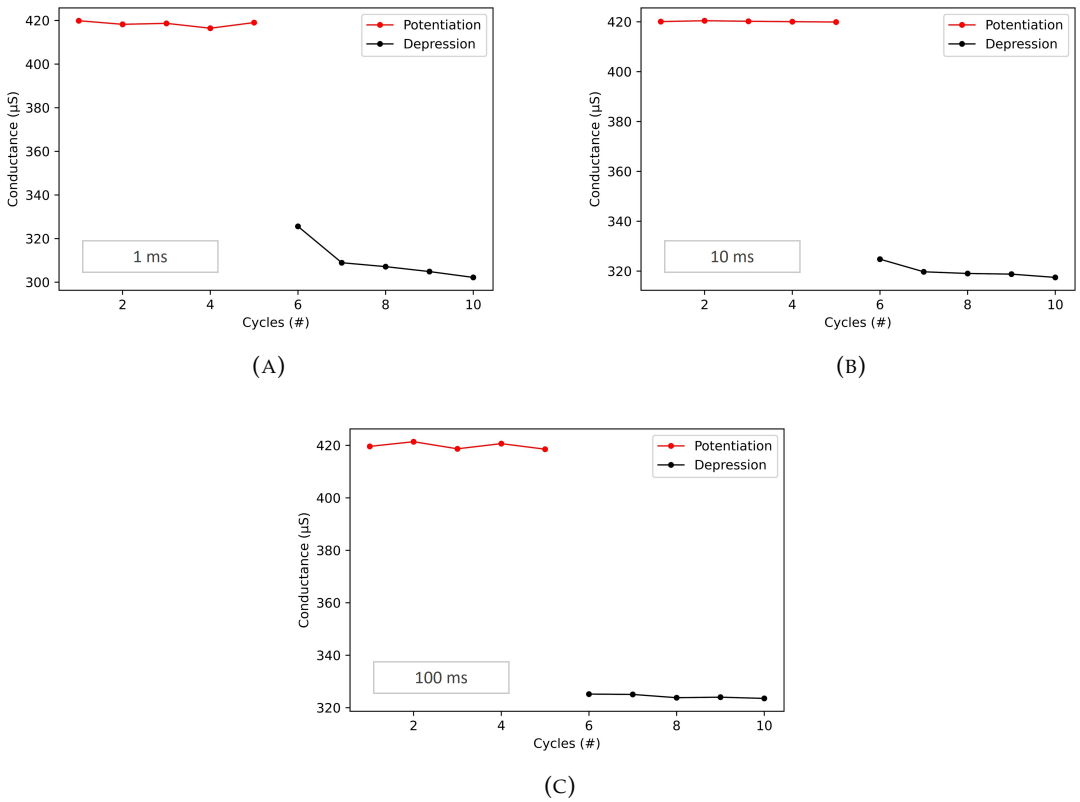

(A) (B)

(C)

FIGURE 4.30: Behaviour displayed by the device resulting from consecutive applied pulses with voltages of -60 mV for potentiation and 90 mV for depression, pulse width of 10 ms and interpulse width of (A) 1, (B) 10 and (C) 100 ms.

With pulse and interpulse width defined for the applied pulses, a study for the best possible potentials to achieve learning abilities was performed. From that study it was concluded that the potentials that achieved better performance of the device were of -200 mV for potentiation and 90 mV for depression. For the potentials of -60 and 90 mV, the device was able to achieve depression but not potentiation, which lead to the increase of the magnitude of the potentiation pulse to -100 mV. With this new potential, potentiation was finally possible, achieving values of 500 μS, contrasting with the 420 μS achieved previously. However, it was still a small increase in conductance, therefore a new increase in the potentiation pulse magnitude was performed, now of -200, reaching the optimal results (fig. 4.31c). With these potentials (-200 mV and 90 mV), the device was able to achieve both potentiation and depression, reaching a maximum conductance of about 600 μS and a minimum conductance of about 350 μS. It presented a steady growth in potentiation and a rapid decrease in depression. Comparing the best potentiation and depression achieved from the present device with the previous device made out of the copper sulphate solution, it is clear that it underperforms. The previous device was able

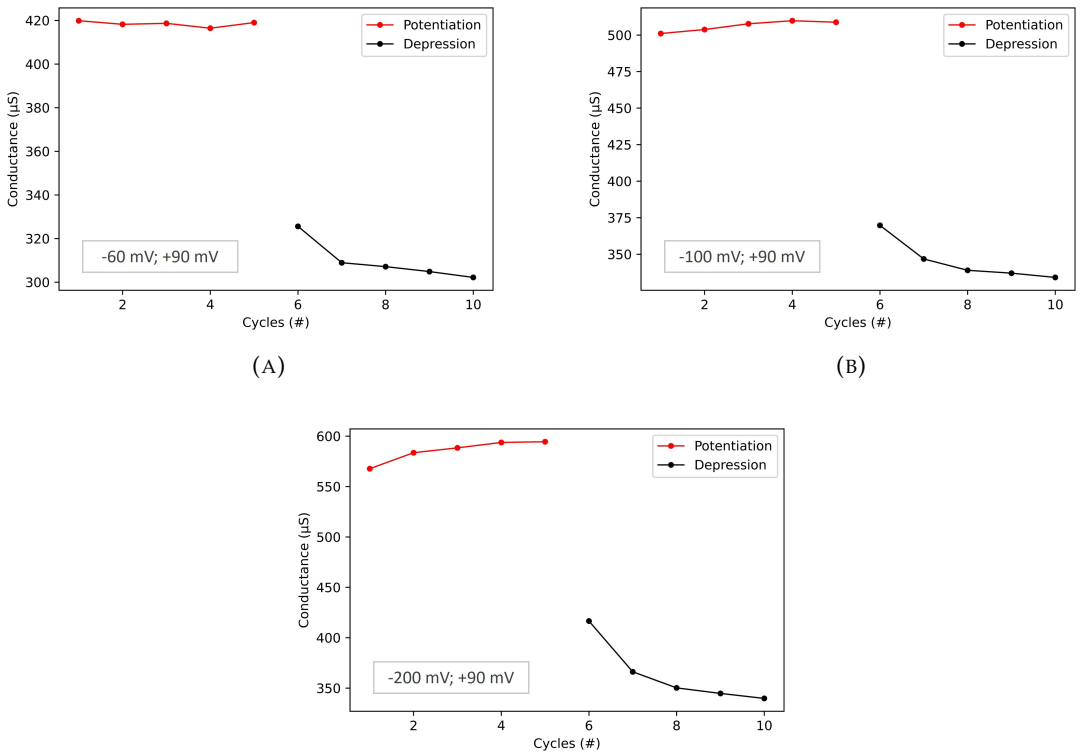

FIGURE 4.31: Behaviour displayed by the device resulting from consecutive applied pulses with pulse width of 10 ms, interpulse width of 1 ms and voltages of (A) -60 mV (for potentiation) and 90 mV (for depression), (B) -100 mV and 90 mV and (C) -200 mV and 90 mV.

to achieve potentiation and depression, with conductance in the order of 1600 and 600 μS, respectively, for smaller operation potential.

4.2.4 Gelling of the mixture

In order to broaden the scope in which the device can be used for, an attempt to gel the DES and copper sulphate mix was made. With the gel form, instead of liquid, problems such as leakage, if used in microchips, and evaporation would no longer be an issue, with the addition that a gel is flexible and can adapt to many shapes (which is ideal for implantable applications, for example). However, after the gelling production, it was noted that the crosslinking did not occur as expected, remaining quite liquid still. This was due to the fact that the water content, for processes of gelling, needs to be extremely well controlled and, since the copper sulphate was hydrated, full cross-linking did not occur. For future work, an adjustment in the recipe for gelling needs to be made in order

to accommodate this specificity. Still, an analysis was carried on, as presented in the next sections.

4.2.4.1 Resistive switching behaviour

For the study of the RS behaviour in the gel, the pulse width and interpulse width of the applied stair-like potential were the same as the ones reported as achieving better results in section 4.2.1. The voltage sweep ranges were varied to test which obtained better results. The obtained RS outcomes can be seen in fig. 4.32a.

As one can see, RS behaviour is present and has similar characteristics as the mix previously characterised, namely, the fact that it begins in the LRS and that it remains volatile, as seen by the arrows that determine the path of the current, which would be expected since the solvent remained the same. However, a difference noted is the fact that for the two higher voltage ranges used, the HRS for the negative portion of potential

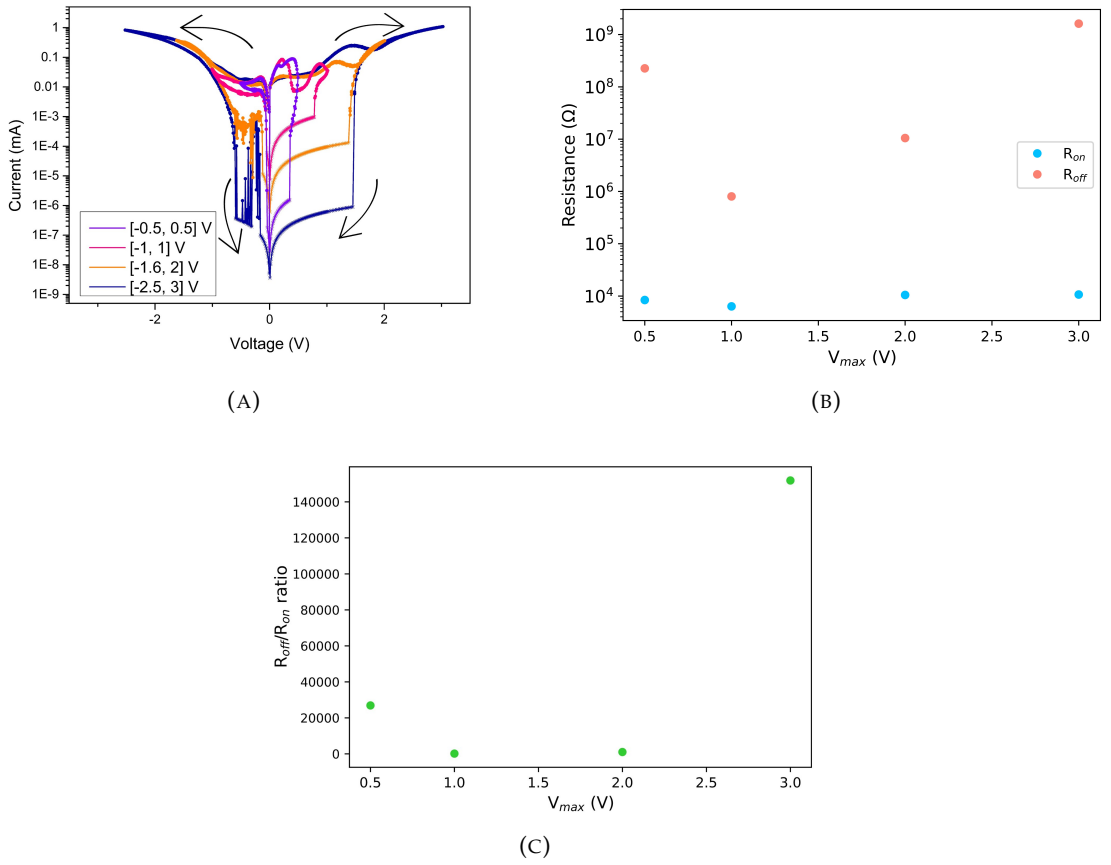

FIGURE 4.32: (A) RS cycles obtained from voltage sweeps with pulse width of 10 ms, interpulse width of 100 ms and potential ranges of [-0.5, 0.5], [-1, 1], [-1.6, 2] and [-2.5, 3] V. (B) R_{On} and R_{Off}, and (C) R_{Off}/R_{On} ratio obtained for each potential range. Reading voltage of 50 mV.

presented an erratic behaviour, which can be an attempt of the device to return to its initial state. Since this did not happen in previous devices, one can assume that the gel used, or its components, are somewhat responsible for this behaviour. Taking a look at the On and Off resistances of the curves, in fig. 4.32b, it is clear that the On resistance remains almost the same ($\sim 10^4$ Ω) no matter what the range of applied potential is, and the Off resistance has more variability, having an initial spike, then decreasing for the second range of potentials, then increasing steadily again until the last range of potentials, varying from $\sim 10^6$ until 10^4 Ω. The same disclaimer made about the R_{Off} values apply to this case. Finally, looking at fig. 4.32c, it is clear that the highest On/Off ratio was provided by the highest range of potential, with a value of over 10^5, which is extremely high as desired, and of equal value as the previous device. The lowest ratio achieved was of 10^2, which is already a good value.

4.2.4.2 Endurance and data retention

Endurance and data retention tests were performed in the device, with results shown in figs. 4.33a and 4.33b.

As far as endurance goes, the device shows good results. It was able to achieve over 5000 cycles, with quite steady states and reliable results. Initially, the R_{Off} and R_{On} presented values of around 1008 and 587 Ω, respectively, and by the end of the cycles they decreased to slightly 912 Ω and 393 Ω. The ratio between resistances obtained was constant at 2, the same as the previous device, which is a low value, but given that the states are very well defined for various cycles, it can still be considered acceptable. Now looking at the data retention results, it is clear that low retention of states occurred, as it would be

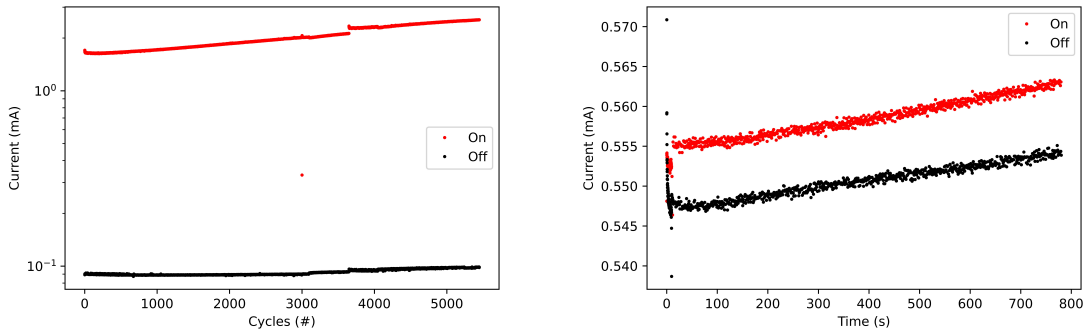

(A) (B)

FIGURE 4.33: (A) Endurance behaviour displayed by the device over 5000 cycles. (B) Data retention of the device over 800 s, at a reading voltage of 50 mV.

expected on a volatile device. Even though one can tell the difference between two states at such close scale, their current and, therefore, resistance values are so close together that they cannot be considered two distinct, well-defined states, making them, basically, the same state (the ratio of resistances is ~ 1).

4.2.4.3 Neuromorphic properties

For potentiation and depression, the same pulse width and interpulse width were used as the ones studied and determined to be the better candidates for the device with the mix of the DES and the copper sulphate. Potentiation and depression characteristics were assessed for 10 consecutive cycles of each, for three different pulse amplitudes, and 30 consecutive cycles of each, for the pulse amplitude with better outcome, as shown in figs. 4.34a, 4.34b, 4.34c and 4.34d.

Initially, the same pulse amplitudes as the ones used for the DES and copper sulphate mix were adopted. Depression was very clear, which meant that its amplitude was well

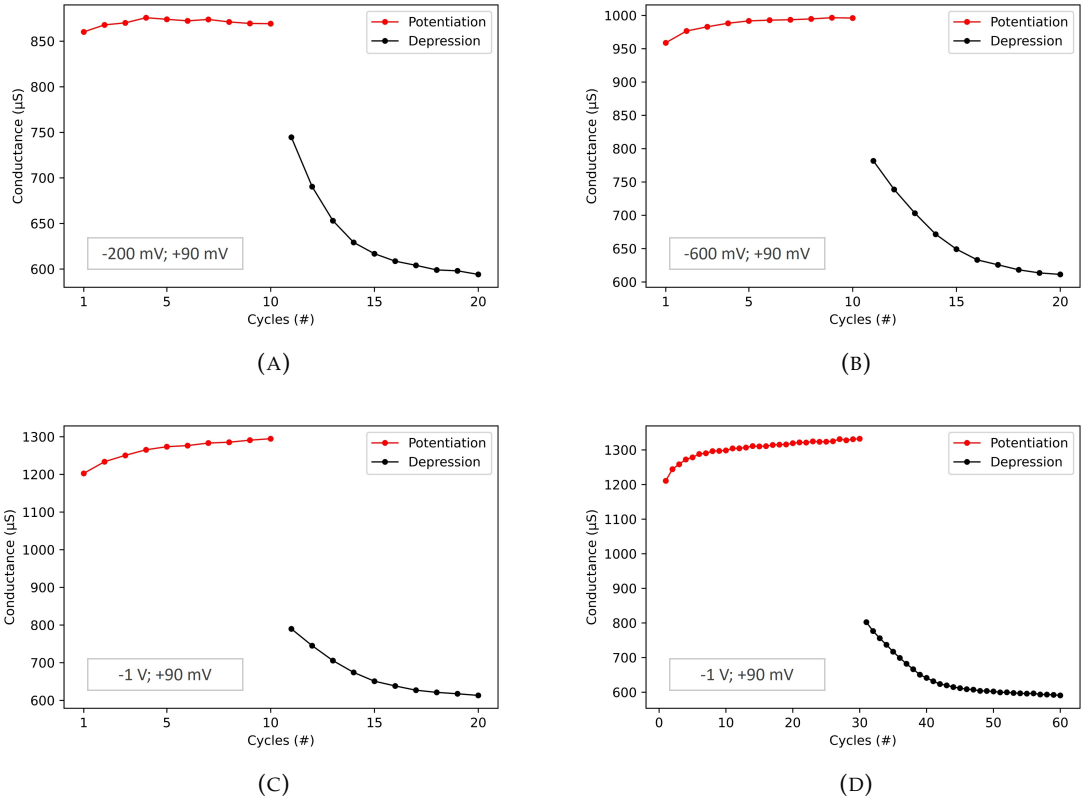

FIGURE 4.34: Behaviour displayed by the device resulting from (A) 10 consecutive applied pulses of -200 mV for potentiation and 10 of 90 mV for depression, (B) -600 and 90 mV, (C) -1 V and 90 mV, and (D) 30 pulses of -1 V and 90 mV, with interpulse width of 1 ms and pulse width of 10 ms.

suited, but as far as potentiation goes, it was very minimal. Conductance achieved a maximum value of 850 μS and a minimum of 600 μS. Because of that, an amplitude of -600 mV instead of -200 mV was tested. Depression was, again, very clear, achieving a conductance minimum of 600 μS, and potentiation started to show, achieving a conductance maximum of 1000 μS. However, it was still low, so a last amplitude rise was tested, of -1 V (fig. 4.34c). As one can tell, potentiation and depression are clearly visible, for both 10 and 30 consecutive pulses, with gradual and constant increase in conductance for potentiation in each cycle, and decrease in conductance for depression in each cycle, except for the initial stimuli of both that suffer a steeper growth and decay. Conductance achieved high values, reaching over 1300 μS for potentiation, and presented a minimum of about 600 μS, for depression. Comparatively with the same solution without the gel process, potentiation and depression presented better values because, although gel diminishes ion movement, the applied voltage was increased drastically compared to the previous device.

4.3 Summary of results

The overall performance of the studied systems is shown in table 4.3. Regarding R_{Off}/R_{On}, it is clear that the better value of 10^5 occurs with the DES (with and without gelling). However, the ratio of the $CuSO_4$ solution by itself may be sufficient depending on the application. Both V_{set} and V_{reset} presented low values for the solution, which can be further improved considering the still large distance between electrodes. Potentiation and depression were obtained in all cases, with better performance for the $CuSO_4$ solution, due to the high achieved condutances for the lowest applied pulses, -60 and 90 mV, which is truly remarkable. High endurance was achieved in all three cases, with the most cycles achieved by the gel. Only the $CuSO_4$ solution showed retention, due to the volatility observed once the DES was introduced in the system. The copper sulphate aqueous solution had a non-volatile behaviour and the eutectic solvent solutions had a volatile behaviour.

TABLE 4.3: Summary of the results obtained on several devices (for $CuSO_4$ concentrations of 0.5 mol/l, 1 mm distance between electrodes, platinum top electrode with a diameter of 0.1 mm and room temperature).

Results	$CuSO_4$	$CuSO_4$ + DES	$CuSO_4$ + DES gel
Highest R_{Off}/R_{On}	10^2	10^5	10^5
V_{set} (V)	$\sim$ -0.07	$\sim$ -0.8	$\sim$ -0.8
V_{reset} (V)	$\sim$ 0.27	$\sim$ 1.2	$\sim$ 1.4
Endurance (cycles)	$>$1000	500	$>$5000
Retention (s)	10^3	-	-
$G_{potentiation}$ (μS)	$\sim$ 1600	$\sim$ 600	$>$1300
$G_{depression}$ (μS)	$\sim$ 600	$\sim$ 350	$\sim$ 600
$V_{potentiation}$ (mV)	-60	-200	-1000
$V_{depression}$ (mV)	90	90	90
Volatility	No	Yes	Yes

Chapter 5

Conclusions and outlook

With the rapid evolution in computer software and the difficulty of hardware to follow it, new computation paradigms arose to solve this issue. Neuromorphic computing emerged as one of the possibilities, being inspired by the brain architecture in humans. In order to mimic the synapses of the brain, that are responsible for information processing and storage of memory in the form of synaptic strength, a new generation of devices surfaced, that present resistive switching. These devices have been the subject of intense study since they were first experimentally discovered, in 2008 [25], however, there is still information lacking when it comes to the use of liquids as the active layer. Liquid solutions are a great candidate to be used in the devices due to their ionic conductivity, their adaptability and flexibility, and easy and low cost of fabrication. In order to, somehow, mitigate this problem, this dissertation came to light.

This work focused on the creation and characterisation of a liquid-based artificial synapse device. It is composed of a copper sulphate solution ($CuSO_4.5H_2O$), a top electrode with variable material and a copper active bottom electrode. Presents bipolar RS, non-volatile behaviour, endurance, and data retention characteristics, all of this at very low power (<300 mV). The conduction mechanism of the device can be described by the formation of a copper filament in the solution that, upon connecting both electrodes, is in the conductive state. This takes place when a favourable electrical field in applied to the device. In order to characterise the devices, several parameters were varied, such as range of applied potentials, solution concentration, temperature of the solution, electrode distance and material of the top electrode, and its response was studied. Four properties were particularly aimed for: i) low current response by the device, because it implies less power consumption, but also less chance of Joule heating effect, that evaporates the water

in the solution quicker and destabilizes the filament, ii) higher ratio between the On and Off states, because it implies less leakage probability, iii) reliability and iv) stability over cycles and time.

As far as the range of applied potentials, it was noted that similar current response and ratio of states were achieved for each one, but that the smaller range had overall better results when it comes to reliability, so, [-300, 300] mV proved to be the most appropriate range of applied potentials. When it comes to the solution concentration, three different ones were used and it was noted that, the higher the concentration, the larger the current response by the device, and the smaller the ratio between On and Off states. It was also noted that the best endurance and data retention properties were achieved by the smallest and intermediate solution concentrations, of 0.1 and 0.5 mol/l. After analysing all the results, the concentration that best balances all the required aspects is the intermediate one. When it came to temperature, the solution was first cooled down until 11°C and then heated up until 72°C. It was noted that as the solution was cooled, the ratio of states remained approximately the same, and the current response of the device diminished and that, as the solution was heated, no clear tendency was found, probably due to the high particle vibration felt in the solution and the water evaporation phenomenon. Overall, the best results were achieved for room temperature. The electrode distance that possessed the best results was the larger one tested, 1.26 mm, because it presented the less current response by the device and the highest ratio of states. As far as the top electrode goes, several materials were tested, and the best results were achieved for the platinum wire with a diameter of 0.1 mm, presenting less current response and higher ratio of states than the others. Furthermore, a study of the diameter of the filaments created was performed using the resistance of a wire formulation, and the results ranged from 89 to 240 nm. The overall state ratios, even though some presented higher values than others, remained in the order of 10^0 - 10^2 which may be a low value for what would be expected of a device with electronic implementation prospects. To further characterise the device, equal pulses were applied, consecutively, with different potentials and potentiation and depression characteristics were tested. The device proved to have potentiation and depression capabilities, with conductance going as high as 1600 μS. Furthermore, this was achieved with pulses that are the same magnitude as the ones seen in the action potential of the cells. Finally, further phenomena were studied, and it was observed that, sometimes, nucleation of copper in the platinum electrode took place due to the overtaking

of the equilibrium potential and a nanobattery effect was present, due to the existence of electromotive forces that caused it.

With the rise of the use of ionic liquids to help enhance the performance of electronic devices, its behaviour in the present device was explored. However, ionic liquids are hard to make and have high cost, therefore, it was chosen to use deep eutectic solvents as an alternative, because they present similar physical and electrical properties, even though their chemistry is different. Furthermore, they are cheap and easy to make. So, a mixture of the DES with the copper sulphate was made, introduced in the device, and analysed. Bipolar RS was achieved, with a range of potentials from [-3, 3] V presenting the best results, with similar current response as the others, but a ratio between states of 10^5, which is a considerable improvement compared to the previous device. It presented endurance over 500 cycles, with very stable and well-defined states but with very low resistance ratio. Some differences were noted in regard to the previous device, mainly that the current path was different, beginning in the low resistive state, as opposed to the high resistive state, and, with the input voltage, moved to the high resistive state, as opposed to the low resistive state. This change in states was expected due to the fact that the DES is highly conductive by itself, however, the mechanism in which the change in states happens is not yet understood. Another difference noted in this device is that it presented volatile behaviour, so, its ability to hold the low resistive state was very poor, when no bias was being applied. Potentiation and depression were also achieved, but conductance reached lower values than the previous device, about 600 μS. A further experiment was made, the gelling of the mixture. However, the high quantity of water present in the copper sulphate prevented the crosslinking from fully taking place, originating still a somewhat liquid device. RS was once more observed with similar characteristics as before. Endurance studies showed highly stable and well-defined states up to 5000 cycles, despite the low ratio between resistances. Finally, potentiation and depression were also achieved, with conductance reaching 1300 μS, which is an improvement compared with the mixture without the gelling.

As for future work, a deep understanding of the behaviour that governs the copper in the first device is needed, due to the high variability of results obtained. This could be pursued through the use of more sophisticated techniques (e.g., SEM to better understand the nucleation mechanism happening) that can shed a light into micro and nanoscopic

processes in the copper, as the reactions are taking place as well as a more controlled measurement environment. A study of its possible implementation in an array of devices is also an important step to fulfil its role in artificial neural networks, as well as its incorporation into flexible and soft electronics, to broaden its spectrum of application. The use of DESs also needs to be further investigated, in order to both understand the conduction mechanism it presents and optimize the mixture with the copper sulphate to obtain the best possible results.

Bibliography

[1] Q. Wan, M. T. Sharbati, J. R. Erickson, Y. Du, and F. Xiong, "Emerging artificial synaptic devices for neuromorphic computing," *Advanced Materials Technologies*, vol. 4, no. 4, pp. 1–34, 2019. [Online]. Available: https://onlinelibrary.wiley.com/doi/abs/10.1002/admt.201900037

[2] Y. Park, M.-K. Kim, and J.-S. Lee, "Emerging memory devices for artificial synapses," *Journal of Materials Chemistry C*, vol. 8, no. 27, pp. 9163–9183, 2020. [Online]. Available: http://dx.doi.org/10.1039/D0TC01500H

[3] F. Corinto, A. Ascoli, and M. Gilli, "Class of all i-v dynamics for memristive elements in pattern recognition systems," in *The 2011 International Joint Conference on Neural Networks*, 2011, pp. 2289–2296. [Online]. Available: https://ieeexplore.ieee.org/document/6033514

[4] C. Dias, H. Lv, R. Picos, P. Aguiar, S. Cardoso, P. P. Freitas, and J. Ventura, "Bipolar resistive switching in Si/Ag nanostructures," *Applied Surface Science*, vol. 424, pp. 122–126, 2017. [Online]. Available: https://doi.org/10.1016/j.apsusc.2017.01.140

[5] M. U. Khan, G. Hassan, and J. Bae, "Soft ionic liquid based resistive memory characteristics in a two terminal discrete polydimethylsiloxane cylindrical microchannel," *Journal of Materials Chemistry C*, vol. 8, no. 38, pp. 13 368–13 374, 2020. [Online]. Available: https://doi.org/10.1039/D0TC03334K

[6] D. Kim and J. S. Lee, "Liquid-based memory and artificial synapse," *Nanoscale*, vol. 11, no. 19, pp. 9726–9732, 2019. [Online]. Available: https://doi.org/10.1039/C9NR02767J

[7] D. Seok Jeong, I. Kim, M. Ziegler, and H. Kohlstedt, "Towards artificial neurons and synapses: A materials point of view," *RSC Advances*, vol. 3, no. 10, pp. 3169–3183, 2013. [Online]. Available: DOIhttps://doi.org/10.1039/C2RA22507G

[8] I. B. Levitan and L. K. Kaczmarek, *The Neuron: Cell and Molecular Biology*, 4th ed., 2015. [Online]. Available: https://doi.org/10.1093/med/9780199773893.001.0001

[9] "Baby's brain begins now: Conception to age 3 — urban child institute." [Online]. Available: http://www.urbanchildinstitute.org/why-0-3/baby-and-brain

[10] M. Devices, "What is an Action Potential, Action Potential Chart, Membrane Potential — Molecular devices," p. 1, 2022. [Online]. Available: https://www.moleculardevices.com/applications/patch-clamp-electrophysiology/what-action-potential

[11] C. Zamarreño-Ramos, L. A. Camuñas-Mesa, J. A. Perez-Carrasco, T. Masquelier, T. Serrano-Gotarredona, and B. Linares-Barranco, "On spike-timing-dependent-plasticity, memristive devices, and building a self-learning visual cortex," *Frontiers in Neuroscience*, vol. 5, no. MAR, pp. 1–22, 2011. [Online]. Available: https://www.frontiersin.org/articles/10.3389/fnins.2011.00026

[12] N. K. Upadhyay, S. Joshi, and J. J. Yang, "Synaptic electronics and neuromorphic computing," *Science China Information Sciences*, vol. 59, no. 6, pp. 1–26, 2016. [Online]. Available: https://doi.org/10.1007/s11432-016-5565-1

[13] Y. Munakata and J. Pfaffly, "Hebbian learning and development," *Developmental Science*, vol. 7, no. 2, pp. 141–148, 2004. [Online]. Available: https://doi.org/10.1111/j.1467-7687.2004.00331.x

[14] Z. Brzosko, S. B. Mierau, and O. Paulsen, "Neuromodulation of Spike-Timing-Dependent Plasticity: Past, Present, and Future," *Neuron*, vol. 103, no. 4, pp. 563–581, 2019. [Online]. Available: https://doi.org/10.1016/j.neuron.2019.05.041

[15] A. Foncelle, A. Mendes, J. Jędrzejewska-Szmek, S. Valtcheva, H. Berry, K. T. Blackwell, and L. Venance, "Modulation of spike-timing dependent plasticity: Towards the inclusion of a third factor in computational models," *Frontiers in Computational Neuroscience*, vol. 12, no. July, pp. 1–21, 2018. [Online]. Available: https://doi.org/10.3389/fncom.2018.00049

[16] N. Deperrois and M. Graupner, "Short-term depression and long-term plasticity together tune sensitive range of synaptic plasticity," *PLoS Computational Biology*, vol. 16, no. 9, pp. 1–25, 2020. [Online]. Available: http://dx.doi.org/10.1371/journal.pcbi.1008265

[17] Q. Zhang, H. Yu, M. Barbiero, B. Wang, and M. Gu, "Artificial neural networks enabled by nanophotonics," *Light: Science & Applications*, vol. 8, no. 1, p. 42, 2019. [Online]. Available: https://doi.org/10.1038/s41377-019-0151-0

[18] I. N. da Silva, D. H. Spatti, R. A. Flauzino, L. H. B. Liboni, and S. F. dos Reis Alves, "Artificial neural networks: A practical course," *Artificial Neural Networks: A Practical Course*, pp. 1–307, 2016. [Online]. Available: https://doi.org/10.1007/978-3-319-43162-8

[19] M. Kubat, "Artificial Neural Networks," *An Introduction to Machine Learning*, pp. 117–143, 2021. [Online]. Available: https://link.springer.com/chapter/10.1007/978-3-030-81935-4_6

[20] F. Amato, A. López, E. M. Peña-Méndez, P. Vaňhara, A. Hampl, and J. Havel, "Artificial neural networks in medical diagnosis," *Journal of Applied Biomedicine*, vol. 11, no. 2, pp. 47–58, 2013. [Online]. Available: https://doi.org/10.2478/v10136-012-0031-x

[21] G. Dede and M. H. Sazli, "Speech recognition with artificial neural networks," *Digital Signal Processing*, vol. 20, no. 3, pp. 763–768, 2010. [Online]. Available: https://doi.org/10.1016/j.dsp.2009.10.004

[22] J. K. Basu, D. Bhattacharyya, and T.-h. Kim, "Use of artificial neural network in pattern recognition," *International journal of software engineering and its applications*, vol. 4, no. 2, 2010. [Online]. Available: https://www.researchgate.net/publication/228566377_Use_of_Artificial_Neural_Network_in_Pattern_Recognition

[23] M. Chattopadhyay, P. K. Dan, S. Majumdar, and P. S. Chakraborty, "Application of neural network in market segmentation: A review on recent trends," *Management Science Letters*, vol. 2, no. 2, pp. 425–438, 2012. [Online]. Available: https://doi.org/10.5267%2Fj.msl.2012.01.013

[24] L. O. Chua, "Memristor - The Missing Circuit Element," *IEEE Transactions on Circuit Theory*, vol. 18, no. 5, pp. 507–519, 1971. [Online]. Available: https://ieeexplore.ieee.org/document/1083337

[25] D. B. Strukov, G. S. Snider, D. R. Stewart, and R. S. Williams, "The missing memristor found," *Nature*, vol. 453, no. 7191, pp. 80–83, 2008. [Online]. Available: https://doi.org/10.1038/nature06932

[26] Y. Ho, G. Huang, and P. Li, "Dynamical properties and design analysis for nonvolatile memristor memories," *Circuits and Systems I: Regular Papers, IEEE Transactions on*, vol. 58, pp. 724 – 736, 2011. [Online]. Available: https://ieeexplore.ieee.org/document/5604689

[27] K. Cho, S. J. Lee, and K. Eshraghian, "Memristor-CMOS logic and digital computational components," *Microelectronics Journal*, vol. 46, no. 3, pp. 214–220, 2015. [Online]. Available: https://doi.org/10.1016/j.mejo.2014.12.006

[28] L. A. Camuñas-Mesa, B. Linares-Barranco, and T. Serrano-Gotarredona, "Neuromorphic Spiking Neural Networks and Their Memristor-CMOS Hardware Implementations," vol. 12, no. 17, 2019. [Online]. Available: https://doi.org/10.3390/ma12172745

[29] Y. Oğuz, "Mathematical Modeling of Memristors," *Memristor and Memristive Neural Networks*, 2018. [Online]. Available: https://www.intechopen.com/chapters/59395

[30] L. Chua and S. M. Kang, "Memristive devices and systems," *Proceedings of the IEEE*, vol. 64, no. 2, pp. 209–223, 1976. [Online]. Available: https://ieeexplore.ieee.org/document/1454361

[31] L. Chua, "Resistance switching memories are memristors," *Applied Physics A 2011 102:4*, vol. 102, no. 4, pp. 765–783, 2011. [Online]. Available: https://link.springer.com/article/10.1007/s00339-011-6264-9

[32] T. Singh, "Hybrid memristor-cmos (memos) based logic gates and adder circuits," *arXiv [cs.ET]*, vol. 1506, pp. 1–11, 2015. [Online]. Available: https://doi.org/10.48550/arXiv.1506.06735

[33] Z. Wang, H. Wu, G. W. Burr, C. S. Hwang, K. L. Wang, Q. Xia, and J. J. Yang, "Resistive switching materials for information processing," *Nature Publishing Group*, vol. 5, no. 3, pp. 173–195, 2020. [Online]. Available: https://www.nature.com/articles/s41578-019-0159-3

[34] A. Sawa, "Resistive switching in transition metal oxides," vol. 11, no. 6, pp. 28–36, 2008. [Online]. Available: https://doi.org/10.1016/S1369-7021(08)70119-6

[35] F. M. Simanjuntak, D. Panda, K.-H. Wei, and T.-Y. Tseng, "Status and prospects of zno-based resistive switching memory devices," *Nanoscale Research Letters*, vol. 11, p. 368, 2016. [Online]. Available: https://doi.org/10.1186/s11671-016-1570-y

[36] F. Chen, Y. Zhou, Y. Zhu, R. Zhu, P. Guan, J. Fan, L. Zhou, N. Valanoor, F. Von Wegner, E. Saribatir, I. Birznieks, T. Wan, and D. Chu, "Recent progress in artificial synaptic devices: Materials, processing and applications," *Journal of Materials Chemistry C*, vol. 9, no. 27, pp. 8372–8394, 2021. [Online]. Available: https://doi.org/10.1039/D1TC01211H

[37] G. Sassine, S. L. Barbera, N. Najjari, M. Minvielle, C. Dubourdieu, and F. Alibart, "Interfacial versus filamentary resistive switching in tio2 and hfo2 devices," *Journal of Vacuum Science & Technology B*, vol. 34, p. 012202, 2016, doi: 10.1116/1.4940129. [Online]. Available: https://doi.org/10.1116/1.4940129

[38] F. Zhuge, K. Li, B. Fu, H. Zhang, J. Li, H. Chen, L. Liang, J. Gao, H. Cao, Z. Liu, and H. Luo, "Mechanism for resistive switching in chalcogenide-based electrochemical metallization memory cells," *AIP Advances*, vol. 5, no. 5, p. 057125, 2015. [Online]. Available: https://aip.scitation.org/doi/abs/10.1063/1.4921089

[39] F. Sun, Q. Lu, S. Feng, and T. Zhang, "Flexible Artificial Sensory Systems Based on Neuromorphic Devices," *ACS Nano*, vol. 15, no. 3, pp. 3875–3899, 2021. [Online]. Available: https://doi.org/10.1021/acsnano.0c10049

[40] S. Batool, M. Idrees, S. R. Zhang, S. T. Han, and Y. Zhou, "Novel charm of 2D materials engineering in memristor: when electronics encounter layered morphology," *Nanoscale Horizons*, pp. 480–507, 2022. [Online]. Available: https://doi.org/10.1039/D2NH00031H

[41] R. Wang, J.-Q. Yang, J.-Y. Mao, Z.-P. Wang, S. Wu, M. Zhou, T. Chen, Y. Zhou, and S.-T. Han, "Recent advances of volatile memristors: Devices, mechanisms, and applications," *Advanced Intelligent Systems*, vol. 2, p. 2000055, 2020. [Online]. Available: https://onlinelibrary.wiley.com/doi/full/10.1002/aisy.202000055

[42] M. S. Feali, "Using volatile/non-volatile memristor for emulating the short-and long-term adaptation behavior of the biological neurons," *Neurocomputing*, vol. 465, pp. 157–166, 2021. [Online]. Available: https://doi.org/10.1016/j.neucom.2021.08.132

[43] A. Citri and R. C. Malenka, "Synaptic plasticity: Multiple forms, functions, and mechanisms," pp. 18–41, 2008. [Online]. Available: https://doi.org/10.1038/sj.npp.1301559

[44] T. Ohno, T. Hasegawa, T. Tsuruoka, K. Terabe, J. K. Gimzewski, and M. Aono, "Short-term plasticity and long-term potentiation mimicked in single inorganic synapses," *Nature Materials*, vol. 10, pp. 591–595, 2011. [Online]. Available: https://doi.org/10.1038/nmat3054

[45] T. Chang, S. H. Jo, and W. Lu, "Short-term memory to long-term memory transition in a nanoscale memristor," *ACS Nano*, vol. 5, pp. 7669–7676, 2011. [Online]. Available: https://doi.org/10.1021/nn202983n

[46] M. Shahsavari, P. Falez, and P. Boulet, "Combining a volatile and nonvolatile memristor in artificial synapse to improve learning in spiking neural networks." Presses Polytechniques Et Universitaires Romandes, 2016, pp. 67–72. [Online]. Available: https://ieeexplore.ieee.org/document/7568628

[47] S. G. Kim, J. S. Han, H. Kim, S. Y. Kim, and H. W. Jang, "Recent Advances in Memristive Materials for Artificial Synapses," *Advanced Materials Technologies*, vol. 3, no. 12, pp. 1–30, 2018. [Online]. Available: https://doi.org/10.1002/admt.201800457

[48] T. Guo, B. Sun, S. Ranjan, Y. Jiao, L. Wei, Y. Norman Zhou, and Y. A. Wu, "From memristive materials to neural networks," *ACS Applied Materials and Interfaces*, vol. 12, no. 49, pp. 54 243–54 265, 2020. [Online]. Available: https://doi.org/10.1021/acsami.0c10796

[49] Q. H. Qin, L. Äkäslompolo, N. Tuomisto, L. Yao, S. Majumdar, J. Vijayakumar, A. Casiraghi, S. Inkinen, B. Chen, A. Zugarramurdi, M. Puska, and S. van Dijken, "Resistive switching in all-oxide ferroelectric tunnel junctions with ionic interfaces," *Advanced Materials*, vol. 28, pp. 6852–6859, 2016, https://doi.org/10.1002/adma.201504519. [Online]. Available: https://doi.org/10.1002/adma.201504519

[50] M. N. Almadhoun, M. Speckbacher, B. C. Olsen, E. J. Luber, S. Y. Sayed, M. Tornow, and J. M. Buriak, "Bipolar resistive switching in junctions of gallium oxide and p-type silicon," *Nano Letters*, vol. 21, pp. 2666–2674, 2021,

doi: 10.1021/acs.nanolett.1c00539. [Online]. Available: https://doi.org/10.1021/acs.nanolett.1c00539

[51] S. Pinto, R. Krishna, C. Dias, G. Pimentel, G. N. Oliveira, J. M. Teixeira, P. Aguiar, E. Titus, J. Gracio, J. Ventura, and J. P. Araujo, "Resistive switching and activity-dependent modifications in ni-doped graphene oxide thin films," *Applied Physics Letters*, vol. 101, 2012. [Online]. Available: https://doi.org/10.1063/1.4742912

[52] S. Goswami, D. Deb, A. Tempez, M. Chaigneau, S. P. Rath, M. Lal, Ariando, R. S. Williams, S. Goswami, and T. Venkatesan, "Nanometer-scale uniform conductance switching in molecular memristors," *Advanced Materials*, vol. 32, no. 42, p. 2004370, 2020. [Online]. Available: https://onlinelibrary.wiley.com/doi/abs/10.1002/adma.202004370

[53] R. Martins, E. Carlos, J. Deuermeier, M. Pereira, R. Martins, E. Fortunato, and A. Kiazadeh, "Emergent solution based igzo memristor towards neuromorphic applications," *Journal of Materials Chemistry C*, vol. 10, no. 6, pp. 1991–1998, 2022. [Online]. Available: https://doi.org/10.1039/d1tc05465a

[54] D. Kim and J. S. Lee, "Designing artificial sodium ion reservoirs to emulate biological synapses," *NPG Asia Materials*, vol. 12, 2020. [Online]. Available: http://dx.doi.org/10.1038/s41427-020-00243-2

[55] H.-J. Koo, J.-H. So, M. D. Dickey, and O. D. Velev, "Towards all-soft matter circuits: Prototypes of quasi-liquid devices with memristor characteristics," *Advanced Materials*, vol. 23, no. 31, pp. 3559–3564, 2011. [Online]. Available: https://onlinelibrary.wiley.com/doi/abs/10.1002/adma.201101257

[56] M. U. Khan, Q. M. Saqib, M. Y. Chougale, R. A. Shaukat, J. Kim, and J. Bae, "Soft and flexible: core-shell ionic liquid resistive memory for electronic synapses," *Microsystems and Nanoengineering*, vol. 7, 2021. [Online]. Available: http://dx.doi.org/10.1038/s41378-021-00305-7

[57] K. Lu, X. Li, Q. Sun, X. Pang, J. Chen, T. Minari, X. Liu, and Y. Song, "Solution-processed electronics for artificial synapses," *Materials Horizons*, vol. 8, pp. 447–470, 2021. [Online]. Available: http://dx.doi.org/10.1039/D0MH01520B

[58] K. Khoshmanesh, S. Y. Tang, J. Y. Zhu, S. Schaefer, A. Mitchell, K. Kalantar-Zadeh, and M. D. Dickey, "Liquid metal enabled microfluidics," *Lab on a Chip*, vol. 17, pp. 974–993, 2017. [Online]. Available: https://doi.org/10.1039/C7LC00046D

[59] M. Zaheer, Y. Cai, A. B. Waqas, S. F. Abbasi, G. Zhu, C. Cong, Z. J. Qiu, R. Liu, Y. Qin, L. Zheng, and L. Hu, "Liquid-metal-induced memristor behavior in polymer insulators," *Physica Status Solidi - Rapid Research Letters*, vol. 14, 2020. [Online]. Available: https://doi.org/10.1002/pssr.202000050

[60] M. Y. Chougale, S. R. Patil, S. P. Shinde, S. S. Khot, A. A. Patil, A. C. Khot, S. S. Chougule, C. K. Volos, S. Kim, and T. D. Dongale, "Memristive switching in ionic liquid–based two-terminal discrete devices," *Ionics*, vol. 25, pp. 5575–5583, 2019. [Online]. Available: https://doi.org/10.1007/s11581-019-03082-6

[61] K. Rajan, A. Chiappone, D. Perrone, S. Bocchini, I. Roppolo, K. Bejtka, M. Castellino, C. F. Pirri, C. Ricciardi, and A. Chiolerio, "Ionic liquid-enhanced soft resistive switching devices," *RSC Advances*, vol. 6, pp. 94 128–94 138, 2016. [Online]. Available: https://doi.org/10.1039/C6RA18668H

[62] E. L. Smith, A. P. Abbott, and K. S. Ryder, "Deep eutectic solvents (dess) and their applications," *Chemical Reviews*, vol. 114, pp. 11 060–11 082, 2014. [Online]. Available: https://doi.org/10.1021/cr300162p

[63] M. Li, C. Wang, Z. Chen, K. Xu, and J. Lu, "New concepts in electrolytes," *Chemical Reviews*, vol. 120, pp. 6783–6819, 2020. [Online]. Available: https://doi.org/10.1021/acs.chemrev.9b00531

[64] C. Wang, C. Wang, Z. Huang, and S. Xu, "Materials and structures toward soft electronics," *Advanced Materials*, vol. 30, pp. 1–49, 2018. [Online]. Available: https://doi.org/10.1002/adma.201801368

[65] N. C. for Biotechnology Information, "Copper sulfate pentahydrate," 2022. [Online]. Available: https://pubchem.ncbi.nlm.nih.gov/compound/Copper-sulfate-pentahydrate

[66] S. Hong, Y. Yuan, C. Liu, W. Chen, L. Chen, H. Lian, and H. Liimatainen, "A stretchable and compressible ion gel based on a deep eutectic solvent applied as a strain sensor and electrolyte for supercapacitors," *Journal of*

Materials Chemistry C, vol. 8, no. 2, pp. 550–560, 2020. [Online]. Available: https://doi.org/10.1039/C9TC05913J

[67] A. P. Abbott, D. Boothby, G. Capper, D. L. Davies, and R. K. Rasheed, "Deep eutectic solvents formed between choline chloride and carboxylic acids: Versatile alternatives to ionic liquids," *Journal of the American Chemical Society*, vol. 126, pp. 9142–9147, 2004. [Online]. Available: https://doi.org/10.1021/ja048266j

[68] A. P. Abbott, R. C. Harris, K. S. Ryder, C. D'Agostino, L. F. Gladden, and M. D. Mantle, "Glycerol eutectics as sustainable solvent systems," *Green Chemistry*, vol. 13, pp. 82–90, 2011. [Online]. Available: https://doi.org/10.1039/C0GC00395F

[69] A. T. S. C. Brandão, R. Costa, A. F. Silva, and C. M. Pereira, "Hydrogen bond donors influence on the electrochemical performance of composite graphene electrodes/deep eutectic solvents interface," *Electrochem*, vol. 3, no. 1, pp. 129–142, 2022. [Online]. Available: https://www.mdpi.com/2673-3293/3/1/9

[70] A. T. Brandão, S. Rosoiu, R. Costa, O. A. Lazar, A. F. Silva, L. Anicai, C. M. Pereira, and M. Enachescu, "Characterization and electrochemical studies of MWCNTs decorated with Ag nanoparticles through pulse reversed current electrodeposition using a deep eutectic solvent for energy storage applications," *Journal of Materials Research and Technology*, vol. 15, pp. 342–359, 2021. [Online]. Available: https://doi.org/10.1016/j.jmrt.2021.08.031

[71] F.-C. Chiu, "A Review on Conduction Mechanisms in Dielectric Films," *Advances in Materials Science and Engineering*, vol. 2014, p. 578168, 2014. [Online]. Available: https://doi.org/10.1155/2014/578168

[72] Y. B. Zhu, K. Zheng, X. Wu, and L. K. Ang, "Enhanced stability of filament-type resistive switching by interface engineering," *Scientific Reports*, vol. 7, p. 43664, 2017. [Online]. Available: https://doi.org/10.1038/srep43664

[73] G. Bersuker and D. Gilmer, "9 - metal oxide resistive random access memory (rram) technology," in *Advances in Non-volatile Memory and Storage Technology*, Y. Nishi, Ed. Woodhead Publishing, 2014, pp. 288–340. [Online]. Available: https://www.sciencedirect.com/science/article/pii/B9780857098030500096

[74] A. V. Fadeev and K. V. Rudenko, "To the Issue of the Memristor's HRS and LRS States Degradation and Data Retention Time," *Russian Microelectronics*, vol. 50, no. 5, pp. 311–325, 2021. [Online]. Available: https://doi.org/10.1134/S1063739721050024

[75] W. Yu, H. Xie, L. Chen, Y. Li, and C. Zhang, "Synthesis and characterization of monodispersed copper colloids in polar solvents," *Nanoscale Research Letters*, vol. 4, no. 5, pp. 465–470, 2009. [Online]. Available: https://doi.org/10.1007/s11671-009-9264-3

[76] "Chapter 1 - electrical double layer around a charged colloidal particle in an electrolyte solution," in *Theory of Colloid and Interfacial Electric Phenomena*, ser. Interface Science and Technology, H. Ohshima, Ed. Elsevier, 2006, vol. 12, pp. 1–38. [Online]. Available: https://www.sciencedirect.com/science/article/pii/S1573428506800244

[77] J. C. Mauro, "Chapter 26 - thermal and electrical conductivities," in *Materials Kinetics*, J. C. Mauro, Ed. Elsevier, 2021, pp. 501–511. [Online]. Available: https://www.sciencedirect.com/science/article/pii/B9780128239070000108

[78] T. Bell, "Electrical Conductivity of Metals," 2020. [Online]. Available: https://www.thoughtco.com/electrical-conductivity-in-metals-2340117

[79] T. Yanagida, K. Nagashima, K. Oka, M. Kanai, A. Klamchuen, B. H. Park, and T. Kawai, "Scaling Effect on Unipolar and Bipolar Resistive Switching of Metal Oxides," *Scientific Reports 2013 3:1*, vol. 3, no. 1, pp. 1–6, 2013. [Online]. Available: https://www.nature.com/articles/srep01657

[80] H. Jiang, X. Y. Li, R. Chen, X. L. Shao, J. H. Yoon, X. Hu, C. S. Hwang, and J. Zhao, "Bias-polarity-dependent resistance switching in W/SiO2/Pt and W/SiO2/Si/Pt structures," *Scientific Reports 2016 6:1*, vol. 6, no. 1, pp. 1–11, 2016. [Online]. Available: https://www.nature.com/articles/srep22216

[81] P. A. Tipler and R. A. Llewellyn, *Modern Physics*, 3rd ed. W. H. Freeman, 1999.

[82] K. Fleck, C. La Torre, N. Aslam, S. Hoffmann-Eifert, U. Böttger, and S. Menzel, "Uniting gradual and abrupt set processes in resistive switching oxides," *Phys. Rev. Applied*, vol. 6, p. 064015, 2016. [Online]. Available: https://link.aps.org/doi/10.1103/PhysRevApplied.6.064015

[83] D. C. Giancoli, *Physics*, 4th ed. Prentice Hall, 1995. [Online]. Available: https://archive.org/details/physicsprinciple00gian_0

[84] I. Valov, E. Linn, S. Tappertzhofen, S. Schmelzer, J. V. D. Hurk, F. Lentz, and R. Waser, "Nanobatteries in redox-based resistive switches require extension of memristor theory," *Nature Communications*, pp. 1–9, 2013. [Online]. Available: https://doi.org/10.1038/ncomms2784

[85] B. Sundén, "Electrochemistry and thermodynamics," *Hydrogen, Batteries and Fuel Cells*, pp. 15–36, 2019. [Online]. Available: https://www.sciencedirect.com/science/article/pii/B9780128169506000026

[86] G. Wang, C. Li, Y. Chen, Y. Xia, D. Wu, and Q. Xu, "Reversible voltage dependent transition of abnormal and normal bipolar resistive switching," *Scientific Reports*, vol. 6, p. 36953, 2016. [Online]. Available: https://doi.org/10.1038/srep36953

[87] A. Milchev, "Nucleation phenomena in electrochemical systems: thermodynamic concepts," *ChemTexts*, vol. 2, no. 1, pp. 1–9, 2016. [Online]. Available: https://doi.org/10.1007/s40828-015-0022-0

[88] D. Grujicic and B. Pesic, "Electrodeposition of copper: The nucleation mechanisms," *Electrochimica Acta*, vol. 47, no. 18, pp. 2901–2912, 2002. [Online]. Available: https://doi.org/10.1016/S0013-4686(02)00161-5

[89] A. Ramos, M. Miranda-Hernández, and I. González, "Influence of Chloride and Nitrate Anions on Copper Electrodeposition in Ammonia Media," *Journal of The Electrochemical Society*, vol. 148, no. 4, p. C315, 2001. [Online]. Available: https://doi.org/10.1149/1.1357176

[90] U. B. Han and J. S. Lee, "Integration scheme of nanoscale resistive switching memory using bottom-up processes at room temperature for high-density memory applications," *Scientific Reports*, vol. 6, no. June, pp. 1–8, 2016. [Online]. Available: http://dx.doi.org/10.1038/srep28966

[91] M. Aarts, S. V. Vliet, R. Bliem, and E. Alarcon-Llado, "Investigation of copper nanoscale electro-crystallization under directed and non-directed electrodeposition from dilute electrolytes," *CrystEngComm*, vol. 23, pp. 3648–3653, 2021. [Online]. Available: https://doi.org/10.1039/D1CE00143D

[92] W. Wang, M. Wang, E. Ambrosi, A. Bricalli, M. Laudato, Z. Sun, X. Chen, and D. Ielmini, "Surface diffusion-limited lifetime of silver and copper nanofilaments in resistive switching devices," *Nature Communications*, vol. 10, no. 1, pp. 1–10, 2019. [Online]. Available: http://dx.doi.org/10.1038/s41467-018-07979-0

[93] M. K. Rahmani, B. D. Yang, H. Kim, H. Kim, and M. H. Kang, "Coexistence of volatile and non-volatile resistive switching in Ni/SiO2/Pt memristor device controlled from different current compliances," *Semiconductor Science and Technology*, vol. 36, no. 9, 2021. [Online]. Available: https://doi.org/10.1088/1361-6641/ac18f7